Atmospheric Sciences Report 79-1

RESEARCH, OPERATIONS, AND EVALUATION IN THE ALBERTA HAIL PROJECT

Volume 2A: Research Meteorology and Modelling

RESEARCH COUNCIL

RESEARCH, OPERATIONS, AND EVALUATION IN THE ALBERTA HAIL PROJECT 1974 - 1978

Volume 2-A
Meteorology and Modelling

by

F.E. Robitaille
M. English
B. Kochtubajda
F. Barlow
T. Krauss
C.M. Sackiw
J. Mason

G.G. Goyer, Head
Atmospheric Sciences Division
Alberta Research Council

1980

THE STORM ENVIRONMENT PROGRAM

F.E. Robitaille
C.M. Sackiw
J. Mason
F. Barlow

TABLE OF CONTENTS

	Page
Introduction	1
Program Objectives	1
Development of a Mobile Rawinsonde System	1
A case study of atmospheric features on days with and without major hailfall	1
Estimating hail potential for convective storms in Alberta	5
Rocky Mountain House Area Genesis Study	9
Conclusions	17
Recommendations	17
References	18

ILLUSTRATIONS

Figure 1.	Making a sounding in the Alberta foothills	2
Figure 2.	Preparing for a sounding near a thunderstorm	2
Figure 3.	The layout of the interior of the Moras tracking vehicle	3
Figure 4.	Time-height sections showing mixing ratio difference, $\Delta w = w_{21}$ Aug. $- w_{27}$ Aug. in g/kg	3
Figure 5.	Time-height sections of dewpoint depression (°C) for 21 August 1975	4
Figure 6.	Time-height sections of dewpoint depression (°C) for 27 August 1975	4
Figure 7.	Time-height sections of wind speed (ms^{-1}) for 21 August 1975	5
Figure 8.	Time-height sections of wind speed (ms^{-1}) for 27 August 1975	5
Figure 9.	Composite parcel energy field ($J\ g^{-1}$) using 33 strong storm soundings.	7
Figure 10.	Composite maximum diameter hail field using 33 strong storm soundings	9
Figure 11.	Schematic showing sounding location areas that give suitable (C and D) and unsuitable (A and B) estimates of instability in the main updraft of a strong convective storm	10
Figure 12.	Phase one of proposed flow patterns leading to activation of thunderstorm formation areas west of Rocky Mountain House	11
Figure 13.	Phase two of proposed flow patterns leading to activation of thunderstorm formation areas west of Rocky Mountain House	12
Figure 14.	Phase three of proposed flow patterns leading to activation of thunderstorm formation areas west of Rocky Mountain House	12
Figure 15.	RAGS location map for 9 August 1978	13
Figure 16.	Observations for leg #1 of RAGS Experiment	14
Figure 17.	Observations for leg #2 of RAGS Experiment	15
Figure 18.	Streamlines near 200 metres above the surface in the early afternoon of 9 August 1978	16
Figure 19.	Network of wind measuring stations proposed for July 1979 to monitor river valley flow on days when thunderstorms form in stippled area	18

REFERENCES

TABLES

Table 1.	Chronology of MORAS participation in the AHP	2
Table 2.	Maximum reasonable values for temperature difference, $T_p - T_m$	6
Table 3.	Parcel energies and maximum hailstone diameters in order of decreasing parcel energies	8
Table 4.	RAGS calendar	11

THE STORM ENVIRONMENT PROGRAM

F. Robitaille
C. Sackiw
J. Mason
F. Barlow

INTRODUCTION

This section summarizes the activities of the Atmospheric Sciences Division's Storm Environment Program during four years of participation in the Alberta Hail Project (AHP). The objectives of the Program are reviewed as well as the in-house development of the unique upper-air measurement system, and the accomplishments of the Program using this system and other AHP data sources. A description of the Rocky Mountain House Area Genesis Study (RAGS) conducted in August 1978 is included. Data from aircraft traverses near preferred convective storm formation areas are analyzed. A role played by river valleys in hailstorm formation and a sequence of events to account for preferred formation areas are suggested. A modest field effort in 1979 to verify this sequence is discussed.

PROGRAM OBJECTIVES

Efforts of the Storm Environment Program have been focused on objectives considered attainable within the AHP. These objectives are:

(1) To identify mesoscale features of the atmosphere on days with and without major hailstorms.
(2) To determine convective instability near hailstorms and, subsequently, determine where soundings can be positioned to best estimate thermodynamic conditions in the airstream feeding the main updraft in the storm core.
(3) To provide sounding location criteria to the Cloud Modelling and Statistical Evaluation Programs to help in the search for evaluation predictors.
(4) To determine why hailstorms form in preferred areas in the Alberta foothills.

The first objective has been met and is discussed later in this section. A definition of representative soundings has been completed based on 1976 data, and inclusion of data from other years is discussed. The last objective can be met following analysis of measurements from a proposed field program for 1979.

DEVELOPMENT OF A MOBILE RAWINSONDE SYSTEM

To detect convective storm circulation systems using soundings, station spacing should be approximately 25 km (Barnes *et al.*, 1971). This suggests that, for the western half of the AHP operational area, a system of eleven stations making soundings every two hours would detect about 80 percent of the hailstorms (Robitaille, 1977).

An alternative to a costly system of fixed stations is to use mobile sounding stations. One such station close to hailstorm areas could detect the same number of storms as two or three fixed stations, depending on meteorological and operational conditions. A smaller and less expensive system incorporating mobile stations can provide the resolution of a larger fixed system.

The concept of mobile stations could not be developed in the 1960s because compact, light-weight rawinsonde tracking equipment was not available. In 1972, however, a solid-state system was placed on the market and the go-ahead to develop an operational prototype for use in Alberta was given. A Weather Measure RD-65 rawinsonde system was acquired in the spring of 1973 and fitted into a one-ton box van. Extensive vehicle modifications and systems trials were performed in-house during 1974 and 1975 and the prototype, designated the MObile RAwinSonde (MORAS), was produced (Figs. 1 and 2). A schematic of the vehicle's internal configuration is shown in figure 3. Table 1 summarizes the history of MORAS from the first successful sounding in 1975 through the 1978 field program. Detailed accounts of MORAS development and operational procedures are contained in two companion reports (Robitaille, 1977; Sackiw and Bergwall, 1977).

A CASE STUDY OF ATMOSPHERIC FEATURES ON DAYS WITH AND WITHOUT MAJOR HAILFALL

With a substantive increase in the number of sounding stations in the AHP, occurrences of hail could be reasonably well-predicted for each convective storm. This requires two-hourly soundings at stations 25 km apart throughout the AHP operational area. Displays of convergence and vertical motion available within hours are used to make the prediction.

Better hail forecasts may also be possible by maximizing the use of MORAS and existing AHP sounding stations. By assuming that sounding features are carried along with the flow from west to east, three dimensional pictures can

TABLE 1
Chronology of MORAS participation in the AHP

Date	Activity
May 1975	First successful test sounding
June 1975	Training soundings; first operational sounding
Summer 1975	92 successful soundings
March 1976	Hydraulic levelling system installed; heavy duty springs and tires added for stability
April to May 1976	L & N Type W recorder installed for more sensitivity; intercomparison sounding with AES Stony Plain (EG)
June 1976	Supply vehicle incorporated into field operations
Summer 1976	109 successful soundings; intercomparison soundings with AHP Rocky Mountain House (RM), Penhold (QF) stations
Summer 1977	48 successful soundings; intercomparison soundings with RM, QF, EG and Intera research aircraft
Summer 1978	25 successful soundings during abbreviated four week field period; intercomparison soundings with RM, QF, EG and Calgary (YC) stations

be created by arranging stations in a north-south line. These pictures can be analyzed for features that occur before hailstorms form. With the capability to detect and display these features, they could provide valuable guidance to operational forecasters.

Two days in 1975, 21 and 27 August, were selected in an effort to detect antecedent features. MORAS was located between the upper-air stations at Rocky Mountain House (RM) and Calgary (YC), near Sundre, on both days. The MORAS, RM, and YC sites made 14 releases on 21 August and 16 on 27 August.

FIGURE 1. Making a sounding in the Alberta foothills.

FIGURE 2. Preparing for a sounding near a thunderstorm.

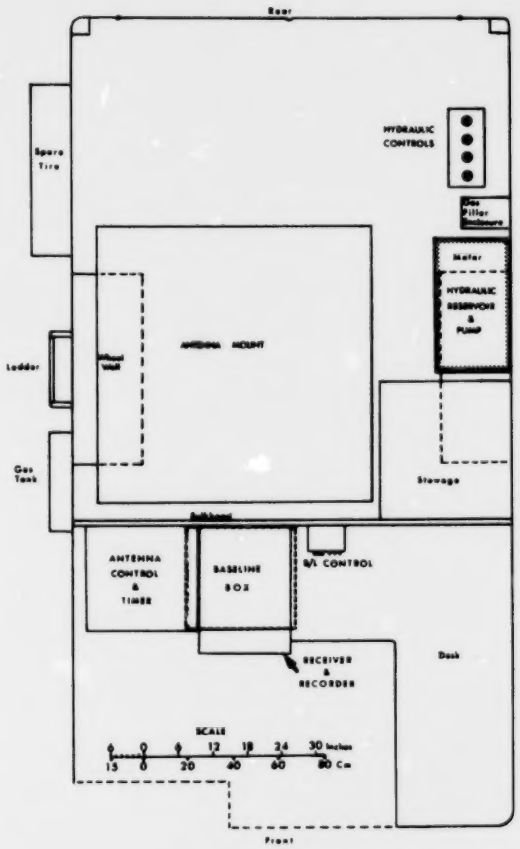

FIGURE 3. The layout of the interior of the MORAS tracking vehicle.

Convective activity on the two days was markedly different. A major hailswath 16 to 20 km wide from near Crimson Lake to south of Camrose occurred on 21 August. Grape size and smaller hail occurred in the western third of the swath and walnut and larger in the remainder. On 27 August, convective activity was isolated with three reports of grape size hail 30 to 35 km northeast of Bashaw and one report of shot size 30 km north-northwest of Rimbey.

Following Ninomiya (1971) fields of instability, moisture, and wind speed were examined for characteristic features. Instability, as represented by calculated parcel energies from the Loaded Moist Adiabatic cloud model (Chisholm, 1970), increased on both afternoons with the highest values on 27 August at YC and RM. Temporal trends, at stations about 80 km apart, showed no direct relation to hailfall intensity. This is not surprising since, as discussed later, this parameter is a reasonable measure of hailfall potential only when it is obtained using soundings ahead of storms.

Higher mixing ratios were present near RM and YC in the low levels on 21 August. This is shown by subtracting the fields for the two days (Fig. 4). However, when the dewpoint depression fields were examined (Figs. 5 and 6), the air mass near RM appeared closer to saturation accounting for lower cloud bases in the northwest part of the AHP area. Lower mixing ratios and low dewpoint depression values were found in the low levels near MORAS, RM, and YC, in the morning of 27 August.

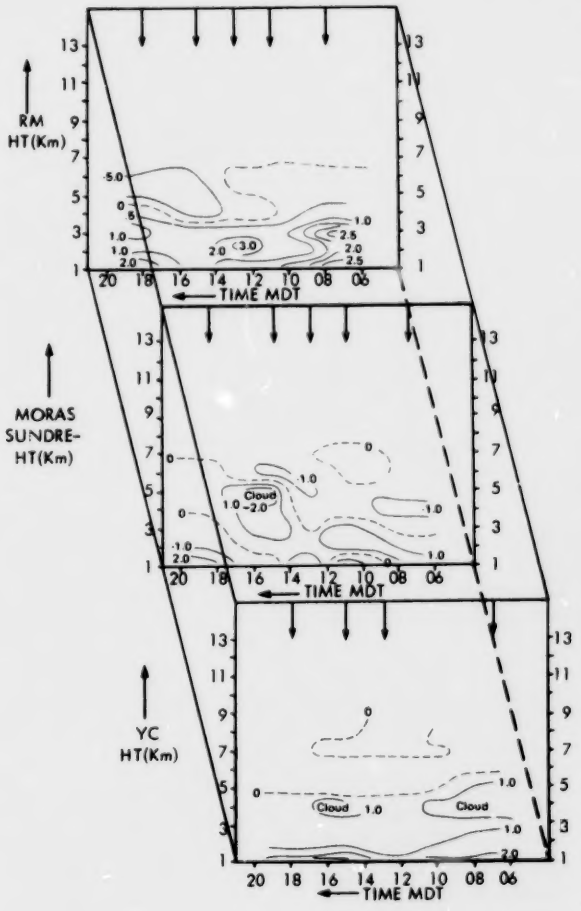

FIGURE 4. Time-height sections showing mixing ratio difference, $\Delta w = w_{21\ Aug.} - w_{27\ Aug.}$ in g/kg. Positive values indicated 21 August 1975 more moist. Arrows refer to rawinsonde release times. Flow from west to east is approximated by time increasing from right to left.

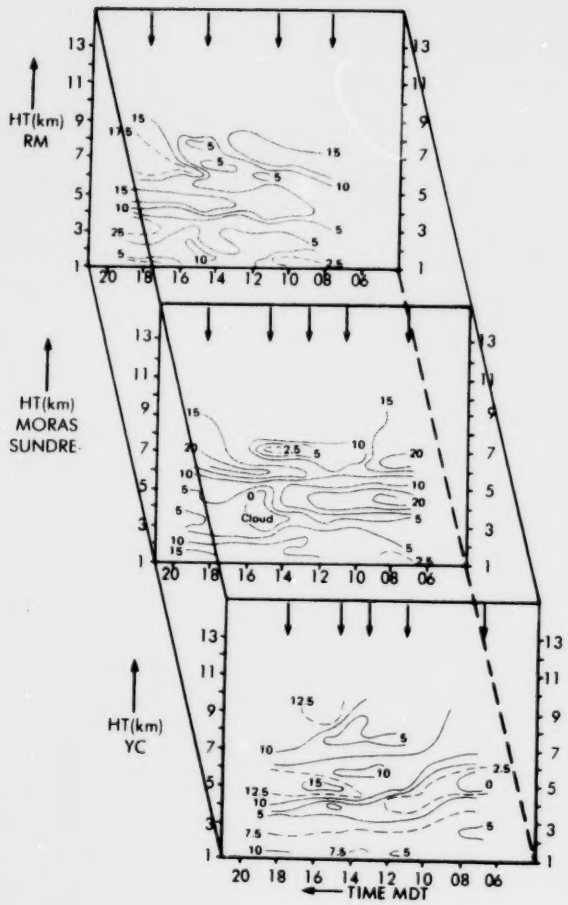

FIGURE 5. Time-height sections of dewpoint depression (°C) for 21 August 1975. Arrows indicate rawinsonde release times. Flow from west to east is approximated by time increasing from right to left.

Wind speeds (Figs. 7 and 8) were a maximum near 11 km over RM which was closest to the major hailswath and also over YC and MORAS suggesting that this phenomenon can be present at stations well-removed from major convective activity. The occurrence of a wind maximum in the low levels, another feature Ninomiya (1971) considered prerequisite for severe convection, could not be seen on either day.

In summary, the occurrence of severe hailfall on 21 August 1975 can be explained by the presence of several atmospheric features. Time-height analysis of soundings showed them as:

(1) Parcel energy dependence on sounding time and location. For severe hailfall, high values of parcel energy are needed.
(2) High moisture content in the low levels and low dewpoint depressions.
(3) Wind speed maxima in the upper levels.

An operational forecaster should watch for these features. If the middle-levels of the atmosphere are expected to cool on a day when these features occur, a forecast of hail should be made. The forecast accuracy depends on the

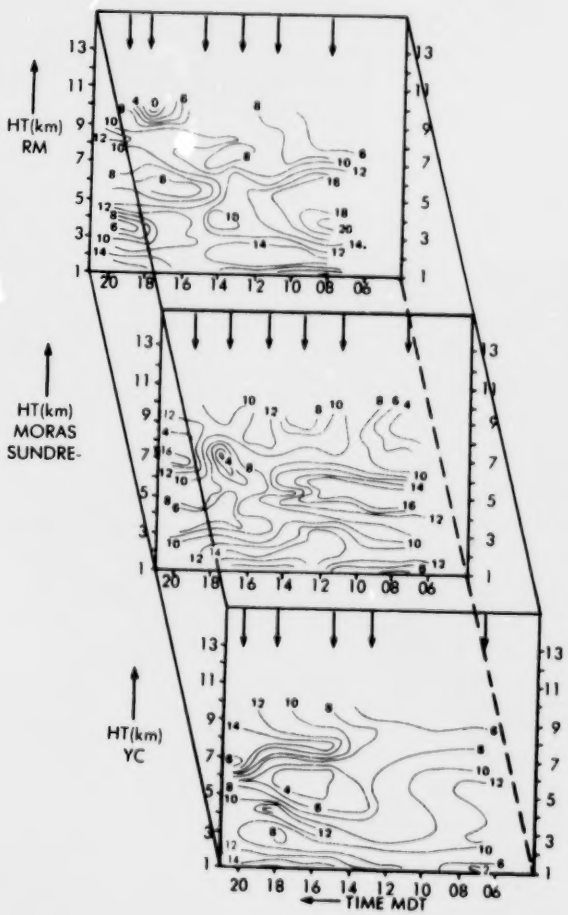

FIGURE 6. Time-height sections of dewpoint depression (°C) for 27 August 1975. Arrows indicate rawinsonde release times. Flow from west to east is approximated by time increasing from right to left.

ability of sounding stations to detect the disturbance associated with an embryonic convective circulation system. The next part of this report examines where these soundings should be located to ensure that the circulations associated with hailstorms are detected.

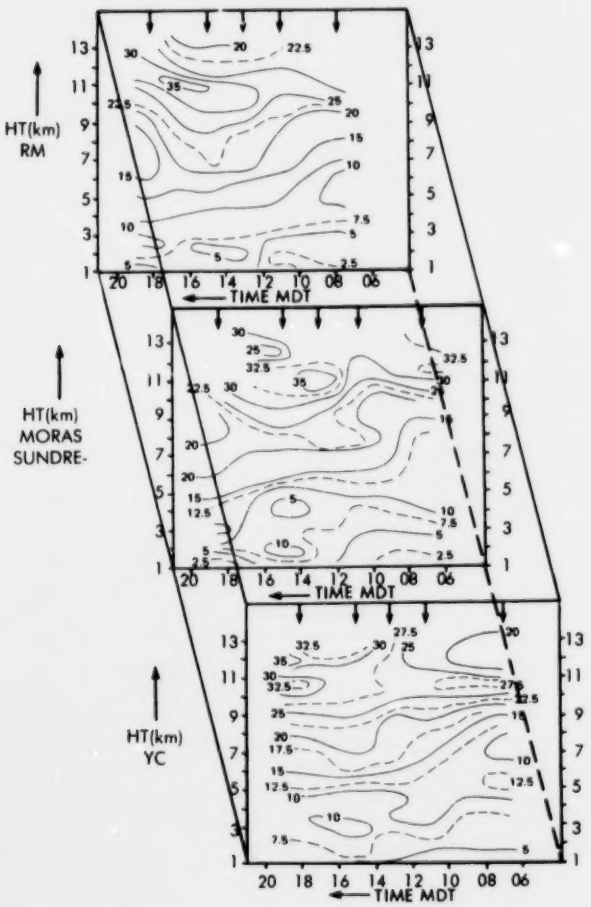

FIGURE 7. Time-height sections of wind speed (ms^{-1}) for 21 August 1975. Arrows indicate rawinsonde release times. Flow from west to east is approximated by time increasing from right to left.

ESTIMATING HAIL POTENTIAL FOR CONVECTIVE STORMS IN ALBERTA

A point estimate of the parcel energy and hail production potential for a convective storm can be made with an upper-air sounding. The computer is used to run the Loaded Moist Adiabatic (LMA) cloud model (Chisholm, 1970, 1973), using data from an upper-air sounding. Parcel energy is computed by the model. Also computed are the maximum vertical velocity in cloud and the temperature at the level at which it occurs. These are read into an empirical nomogram to give the point estimate of maximum hail size (Maxwell, 1974; Renick and Maxwell, 1978). If simultaneous soundings are available around a convective storm, a field of point estimates can be obtained. Locations that give reasonable point estimates are obtained by contouring the parcel energy field and using Chisholm's (1973) guidelines for the storm intensity in question. Soundings that are properly located to give reasonable parcel energy estimates are assumed to give reasonable estimates of hail production potential.

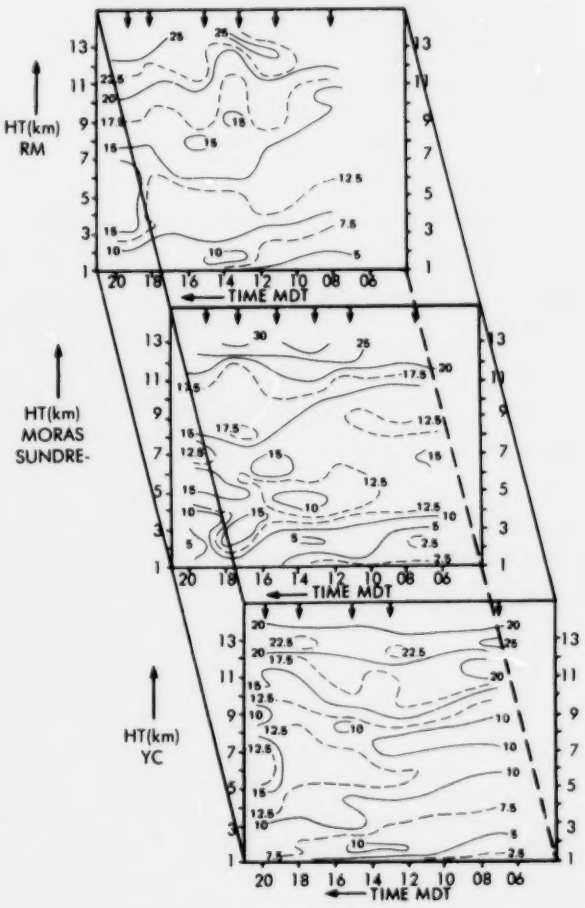

FIGURE 8. Time-height sections of wind speed (ms^{-1}) for 27 August 1975. Arrows indicate rawinsonde release times. Flow from west to east is approximated by time increasing from right to left.

A rawinsonde network of sufficient size does not exist in Alberta to allow construction of contoured fields around a particular storm. An alternative method which approximates these fields is needed. One method is to combine point estimates for many different storms. This is done by placing the origin of a polar coordinate system on storm centers and pointing the zero degree radial in the direction of storm motion. Sounding locations are plotted in this spatial system to give a simulated field of point estimates. These are related to the real fields around a particular storm with the following assumptions:

(1) Parcel energy and hail production potential for a convective storm are dependent on its intensity. Intensity is equated to maximum equivalent radar reflectivity factor, Z_e, as indicated on a one to two degree antenna elevation angle plan position indicator (PPI) display.

(2) Parcel energy and hail production potential from a sounding depend on sounding location with respect to the storm center.

(3) Cloud seeding effects on ambient temperature and dewpoint vertical profiles are small.

(4) Cloud seeding does not affect storm direction of motion.

To carry out this alternative method, radiosonde ascents on AHP declared haildays during the 1976 research field program are considered. A subset of these is used and consists of soundings released from 20 to 100 km away from storm centers. This subset is stratified into weak (20 $\leq Z_e \leq$30 dBZ) and strong (40 $\leq Z_e \leq$ 60 dBZ) storm soundings. Cases of stationary or slowly moving storms are excluded. A total of 16 point estimates are available for the composite weak storm and 33 for the composite strong storm.

To run the LMA model, the temperature and dewpoint of air parcels near convective cloud base are needed. These properties can sometimes be explained by dry adiabatic ascent from near the ground (Marwitz, 1972). In other cases, mixing in the subcloud layer prior to such ascent is required. As examples, Hudson (1970) in a study of horizontal moisture convergence and convective cloud formation used 100 mb, Fankhauser and Mohr (1977) in a study of hailstorms in northeast Colorado use 50 mb, and Barge and Bergwall (1976) in a report on fine-scale radar structure of Alberta convective storms also use 50 mb. The average of these pressures, 75 mb, is used for this study. When the LMA indicates high parcel energy and cloud freezing level exceeding 4.4 km, the sounding is not used since the Maxwell nomogram overestimates maximum hailstone diameter (Renick and Maxwell, 1978).

The convective temperature, T_p, generated by mixing the lowest 75 mb during each LMA run is examined. A range of values considered reasonable for locations within 40 km of the sounding station are defined by

$$T_m \leq T_p \leq T_m + \Delta_1 (r,\theta) + \Delta_2 (t)$$

where T_p is the convective temperature; T_m is the surface temperature measured at the station at release time; Δ_1 allows for the presence of a "hot spot" at radial distance r and bearing angle θ; Δ_2 allows for the effect of the diurnal heating cycle at time t. A maximum value for Δ_1, near 3C° has been observed elsewhere (Wilk *et al.*, 1976; Chalon *et al.*, 1976) and is used here. Δ_2 is estimated by using Calgary mean hourly temperatures for 1951 through 1960 inclusive (Harley and Cudbird, 1969) for the summer months. Table 2 shows the largest values for the difference, $T_p - T_m$, that are accepted. If $T_p - T_m$ exceeds these values, T_p is forced to a lower value by reducing the depth of the mixed layer while increasing the parcel mixing ratio to minimize the change in the cloud process curve. Similarly, when $T_p - T_m$ is negative, T_p is set equal to T_m by increasing the depth of the mixed layer while decreasing the parcel mixing ratio. After these adjustments, a second LMA run is made. If reasonable mixing conditions do not produce convective cloud, the LMA output message "base does not fit, input new one" appears and zeros are entered in the composite fields.

TABLE 2
Maximum reasonable values for temperature difference, $T_p - T_m$

Release Time (MDT)	$T_p - T_m = \Delta_{1\,MAX} + \Delta_{2\,MAX}$		
	June	July	August
1100	5.8	6.7	6.5
1200	4.9	5.4	5.3
1300	4.2	4.6	4.5
1400	3.6	3.8	3.7
1500	3.0	3.0	3.0
1600	3.0	3.0	3.0
1700	3.0	3.0	3.0
1800	3.0	3.0	3.0

Parcel energies and maximum hail diameters for weak and strong storm soundings are listed in table 3. Little spatial variability appears for the weak soundings with parcel energies less than 0.20 Jg^{-1} in 14 of 16 cases. This agrees with earlier estimates of typical parcel energies for storms that do not penetrate the tropopause (Chisholm, 1970). The strong storm sounding composite parcel energy field is shown in figure 9. Values approaching 0.60 Jg^{-1} and higher appear mostly in the forward two quadrants skewed towards the right flank suggesting a typical lower limit for inflow areas in storms of this intensity. This is slightly higher than the 0.45 Jg^{-1} guideline suggested by Chisholm (1970) for the main core of storms that significantly penetrate the tropopause.

Two LMA output parameters, the maximum vertical velocity in the convective cloud and the altitude at which it occurs, are used with an empirical nomogram (Maxwell, 1974) to estimate maximum diameter hail. The maximum size hail likely is taken as an indication of the hail production potential. Figure 10 shows this parameter for the strong storm soundings.

The composite parcel energy field for the strong convective storm is an approximation to the field surrounding an isolated, well-developed thunderstorm characterized by the following:

(1) A core cloud with a 15 to 20 km radius (Browning, 1965; Newton 1966) which protects the main updraft from significant entrainment allowing it to persist in strong ambient vertical wind shear.
(2) Low-level inflow in part of the right-front quadrant (Browning and Ludlam, 1960, 1962; Donaldson, 1962; Browning and Donaldson, 1963; Browning, 1965) or occasionally in part of the left-front quadrant (Hammond, 1967).
(3) An anvil cloud elongated parallel to the upper tropospheric wind usually to the left of storm motion (Lemon, 1977). This cloud can extend 60 km or more downwind from the leading edge of the storm core and 20 km upwind from the trailing edge (Newton, 1966; Palmén and Newton, 1969).

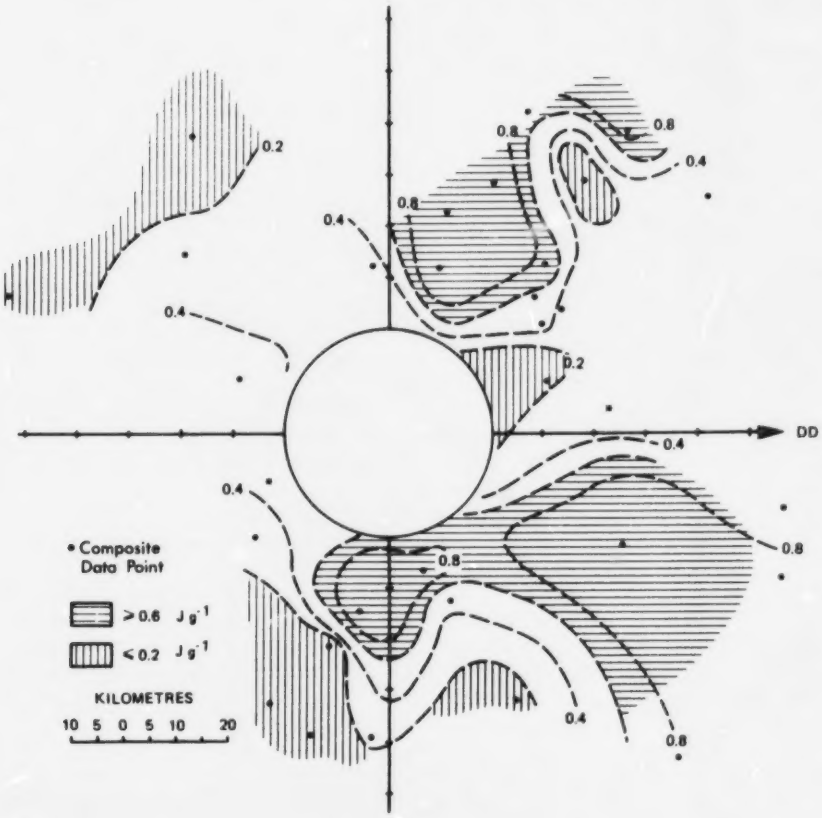

FIGURE 9. Composite parcel energy field (J g^{-1}) using 33 strong storm soundings.

TABLE 3

Parcel energies and maximum hailstone diameters in order of decreasing parcel energies. Temperatures differences, $T_p - T_m$, constrained to limits in Table 1 for all second LMA runs. Reasonable (R) and unreasonable (U) temperature differences indicated. Quadrant numbers: 1 = right front, 2 = right rear, 3 = left rear, 4 = left front.

Quadrant Number	Bearing/ Distance (km)	$T_p - T_m$ (C°)	LMA Run #1 Parcel Energy (J g^{-1})	LMA Run #1 Maximum Hail Diameter (cm)	LMA Run #2 Parcel Energy (J g^{-1})	LMA Run #2 Maximum Hail Diameter (cm)
Strong convective storm soundings (40≤dBZ≤ 60)						
1	025/50	1.4 (R)	1.69	>5.2	—	—
4	288/32	3.0 (R)	1.12	>5.2	—	—
2	099/34	1.3 (R)	1.09	>5.2	—	—
4	286/44	4.0 (U)	1.07	>5.2	1.14	>5.2
1	089/27	2.0 (R)	1.04	>5.2	—	—
4	294/52	1.4 (R)	0.96	>5.2	—	—
1	020/85	3.2 (U)	0.94	>5.2	0.93	>5.2
1	075/27	0.7 (R)	0.93	>5.2	—	—
4	309/73	2.6 (R)	0.93	>5.2	—	—
1	048/84	1.4 (R)	0.80	4.2	—	—
4	314/44	0.7 (R)	0.78	4.2	—	—
4	294/66	2.5 (R)	0.70	4.2	—	—
1	062/20	0.4 (R)	0.63	4.2	—	—
2	157/24	5.8 (U)	0.61	4.2	0.51	2.6
4	318/37	0.5 (R)	0.58	4.2	—	—
3	200/26	0.3 (R)	0.57	2.6	—	—
4	325/33	0.4 (R)	0.46	2.6	—	—
4	308/61	12.7 (U)	0.45	2.6	Base does	not fit
1	070/34	2.5 (R)	0.41	2.6	—	—
3	265/32	2.2 (R)	0.39	2.6	—	—
4	325/40	2.9 (R)	0.39	1.6	—	—
4	354/42	1.5 (R)	0.29	1.6	—	—
3	222/52	4.9 (U)	0.28	1.6	0.23	1.6
2	141/32	1.9 (R)	0.24	1.6	—	—
2	104/60	7.6 (U)	0.21	0.8	Base does	not fit
2	093/58	1.3 (R)	0.21	0.8	—	—
1	065/56	0.3 (R)	0.17	0.8	—	—
4	342/32	0.2 (R)	0.16	0.8	—	—
3	238/68	5.6 (U)	0.10	0.2	0.06	0.2
3	200/77	3.7 (R)	0.10	0.8	—	—
1	011/81	2.9 (R)	0.07	0.2	—	—
2	113/55	2.7 (R)	0.06	0.2	—	—
2	105/42	1.0 (R)	0.02	0.0	—	—
Weak convective storm soundings (20 ≤ dB ≤ 30)						
4	298/31	0.8 (R)	0.32	1.6	—	—
4	299/60	6.8 (U)	0.23	0.8	0.00	0.0
2	114/63	5.5 (U)	0.14	0.8	0.09	0.2
2	190/58	2.1 (U)	0.13	0.8	—	—
3	130/29	7.7 (U)	0.11	0.8	0.08	0.2
4	347/27	0.7 (R)	0.08	0.2	—	—
3	198/35	0.3 (R)	0.05	0.2	—	—
3	203/56	2.6 (R)	0.04	0.0	—	—
2	113/74	0.0 (R)	0.03	0.0	—	—
1	070/73	0.5 (R)	0.03	0.0	—	—
1	011/66	4.5 (U)	0.03	0.0	0.00	0.0
4	353/63	0.8 (R)	0.01	0.0	—	—
1	020/29	0.1 (R)	0.01	0.0	—	—
4	306/66	3.3 (U)	0.01	0.0	0.01	0.0
4	336/32	-0.6 (U)	0.00	0.0	0.00	0.0
1	065/42	-1.1 (U)	Base does	not fit	0.00	0.0

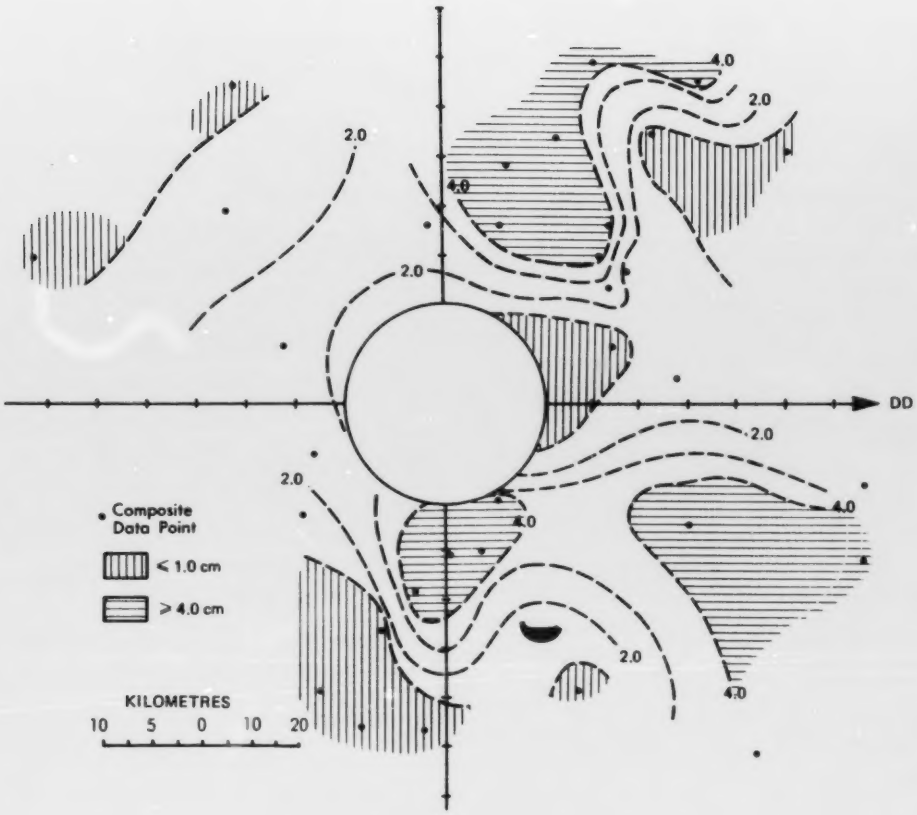

FIGURE 10. Composite maximum diameter hail field using 33 strong storm soundings. Diameters are in cm.

(4) A region of downdraft air extending several tens of kilometres behind the storm core in the low levels (Newton, 1966; Palmén and Newton, 1969). The parcel energy field in figure 9 is superimposed on these features and four distinct regions are identifiable (Fig. 11). Preferred areas for soundings are C, in the right front quadrant where inflow into the storm core originates, and D, in the left front quadrant where ambient air produces parcel energy similar to that in the main updraft. Two areas not recommended are A where downdrafts lower the parcel energy by cooling the low levels, and B where the shade of the anvil cloud lowers the parcel energy by depressing surface temperatures.

ROCKY MOUNTAIN HOUSE AREA GENESIS STUDY

In a unique study Lawford (1970) used initial bearings to lightning strikes from Alberta Forest Service observations from 1962 to 1968 to identify preferred thunderstorm formation areas. Precipitation data were not available and, consequently, he could not distinguish hailstorms from thunderstorms.

This section reports on efforts to determine why convective storms form in preferred areas in the foothills. Convective storms include thunderstorms with and without hail at the ground. It is assumed that preferred thunderstorm formation areas coincide with preferred hailstorm formation areas.

Two of the areas found by Lawford are in the Alberta foothills over elevated terrain between river valleys (Fig. 12). Hailswath climatologies confirm the preferred area southwest of Rocky Mountain House (RM) (Wojtiw, 1975; Deibert and Renick, 1975; Deibert, 1976, 1977, 1978). Low population density precludes confirmation of the area northwest of RM by this method. However, an analysis of radar data for 1969 through 1977 reveals that many echoes form northwest of RM. Preferred areas not considered are those outside the AHP operational area (Deibert, 1978).

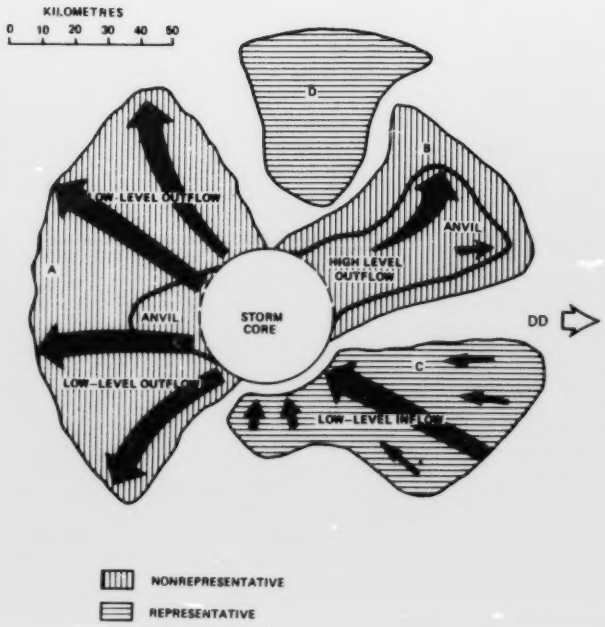

FIGURE 11. Schematic showing sounding location areas that give suitable (C and D) and unsuitable (A and B) estimates of instability in the main updraft of a strong convective storm.

Convective clouds with vertical extent sufficient to produce precipitation at the ground in or near the areas indicated in figure 12 occur often. Convergence and upward vertical motion necessary for these clouds to form must also tend to occur near these areas. A proposed sequence of events that can explain this phenomenon is shown in figures 12, 13, and 14. This sequence does not need to be triggered by the convergence and vertical motion that accompanies cyclones and fronts.

During the first phase (Fig. 12), surface[1] winds are light and variable and no fronts or cyclones are present. These conditions occur quite often during morning hours in the summer. Southeasterly or easterly surface flow in the morning causes the sequence to be completed earlier in the day. Flow in the layer somewhat above the surface and below cloud base is predominantly from the south indicative of warm air advection. Southwesterly winds at 500 mb remain nearly perpendicular to the continental divide for the entire sequence. Scattered cumulus clouds may be present during this phase.

[1]Surface in the context of this section refers to the standard level at which winds are measured for synoptic weather observations, typically about 10 metres above ground.

Southeasterly or easterly surface flow begins during phase two (Fig. 13); this is in response to solar heating of elevated terrain to the west. A gradient from high pressure in southeastern Alberta to low pressure in the lee-of-the-mountains can enhance this flow. Channelling of surface winds, an important effect in other mountainous areas (Fosberg *et al.*, 1978), and in other river valleys (Powe, 1968), is hypothesized to begin (Fig. 13). At one kilometre above the surface, the flow begins to reflect the first towering cumulus clouds. The centers of preferential development areas during this phase are displaced somewhat southwest of those for convective storms to allow for horizontal motion during the time between the towering cumulus and convective storm stages.

In the last phase (Fig. 14), the width and depth of channelled flow reaches its maximum. Convective storms are predominantly located in the preferred areas in figure 14. As the day progresses, convective storms move out of the preferred areas sometimes producing hail.

The Rocky Mountain House Area Genesis Study (RAGS) was designed to measure horizontal winds with an aircraft flying well below cloud base on a day with deep convection. The prerequisite for towering cumulus in the foothills was to guarantee aircraft measurements during phase two. Phase three, aircraft measurements were not planned because of commitments to other missions. A way to confirm flow patterns in all phases is discussed in the recommendations section.

RAGS was carried out on 9 August 1978 with the University of Wyoming Queen Air aircraft[2] supported by a network of sounding and pibal stations (Fig. 15). The aircraft flew two early afternoon low level traverses while the network made hourly releases and surface observations (Table 4). Aircraft instrumentation and operating characteristics are described elsewhere (Cooper, 1978). Soundings were tracked to 600 mb and pibals to 3 km AGL. Tracking angles were recorded every 30 seconds for more detail in the vertical.

Wind flags, selected temperatures and dewpoints at flight level and convective clouds are shown in figures 16 and 17. Aircraft winds are ten second running averages plotted for each minute. Network winds are those measured at flight level when the aircraft was closest to each station. Convective cloud nephanalyses are constructed from slides taken by an observer on the aircraft.

[2] Personnel from Wyoming instrumental in the success of the aircraft measurement portion of the experiment were J. Marwitz, scientist on board; T. Krauss, student observer on board; and W. Sand, pilot.

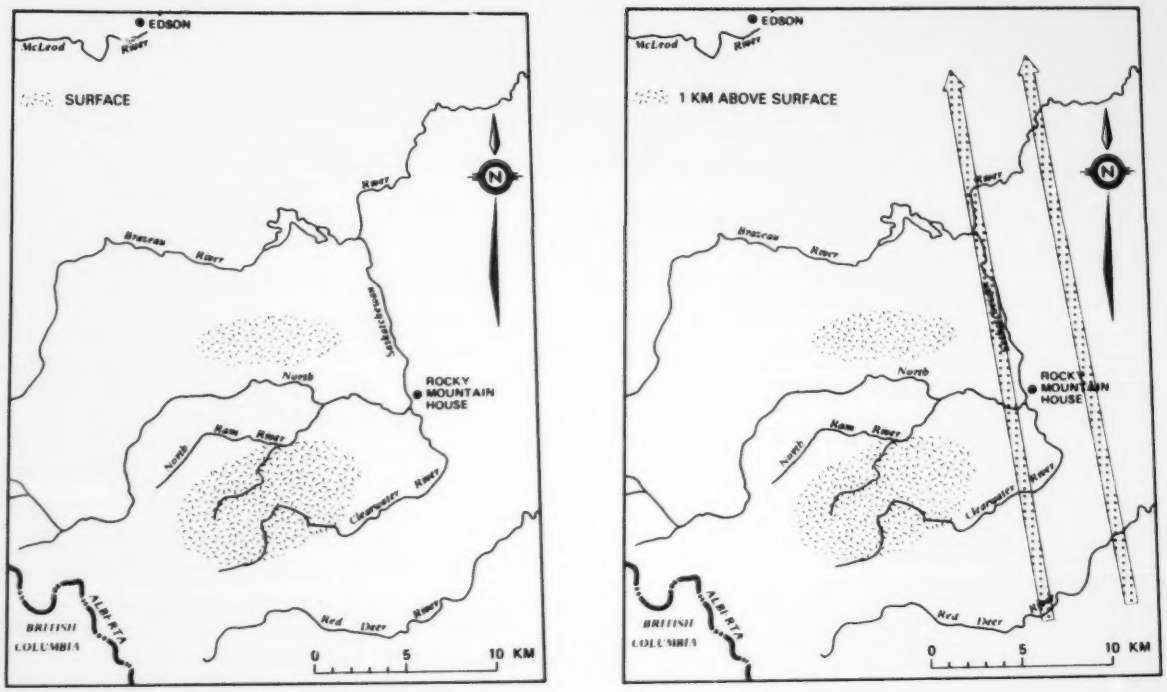

FIGURE 12. Phase one of proposed flow patterns leading to activation of thunderstorm formation areas (stippled) west of Rocky Mountain House.

TABLE 4
RAGS Calendar

TIME MDT	10	11	12	13	14	15	16	17
9/8/77								
MORAS	■	■	■	■	■	■	■	■
YRM	■	■	■	■	■	■	■	■
PIBAL 1	◆	◆	◆	◆	◆	◆	◆	◆
PIBAL 2	◆	◆	◆	◆	◆	◆	◆	◆
PIBAL 3		◆	◆	◆	◆	◆	◆	◆
A/C WYOMING			—	—	—	—		
A/C SOUNDING						▲		
S-BAND RADAR	—	—	—	—	—	—	—	—

Assuming steady flow and referencing measurements to a common surface, the complete flight is shown in figure 18. Streamlines show inflow and convergence associated with areas of towering cumulus.

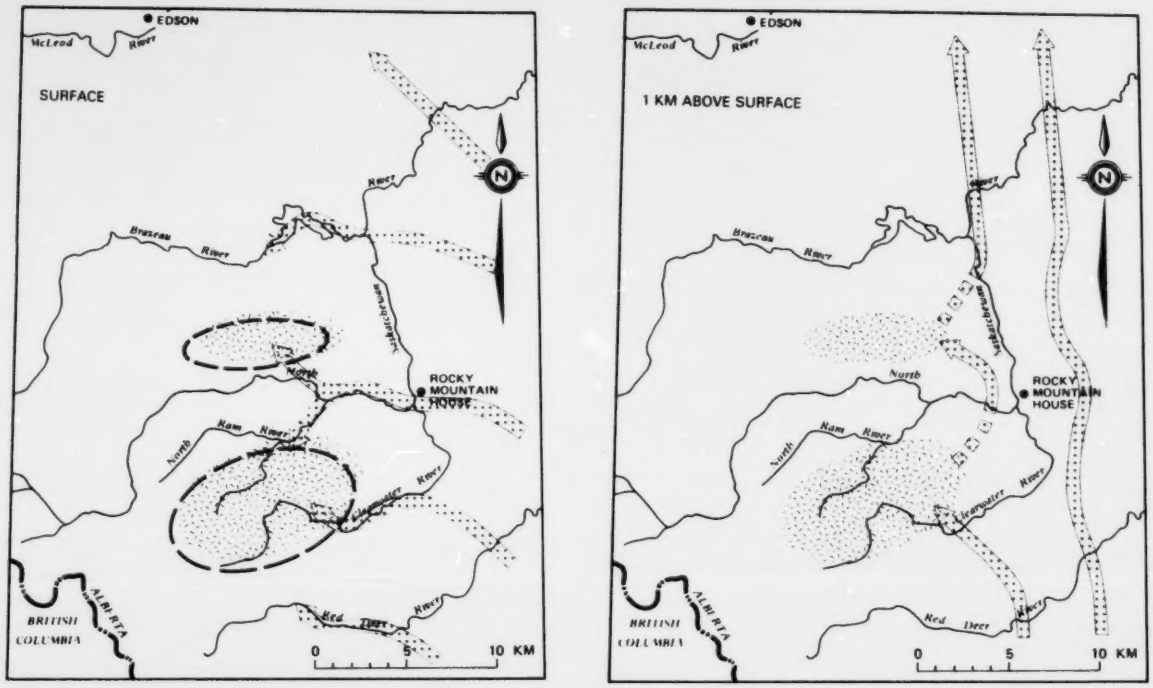

FIGURE 13. Phase two of proposed flow patterns leading to activation of thunderstorm formation areas (stippled) west of Rocky Mountain House. Dashed flow lines are to show regions where parcel motion affected substantially by vertical winds.

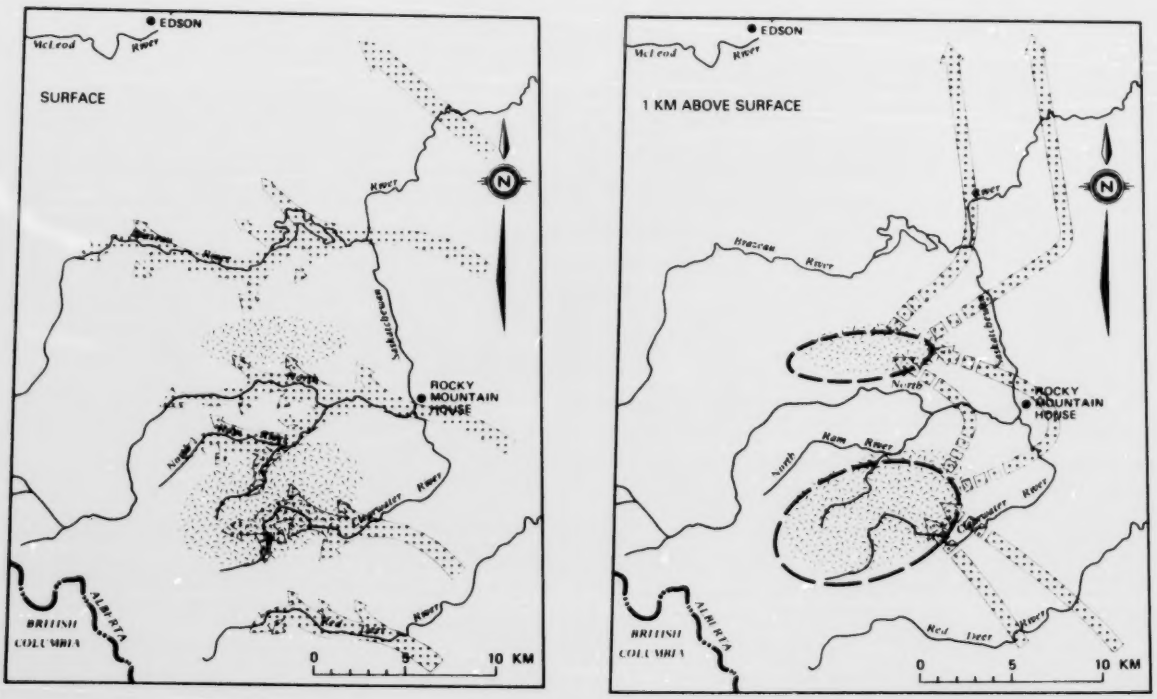

FIGURE 14. Phase three of proposed flow patterns leading to activation of thunderstorm formation areas (stippled) west of Rocky Mountain House. Dashed flow lines are to show regions where parcel motion affected substantially by vertical winds.

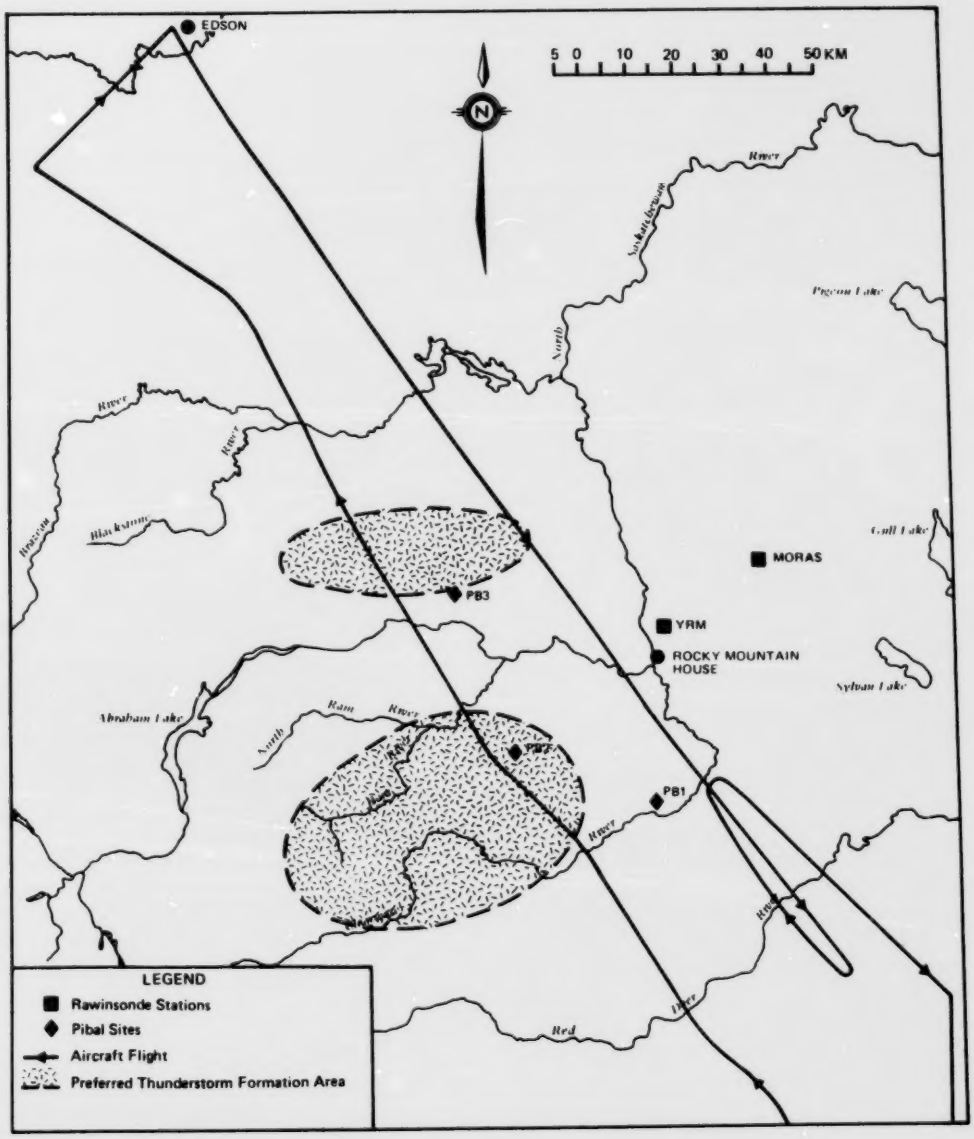

FIGURE 15. RAGS location map for 9 August 1978.

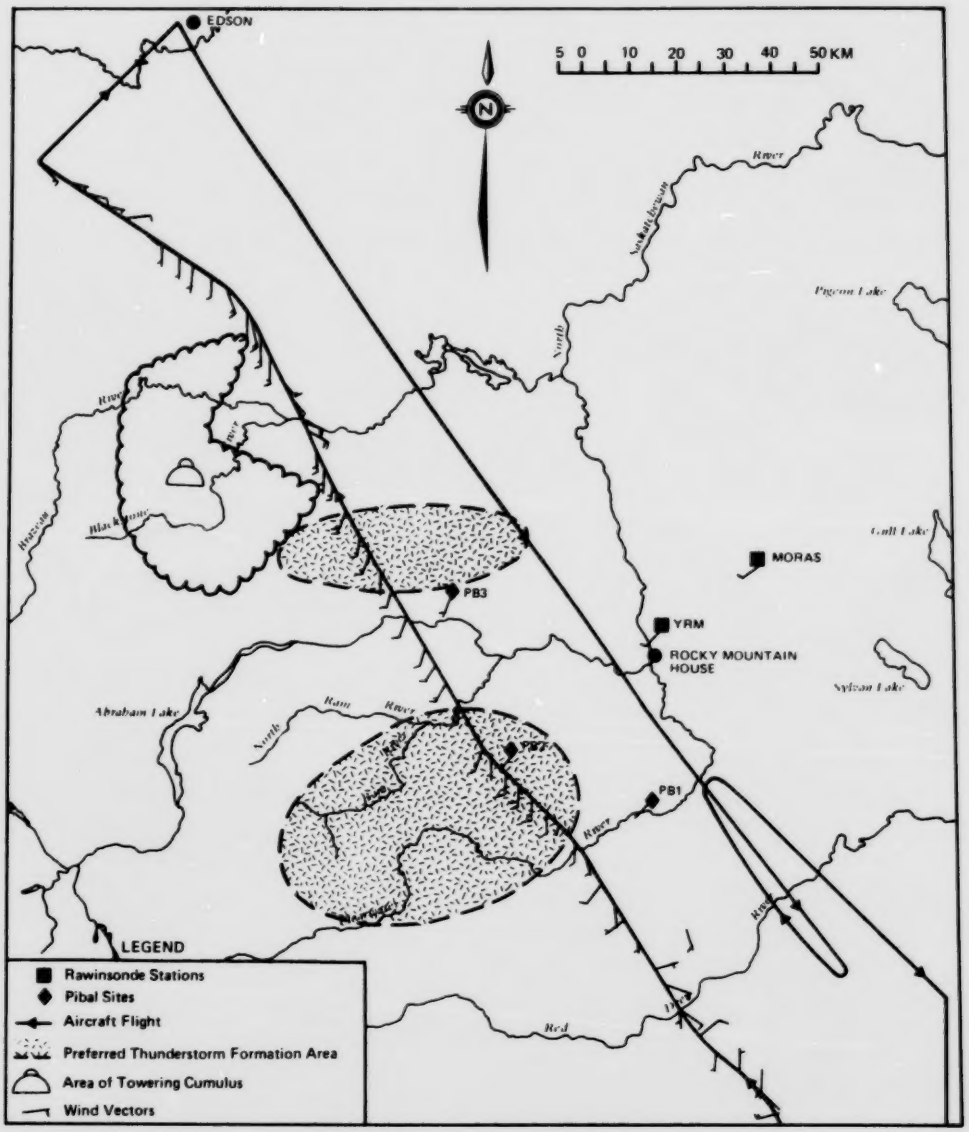

FIGURE 16. Observations for Leg #1 of RAGS experiment.

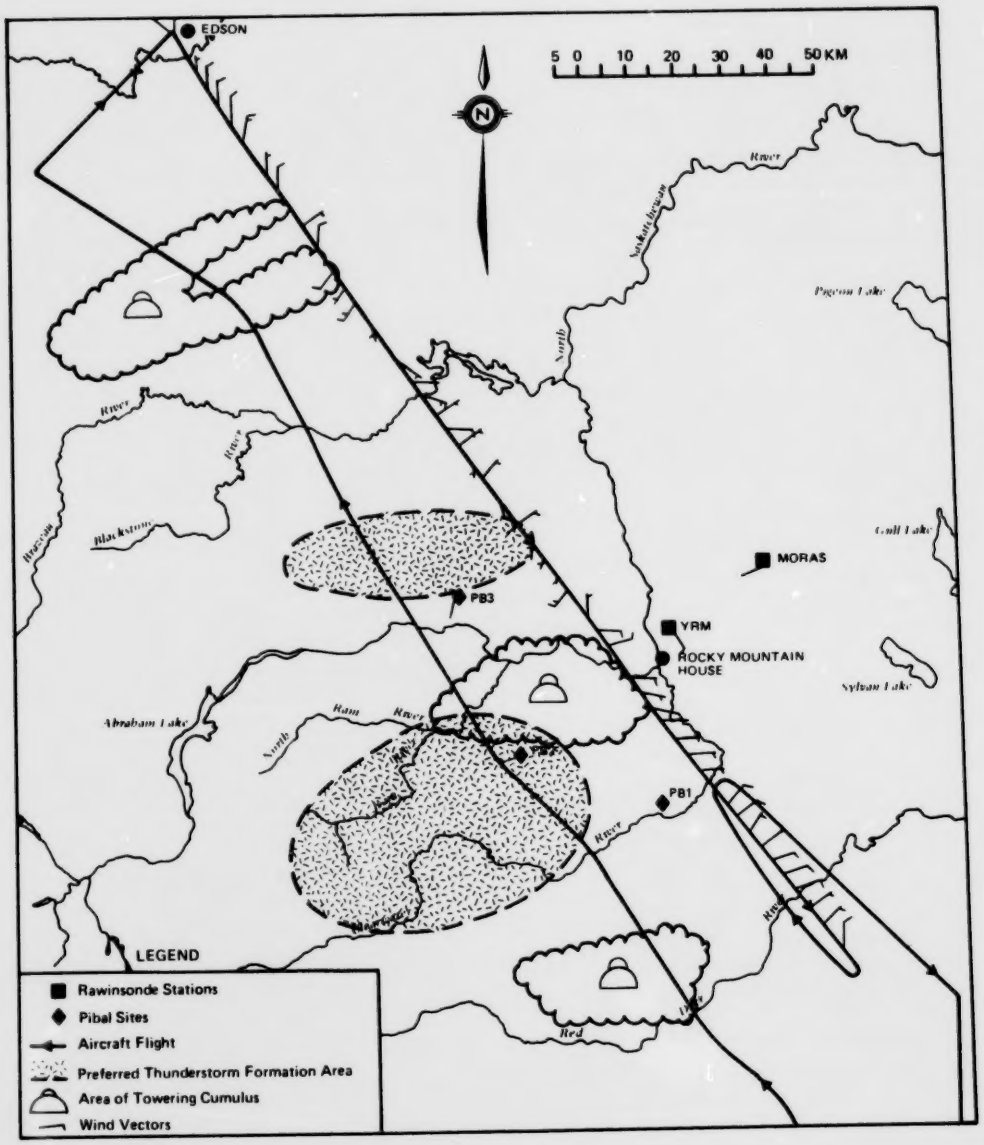

FIGURE 17. Observations for Leg #2 of RAGS experiment.

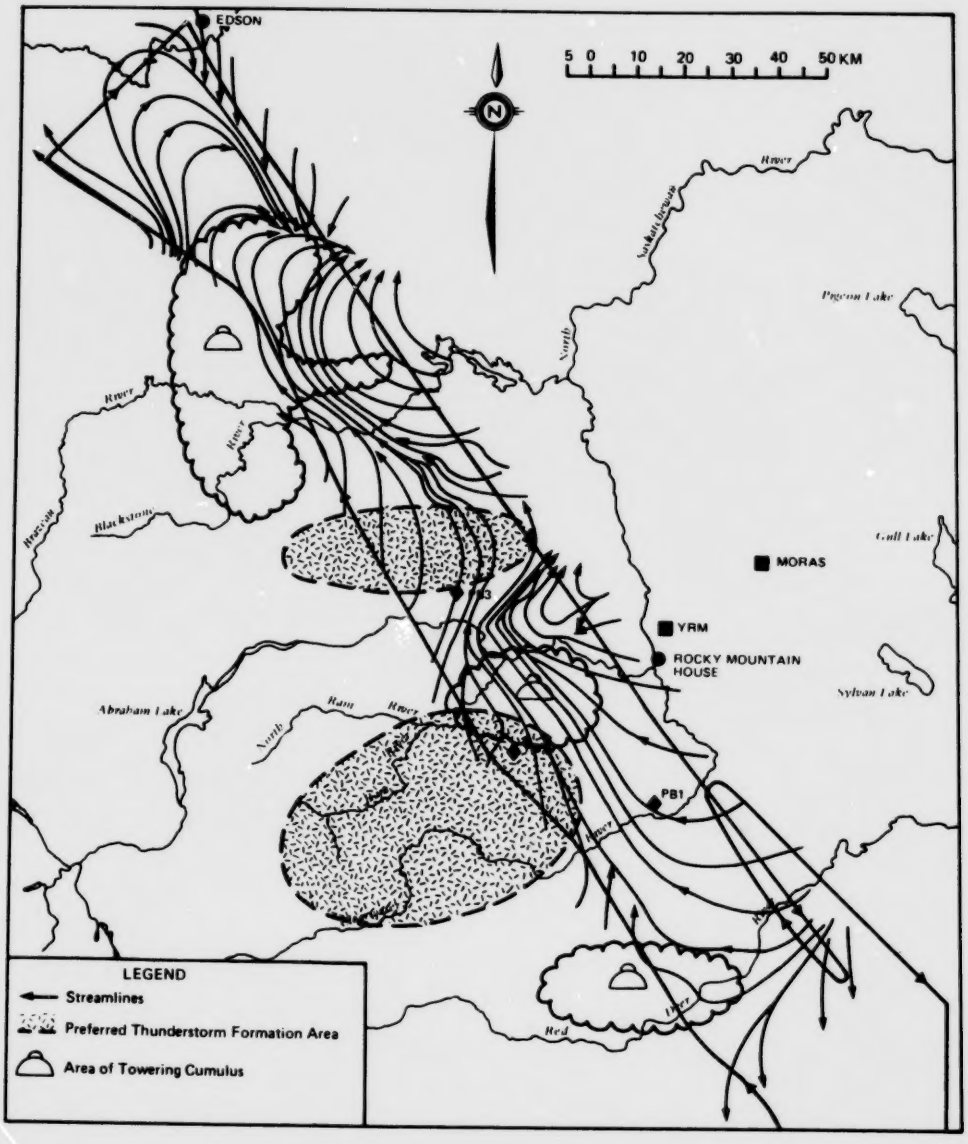

FIGURE 18. Streamlines near 200 metres above the surface in the early afternoon of 9 August 1978.

During the first traverse, towering cumulus appear near the headwaters of the Brazeau River (Fig. 16). Counter-clockwise turning of the wind along the traverse east of this region is clearly evident and may be indicative of channelling thought to begin near the surface and to increase in strength and horizontal and vertical extent as the day progresses (see Figs. 13 and 14).

Additional regions of towering cumulus appear during the second traverse (Fig. 17) west of Rocky Mountain House and near the headwaters of the Red Deer River. Inflow for both areas is from the east. The area found earlier is now subjected to flow from the north. Combining measured winds and streamline analysis, convergence on the order of $1X10^{-3}$ s^{-1} over a 25 km by 25 km square enclosing the most northerly region of towering cumulus from the ground to 300 m AGL is computed. If this convergence occurs throughout the depth of the air column up to cloud base near 3000 m AGL, vertical velocities of three to five m s^{-1} are computed. These are reasonable for the type of cloud observed.

In summary, aircraft wind measurements made during phase 2 indicate a turning of the wind due to channelling by the Brazeau River valley or due to circulations driven by the towering cumulus clouds themselves. A combination of the two factors may be in operation.

To determine if channelling precedes convective storm formation in the preferred area southwest of Rocky Mountain House, a field experiment to measure the wind at several levels in the sub-cloud layer at select points along two river valleys is suggested. This experiment is described in the recommendations section.

CONCLUSIONS

From 1975 through 1978, the Storm Environment Program participated in the AHP and operated MORAS to obtain more than 275 soundings. Comparisons with other rawinsonde stations indicated that the system performed well for a prototype (Robitaille, 1977). However, the speed of motion of convective systems limited the ability of MORAS to obtain more than one sounding in front of a particular storm.

Coordinated sounding programs involving MORAS and the fixed stations were run successfully on several days. Two days in 1975, 21 and 27 August, had serial soundings which were subjected to cross-sectional analysis. Differences in sounding structure from station to station were significant. On 21 August, a day with large hail, the conditions required for convective storm formation were easiest to find in the soundings closest in time and space to the major hailstorm.

A study of 1976 hailday soundings revealed that potential for hail production in isolated, well-developed convective storms can be estimated using soundings approximately 20 to 80 km ahead of the storms and away from the areas shaded by anvils. Soundings behind storms and underneath anvils underestimated this potential.

An experiment in 1978 revealed marked turning of the wind a few kilometres upwind of towering cumulus in the Alberta foothills. This can be reconciled with a proposed sequence of events leading to the activation of preferred thunderstorm formation areas northwest and southwest of Rocky Mountain House.

RECOMMENDATIONS

To support future programs in hail suppression, the following recommendations are made:

(1) Mobile sounding capability should be increased to produce more representative soundings during each hail season. Two additional systems could monitor the convective storm breeding grounds west of Rocky Mountain House. Both systems should have dual rear wheels, automatic tracking capabilities, heated and insulated work areas, and alternative methods of levelling.

(2) Efforts to pinpoint where soundings should be made to reasonably estimate convective storm hail production potential should be expanded. Inclusion of data from 1975, 1977, 1978, and 1979 would increase the number of types of composite storms. Changes in hail production potential during intensification and decay of convective storms could be estimated and verified by comparisons with measured hailfalls.

(3) The events in figures 12, 13, and 14 hypothesized to occur on days when preferred formation areas are active should be tested by observations. To do this, a network of pibal stations operating during convective periods in July 1979 is suggested (Fig. 19). The strength and depth of channelling by the Clearwater and Ram River valleys could be monitored and related to the onset and development of convective clouds.

(4) Development of computerized processing and analysis should include objective streamline and trajectory packages. An interactive program to identify and track first echoes is suggested. First-echo location climatologies for various meteorological conditions could be developed. The manager of a hail suppression program could refer to this climatology and deploy patrol and seeder aircraft to areas likely to be active.

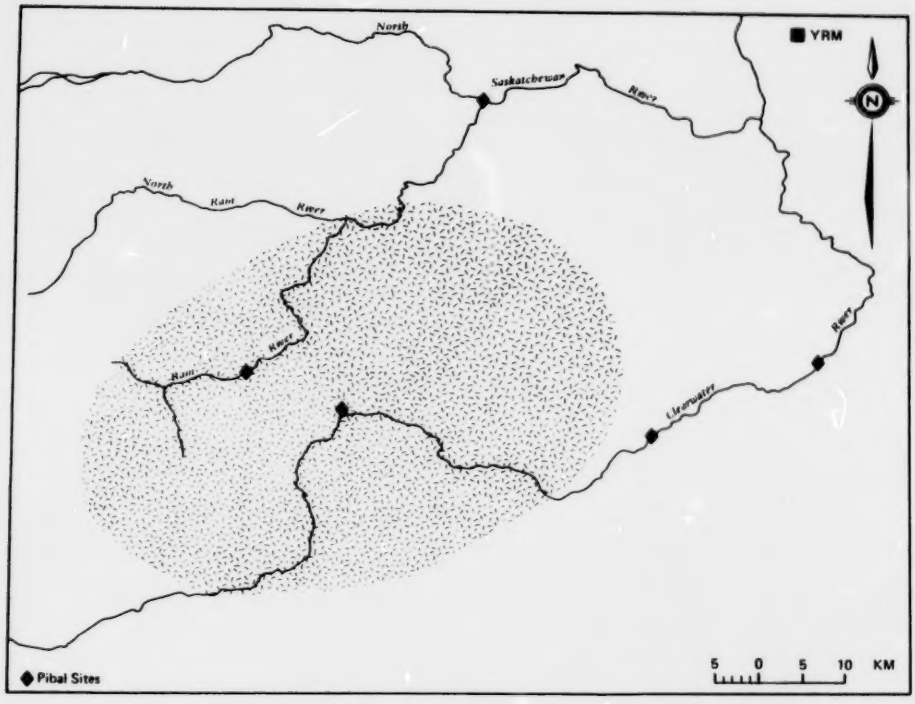

FIGURE 19. Network of wind measuring stations (shown by ◆) proposed for July 1979 to monitor river valley flow on days when thunderstorms form in stippled area.

REFERENCES

Barge, B.L. and F. Bergwall (1976): Fine-scale structure of convective storms associated with hail production; Atmospheric Sciences Report 76-2, Volume 1, Alberta Research Council, Edmonton, Alberta, 43 pages.

Barnes, S.L., J.H. Henderson and R.J. Ketchum (1971): Rawinsonde observation and processing techniques at the National Severe Storms Laboratory; NOAA Technical Memorandum ERL NSSL-53.

Browning, K.A. and F.H. Ludlam (1960): Radar analysis of thunderstorms; Technical Note No. 5, Imperial College, London, 106 pages.

_____ (1962): Airflow in convective storms; Quarterly Journal Royal Meteorology Society, 88, pages 117-135.

Browning, K.A. and R.J. Donaldson (1963): Airflow and structure of a tornadic storm; Journal of Atmospheric Sciences, 20, pages 535-545.

Browning, K.A. (1965): A family outbreak of severe local storms in Oklahoma on 26 May, 1963, Part 1, AFCRL-65-695(1); Special Report No. 32, 346 pages.

Chalon, J.P., J.C. Fankhauser and P.J. Eccles (1976): Structure of an evolving hailstorm, Part 1: General characteristics and cellular structure; National Hail Research Experiment Technical Report No. 76/1, Boulder, Colorado, 29 pages.

Chisholm, A.J. (1970): Estimate of the precipitation growth environment in the updraft core of Alberta hailstorms; preprints, Conference on Cloud Physics, Fort Collins, American Meteorological Society, Boston, pages 151-152.

_____ (1973): Alberta Hailstorms, Part 1: Radar case studies and airflow models; Meteorological Monograph No. 36, Boston, American Meteorological Society, pages 1-36.

Cooper, W.A. (1978): Cloud physics investigations by the University of Wyoming in HIPLEX 1977, Department of Atmospheric Sciences Report No. A5119, pages 42-75.

Deibert, R.J. and J.H. Renick (eds.) (1975): Alberta hail project field program 1974; Alberta Agriculture, IWMB Report 1, Three Hills, Alberta, 37 pages.

Deibert, R.J. (ed.) (1976): Alberta hail project field program 1975; Alberta Agriculture, AWMB Report 2, Three Hills, Alberta, 67 pages.

——— (1977): Alberta hail project field program 1976; Alberta Agriculture, AWMB Report 4, Three Hills, Alberta, 82 pages.

——— (1978): Alberta hail project field program 1977; Alberta Agriculture, AWMB Report 6, Three Hills, Alberta, 92 pages.

Donaldson, R.J. (1962): Radar observations of a tornado thunderstorm in vertical section; Report No. 8, National Severe Storms Project, U.S. Weather Bureau, Washington, D.C., 21 pages.

Fosberg, M.A., W.E. Marlatt and L. Krupnak (1976): Estimating airflow patterns over complex terrain; USDA Forest Service Research Paper RM-162, Fort Collins, Colorado, USA, 16 pages.

Fankhauser, J.C. and C.G. Mohr (1977): Some correlations between various sounding parameters and hailstorm characteristics in northeast Colorado; Proceedings 10th Conference on Severe Local Storms, American Meteorology Society, Omaha, Nebraska, pages 218-225.

Hammond, G.R. (1967): Study of a left-moving thunderstorm of 23 April, 1964; Technical Memoirs, No. 31, National Severe Storms Laboratory, Norman, Oklahoma.

Harley, W.S. and B.S.V. Cudbird (1969): Canadian Meteorological Memoirs, No. 19; Department of Transport, Meteorological Branch, Toronto, Ontario, Table 7.

Hudson, H.R. (1970): On the relationship between horizontal moisture convergence and convective cloud formation; ESSA Technical Memoirs, ERLTM-NSSL 45, NSSL, Norman, Oklahoma, 29 pages.

Lawford, R.G. (1970): The behavior of thunderstorms over Alberta forests; M.Sc. Thesis, Department of Geography, University of Alberta, 176 pages.

Lemon, L.R. (1977): Severe thunderstorm evolution: Its use in a new technique for radar warnings; Proceedings 10th Conference on Severe Local Storms, American Meteorological Society, Omaha, Nebraska, pages 77-80.

Maxwell, B. (1974): Meteorological Section: Alberta Hail Project Field Program 1974; Report No. 1, Interim Weather Modification Board, Alberta Agriculture, Three Hills, Alberta, 20 pages.

Marwitz, J.D. (1972): The structure and motion of severe hailstorms; Parts I, II, and III. Journal of Applied Meteorology, II, pages 166-201.

Newton, C.W. (1966): Circulations in large sheared cumulonimbus; Tellus, 18, pages 699-713.

Ninomiya, K. (1971): Mesoscale modification of synoptic situations from thunderstorm development as revealed by ATS III and aerological data; Journal of Applied Meteorology, 10, pages 1103-1121.

Palmén, E. and C.W. Newton (1969): Atmospheric Circulation Systems, Chapter 13, Convective systems in middle latitudes; Academic Press, New York and London, pages 390-425.

Powe, N.N. (1968): The influence of a broad valley on the surface winds within the valley; Department of Transport, Meteorology Branch, TEC 668, February, Toronto, 9 pages, 6 tables.

Renick, J.H. and B. Maxwell (1978): Forecasting hail in Alberta; Meteorological Monograph No. 38, Boston: American Meteorological Society, pages 145-151.

Robitaille, F.E. (1977): Development and use of a mobile rawinsonde system, Atmospheric Sciences Division Report 77-1, Alberta Research Council, Edmonton, Alberta, 25 pages.

——— (1978): An estimate of the spatial variability of instability around convective storms in Alberta; paper presented at Twelfth Annual Congress of Canadian Meteorological and Oceanographic Society, 31 May to 2 June, 1978, London, Ontario.

Sackiw, C. and F. Bergwall (1977): MObile RAwinSonde training and reference manual; Atmospheric Sciences Division Report 77-2, Alberta Research Council, Edmonton, Alberta, 37 pages.

Wilk, K., K. Gray and C. Clark (1976): Objectives and accomplishments of the NSSL 1975 Spring Program: Observational Program; NOAA Technical Memoirs ERL NSSL-78.

Wojtiw, L. (1975): Climatic summaries of hailfall in central Alberta; Atmospheric Sciences Division Report 75-1, Alberta Research Council, Edmonton, Alberta, 102 pages.

THE CLOUD MODELLING PROGRAM

M. English

B. Kochtubajda

F. Barlow

TABLE OF CONTENTS

	Page
Introduction	21
Objectives	21
The growth of hailstone embryos	21
The approach	21
Present position	22
Simple numerical cloud models as potential tools in evaluating hail suppression techniques	22
Review	22
The objective	22
The cloud model	22
The data	23
Forecast verification of maximum hailstone size	24
Forecast verification of maximum radar echo height	26
The predictors	26
Model predictors	26
Synoptic predictors	28
Seeding predictors	28
Relationships among the various predictors	28
The response variables	32
Response variables derived from hail reports	32
Response variables from radar data	33
Relationships between the response variables	33
Correlations between predictor and response variables for all storms	33
Some predictor — response relationships	35
Predictor — response pairs	35
HCTM with RMHS	35
HCTM with MRT	39
HCTM with AREA	39
HCTM with SV3	39
MAXPE with RMHS	41
MAXPE and MRT	41
MAXPE with AREA	41
MAXPE with SV3	42
PMXSZ with RMHS	42
PMXSZ with MRT	42
PMXSZ with AREA	42
PMXSZ with SV3	42
Multiple linear regressions	42
Conclusions	43
Hailstorm Climatology	43
Comparison between the storms of 1975 and those of 1976	43
Comparison between seeded and not-seeded storms	43
Distributions of reported maximum hailstone diameter	44
Storms with negative buoyancy at cloud base	45
Seeding statistics	45
Summary and Conclusions	45
The simulation of the growth of hail embryos	45
Simple numerical cloud models as potential tools in evaluating hail suppression techniques	45
Acknowledgments	47
References	47

ILLUSTRATIONS

Figure 1. Number of occurrences of each reported maximum size category for each predicted size category for all hailstorms from 1975 and 1976 23

Figure 2. Predicted maximum radar echo height plotted against measured maximum radar echo height for all storms from 1975 and 1976 26

Figure 3. Scatter diagram of HCTM (cld top ht) Versus MRT (max radar top) for all storms from 1975 and 1976 39

Figure 4. Scatter diagram of MAXPE (parcel energy) versus AREA (hailswath area) 42

Figure 5. Scatter diagram of PMXSZ (predicted max. diam.) versus RMHS (reported max. diam.) 43

TABLES

Table 1. Forecast verification of maximum hailstone size 25

Table 2. Forecast verification of maximum radar echo height 27

Table 3. Predictors from the LMA model 28

Table 4. Wind predictors 28

Table 5. Seeding predictors 28

Table 6. Correlations between predictors for all hailstorms from 1975 and 1976 30

Table 7. Response variables calculated from hail reports sent in by voluntary observers 32

Table 8. Correlations between response variables of all hailstorms from 1975 and 1976 34

Table 9. Correlations between predictors and response variables for all hailstorms from 1975 and 1976 36

Table 10. Correlations between various predictor — response pairs for not-seeded and seeded storm samples 40

Table 11. Multiple regression results 44

APPENDIX

Determining the cloud base 49

THE CLOUD MODELLING PROGRAM

M. English
B. Kochtubajda
F. Barlow

INTRODUCTION

OBJECTIVES

The cloud modelling program was started in November, 1974. At that time, two projects were identified as the top priorities for study by the Cloud Modelling Group. These two projects were:

(a) to study possible means by which numerical cloud models could assist in evaluating the hail suppression project and
(b) to simulate numerically the growth of hail embryos, both natural and artificial, in order to develop a firm theoretical foundation for cloud seeding as a means of suppressing hail and also to refine and improve seeding techniques.

Considerable effort has been devoted to both of these objectives in the past four years. The study of the use of numerical models for evaluation purposes is now virtually complete. Thus, much of this report deals with the evaluation aspect of the work done by the Cloud Modelling Group. The simulation of the growth of hail embryos is well underway, but will require considerably more time and effort to reach fruition. To a large extent, the need for actual in-cloud measurements to provide a firm foundation for the numerical model of hail embryo growth spawned the Cloud Physics Program which was started in the summer of 1978. Data from the cloud physics field experiment of August 1978 have become available only very recently. Furthermore, preliminary analyses to be done by others have not yet been completed. It is clear, therefore, that no results are yet available from the simulation of the growth of embryos study. However, a summary of the model being developed is given in the next section.

A number of peripheral problems, not covered in this report, have also been investigated during the four years of the Cloud Modelling Program. These peripheral problems will be covered in separate technical reports, but are summarized briefly here. Numerous night-time experiments on the melting of hailstones on the ground were conducted. The purpose of these experiments was to determine how much the maximum hailstone size might have decreased if the voluntary observers looked at the hail, from a night-time storm, the next morning. Another problem investigated was to compare cloud-base temperatures and heights from some aircraft observations, made between 1968 and 1970, to those determined from surface temperatures and dew points. Also, some calculations of the dispersion of AgI from cloud-base seeding were made to determine optimum seeding locations. Considerable time was also spent in extracting data to determine other response variables.

THE GROWTH OF HAILSTONE EMBRYOS

The Approach

In simulating the growth of hailstone embryos, an approach very similar to that of English (1973) (who simulated the growth of hailstones from the embryo stage) is being followed. This entails the use of an empirical cloud model to provide the details of the environment in which the embryos grow from some initial stage. The growth of the embryos is then calculated using very detailed theoretical microphysics. The model presently in use is two-dimensional, the two dimensions being height and horizontal distance, and time-dependent. This approach has the disadvantage of not allowing any interactions between the dynamics and the microphysics. But a hybrid model of this type requires much less computer time and ensures that the dynamic framework is reasonable. Models of the purely theoretical type often do not reproduce the dynamics of clouds very well. Working in two dimensions rather than three is a further limitation, but it is a necessary restriction if computer time is to be kept to reasonable limits.

The empirical cloud model used by English (1973) was derived mainly from radar and cloud-photography data. However, the new growth zone, where hailstone embryos are believed to originate (Barge and Bergwall, 1976) is not radar detectable. Thus, some problems were encountered in deriving a reasonable dynamic framework for the growth of hailstone embryos.

As a starting point for calculating the growth of hailstones, English (1973) assumed the existence of hailstone embryos at various reasonable locations. The size, nature, and density of these hailstone embryos were fairly well known from thin sections of hailstones collected on the ground. No similar information can be obtained about the origin of hailstone embryos (the "embryos" of the embryo) from hailstones collected on the ground. Thus, further problems were encountered in finding a reasonable starting point for the simulation of the growth of hailstone embryos.

It seemed obvious, then, that in order to derive a reasonable dynamical framework and a reasonable starting point for calculating the growth of embryos, measurements inside the new growth zone were necessary. Others were also interested in measurements inside the new growth zone of hailstorms, chiefly to confirm Barge and Bergwall's (1976) conclusions that hail growth starts in the new growth zone. Thus, the "Cloud Physics Research Aircraft Program" was initiated in 1978. (For further details on this program, see English *et al.*, 1980).

Present Position

The theoretical model for the treatment of the microphysical processes is complete. Measurements made in August 1978 for the "Cloud Physics Research Aircraft Program" will provide the dynamic framework and the starting point for the calculations. It is to be expected that the required empirical model will be available before the end of 1980. The cloud-physics data will likely be useful also in testing and fine-tuning the eventual model for the simulation of the growth of hail embryos.

SIMPLE NUMERICAL CLOUD MODELS AS POTENTIAL TOOLS IN EVALUATING HAIL SUPPRESSION TECHNIQUES

REVIEW

The Objective

To evaluate a hail suppression project, it is necessary to compare two samples of data, one for natural storms and one for treated storms. Judging from the results of Warner (1976) and Wong (1977) it appears likely that any possible effects due to treatment would be considerably smaller than the natural variation in the hailfall. Thus, some means must be found for taking the natural variation into account. Randomly choosing storms to be treated over a long period of time is a method often used. However, because of the many years of data required to reach a statistically significant result for a randomized experiment, it is highly desirable to find some "predictor" variables, or covariates, to explain some of the natural variability and thus reduce the noise level. Good predictor variables can dramatically reduce the sample size required to detect a treatment effect. Flueck and Mielke (1977) suggest that a correlation coefficient, obtained from a regression of response on predictor variables, of 0.1 to 0.3 would be of minor help, of 0.4 to 0.6 of major help, and of 0.7 or better of enormous help in detecting a treatment effect. (Response variables are measurements of the hail produced.) Accordingly, some simple cloud models have been studied with a view to determining a few predictor variables to be used in evaluating a hail suppression project.

The intent of this study can be said to have been to identify a number of useful predictor variables and to develop relationships between these predictor variables and some response variables. In particular, simple linear regression models and more complex multiple linear regression models have been developed for not-seeded and seeded storms. For the simpler relationships, apparent differences between not-seeded and seeded storms have been tested for statistical significance.

The Cloud Model

For this study, the cloud models must necessarily be simple since a statistical evaluation requires doing exactly the same thing many times. During the summer of 1975, the Alberta Hail Project utilized two steady-state, one-dimensional cloud models routinely to assist the forecaster with his daily forecast. The two models were the Loaded Moist Adiabatic (LMA) model and the Hirsch model. The LMA model (Chisholm, 1970) was used on the project as a forecasting tool from about 1970 to 1976 and is simply parcel theory with water loading taken into account. Combined with the Maxwell nomogram (Renick and Maxwell, 1977), it can predict the category of the maximum hail size. The Hirsch model is somewhat more plausible, physically, than the LMA model since it takes entrainment into account and also includes some microphysics, although in a very simple form (Hirsch, 1971). English (1976) found that, as an operational forecasting tool, both models proved unreliable chiefly due to frequent difficulties in estimating the required afternoon temperature and moisture conditions. However, when reliable input data were used, both the Hirsch model and the LMA model were found to predict maximum hailstone size and maximum storm top quite well. Correlation coefficients between model predictions and observations seemed to be quite similar for both models. However, the Hirsch model seemed to be a little more sensitive to the quality of the input data than the LMA model. This may be due to the fact that the Hirsch model requires an additional input parameter, namely the radius of the updraft region. For this reason, the LMA model was used exclusively in all subsequent work.

The LMA model requires only a temperature and humidity sounding, representative of the storm environment, and some fairly accurately determined cloud-base parameters as input. These input parameters can be measured prior to seeding and are not expected to be affected by seeding. Thus, results from the LMA model could serve as predictors of the natural ability of a storm to produce hail.

Since cloud-base temperatures and heights are not routinely measured for all storms occurring in the Alberta Hail Project Area, these input parameters were obtained indirectly. The various methods used to obtain these parameters are described in Appendix 1. For all results presented in this report, cloud-base temperatures and

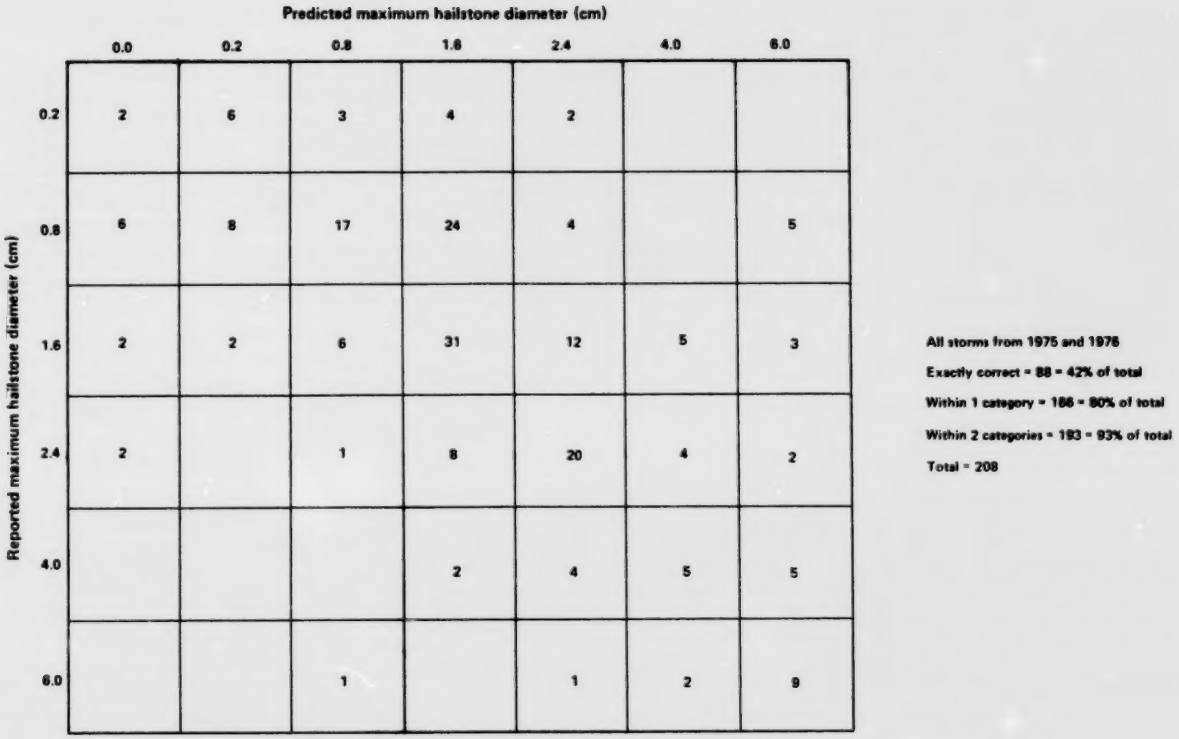

FIGURE 1. Number of occurrences of each reported maximum size category for each predicted size category for ALL HAILSTORMS FROM 1975 and 1976. Maximum hail size is reported in terms of familiar objects; shot, pea, grape, walnut, golfball or larger than golfball. The mean diameter for each size category, from Wojtiw (1975) is shown. Model predictions are exactly correct for 88 out of the 208 storms (42 percent of total), within one size category for 166 storms (80 percent) and within two size categories for 193 storms (93 percent).

heights were determined from surface temperatures and dewpoint temperatures.

The Data

Data collected during the summers of 1975 and 1976 by the Alberta Hail Project were used. From radar and hail card data (the latter being obtained from voluntary observers) all hailstorms[1] that occurred in the project area were identified. Then, the best available sounding was chosen for each storm. Within the project area (about 48,000 km^2) there are three fixed stations where two temperature, humidity, and wind soundings are taken routinely each day. In addition, a mobile rawinsonde unit can take additional soundings. "Representative" soundings were available for only about one quarter of the storms.[2] Cloud-base temperatures and heights were obtained from subjectively interpolated hourly surface temperatures and dew points. Only six stations are located in the project area where surface temperatures and dew points are recorded every hour. As nearly as was possible, the surface temperature and dew point used were those appropriate to the location of the maximum development of the storm (as judged from radar data), and at a time of about one half hour before that maximum development.

1 A hailstorm is defined as any storm to which one or more hail reports could be attributed. A storm is defined by its radar echo envelope, in particular, by the minimum detectable signal envelope which is approximately 20 dBZ. Any distinct echo was labelled as a separate storm. However, if two echoes merged, the two storms together were treated as a single storm.

2 A "representative" sounding is one taken 20 to 80 km in front of the storm and removed from the area shaded by the anvil (see Robitaille *et al.*, 1979) and taken less than two hours ahead of the storm.

A total of fourteen potential predictor variables were extracted from the model results for each storm. In addition, four predictor variables were calculated from the wind hodographs, since wind speed and direction are thought to be important factors in hailstorm development (Chisholm and Renick, 1972).

The storms were classified as seeded or not-seeded. Any storm into which one or more flares was dropped or under which one or more flares was burnt was classified as a seeded storm. Although in 1975 and 1976 the project area was divided into a randomized seeding area (the north) and an operational seeding area (the south), all storms from both areas were included in the data sample. Numerous seeding parameters, designed to bring to light differences in seeding techniques, have also been calculated for all seeded storms.

Lastly, as many as 17 response variables (actual measures of the hailfall produced by a storm or storm characteristics) were calculated, mostly from the hail card data. Only the maximum radar echo height was obtained from radar data. Hopefully, more accurate measures of hailfall will become available in the future.

The bulk of this voluminous data base is documented in Kochtubajda and English (1980); the predictor and response variables for each storm are listed in Barlow *et al.* (1980).

FORECAST VERIFICATION OF MAXIMUM HAILSTONE SIZE

Figure 1 shows how well the LMA model, combined with the Maxwell nomogram (Renick and Maxwell, 1977), can predict the maximum size of hailstones produced by a storm. The fact that, for 80 percent of the storms, the predicted maximum hailstone size is within one category of the reported maximum hailstone size suggests that at the very least, predicted maximum hailstone size could be used to stratify data for a statistical evaluation.

However, for a number of storms, the predicted maximum hailstone size is very different from the reported maximum size. A close inspection of these "outlier" storms shows that all the storms for which maximum hailstone size is grossly underpredicted were night-time storms while many of the storms for which maximum hailstone size is grossly overpredicted were "in-the-mountains" storms.

Chisholm (private communication) suggested that, often, at night, a very shallow inversion is set up and that night-time hailstorms actually feed from the warmer air at the top of the inversion rather than from the colder surface air. Little information is available on the vertical distribution of temperature in Alberta. However, the CBC Edmonton Tower does have temperature sensors at two heights, one at 33 ft above ground, the other at 300 ft above ground. A perusal of these temperature records shows that on many of the days on which night-time storms occurred in the project area, the temperature at 300 ft was warmer than that at 33 ft for most of the night. A list was made of the first hour on each day when the 300 ft temperature was warmer than the 33 ft one. This list suggests that an inversion can set in as early as 1700 MDT, but the average time for an inversion to set in is about 2000 MDT. Data from a Calgary Tower were also examined, but this tower is apparently located in a depression and so would not be representative of the plains. In any case, the average time of onset of an inversion seemed to be about an hour later than at the Edmonton tower.

In the mountains, there are few observers to report hailstone size. Thus the reported maximum hailstone size may be underestimated considerably.

Table 1 shows the data of figure 1 separated into various subsets. From table 1, it is apparent that maximum hailstone size is predicted somewhat more accurately for the storms of 1975 than for those of 1976. One reason for this may be that there are more "outliers" in the 1976 data than in the 1975 data.

English (1976) showed that the accuracy with which the maximum hailstone size of a storm could be predicted was considerably improved when "a representative sounding" was used as input into the model. Data presented in table 1 is consistent with this finding. However, the sample sizes are reduced to one quarter of the original samples.

The lack of accuracy in the data used as input into the model is not the only factor responsible for large discrepancies between predicted and reported maximum size. Obviously, the error in the reported maximum size can be appreciable also. The reported maximum size is an estimated value derived by considering only small samples of the hailfall from a storm. To assess the possible magnitude of the error due to these factors, all storms which produced less than five hail reports from the voluntary observers were deleted from the data sample. From table 1, it is apparent that the accuracy of the predictions is improved slightly by dropping from the sample all the storms with less than five hail reports. Combining this restriction with that of a representative sounding leads to extremely small sample sizes and to no further improvement of the agreement between predictions and observations.

It is conceivable that some of the apparent difference between predicted and reported maximum hail size is due to seeding effects. The data in table 1 shows that not only is the agreement between predicted and reported maximum size slightly worse for the not-seeded-storms sample than for the all-storms sample, but also that most of the "outliers" are in the not-seeded sample. This is not surprising. Most of the "outliers" have been shown to pertain to storms that occurred at night or that occurred in

TABLE 1
Forecast Verification of Maximum Hailstone Size

Sample number	Sample	Number of storms in sample	% of storms for which predicted and observed max size are identical	% of storms for which predicted and observed max size are within 1 category	% of storms for which predicted and observed max size are within 2 categories	Number of outliers
1	All hailstorms from 1975 + 1976	208	42	80	93	15
2	All hailstorms from 1976	109	32	74	91	10
3	All hailstorms from 1975	99	54	86	95	5
4	All hailstorms from 1975 and 1976 with representative soundings	46	46	89	96	2
5	All hailstorms from 1976 with representative soundings	24	50	75	92	2
6	All hailstorms from 1975 with representative soundings	22	41	100		
7	All hailstorms from 1976 and 1975 with 5 or more hail reports	117	47	85	97	4
8	All hailstorms from 1976 with 5 or more hail reports	56	36	82	96	2
9	All hailstorms from 1975 with 5 or more hail reports	61	57	89	97	2
10	All hailstorms from 1976 and 1975 with representative soundings and 5 or more hail reports	25	44	88	100	
11	All hailstorms from 1976 with representative soundings and 5 or more hail reports	14	43	79	100	
12	All hailstorms from 1975 with representative soundings and 5 or more hail reports	11	45	100		
13	All not-seeded hailstorms from 1975 and 1976	106	39	76	88	13
14	All not-seeded hailstorms from 1976	64	31	70	84	10
15	All not-seeded hailstorms from 1975	42	50	86	93	3
16	All not-seeded hailstorms from 1975 and 1976 with representative soundings	22	59	82	91	2
17	All not-seeded hailstorms from 1976 with representative soundings	14	64	71	86	2
18	All not-seeded hailstorms from 1975 with representative soundings	8	50	100		
19	All not-seeded hailstorms from 1975 and 1976 with 5 or more hail reports	51	43	88	94	3
20	All not-seeded hailstorms from 1976 with 5 or more hail reports	30	37	87	93	2
21	All not-seeded hailstorms from 1975 with 5 or more hail reports	21	52	90	95	1
22	All not-seeded hailstorms from 1975 and 1976 with representative soundings and 5 or more hail reports	8	63	88	100	
23	All seeded hailstorms from 1975 and 1976	102	46	83	98	2
24	All seeded hailstorms from 1976	45	33	80	100	
25	All seeded hailstorms from 1975	57	56	86	96	2
26	All seeded hailstorms from 1975 and 1976 with representative soundings	25	32	92	100	
27	All seeded hailstorms from 1976 with representative soundings	10	30	80	100	
28	All seeded hailstorms from 1975 with representative soundings	15	30	100		
29	All seeded hailstorms from 1975 and 1976 with 5 or more hail reports	66	50	83	98	1
30	All seeded hailstorms from 1976 with 5 or more hail reports	26	35	77	100	
31	All seeded hailstorms from 1975 with 5 or more hail reports	40	60	88	98	1
32	All seeded storms from 1975 and 1976 with representative soundings and 5 or more hail reports	17	35	88	100	

the mountains. Such storms are not likely to be seeded. Furthermore, predictions of maximum size are somewhat more accurate for the not-seeded storms of 1975 than for the not-seeded storms from 1976. Again, the 1976 not-seeded storms sample contain many more "outliers" than does the 1975 not-seeded storms sample.

It is interesting to note that the difference in forecast verification for 1975 and 1976 storms is not as marked for the seeded-storms samples as it is for the not-seeded storms samples. Note that the seeded storm sample for 1975 contains two outliers, whereas the seeded storm sample for 1976 contains no outliers.

FORECAST VERIFICATION OF MAXIMUM RADAR ECHO HEIGHT

Chisholm (1973) found that the LMA model gave radar echo tops (defined as the height where the calculated updraft speed decreases to 10 ms^{-1}) that agreed within ± 0.8 km with the radar storm tops in 75 percent of the cases he analyzed. However, Chisholm analyzed only relatively large hailstorms, that is, those that occurred on days when twenty or more hail reports were received for the project area from the voluntary observers.

The agreement shown in figure 2 between predicted radar echo top (HETM) and measured maximum radar echo height (MRT) is not that good. The predicted and measured radar echo top are within 2 km for 77 percent of the storms. The probable errors in MRT likely would be a maximum of about 1½ km and an average of about ± 1 km. Allowing for some error in the predicted radar echo top, a difference of 2 to 3 km between the predicted and measured radar echo top is not unreasonable. There are twelve storms for which the difference between predicted and measured radar echo top is greater than 3.0 km.

It is interesting to compare the "maximum size outliers" with the "maximum radar echo height outliers". No value for MRT could be determined for all of the storms for which the maximum hailstone size was grossly underpredicted. Reasons for this would be that the storm occurred after the radar data logging had been terminated, or the storm spent most of its lifetime in the vicinity of the radar site, or some problem was encountered with the radar data. All the storms for which the maximum hailstone size was grossly overpredicted, show a positive value, greater than one for HETM-MRT, indicating that the maximum radar echo height is also overpredicted for these storms.

It is obvious from figure 2 that the LMA model tends to overpredict maximum radar echo height. This may be due to the manner in which the cloud base was determined.

The data in figure 2 are separated into a number of subsets in table 2. From table 2 it is apparent that there is little difference in the accuracy with which maximum radar echo height is predicted for the storms of 1975 and those of 1976. It is also apparent that no consistent improvement in forecast verification is obtained by using only storms with representative soundings.

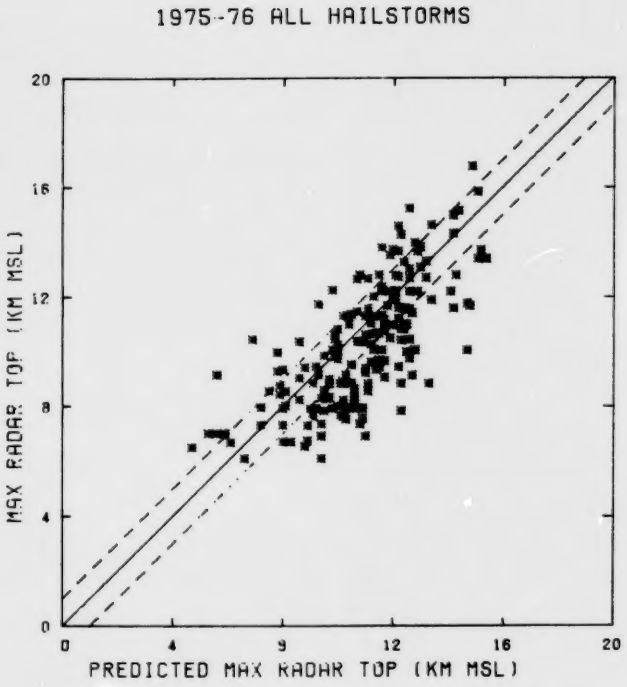

FIGURE 2. Predicted maximum radar echo height plotted against measured maximum radar echo height for all storms from 1975 and 1976. Predicted and measured maximum echo height are within 1 km for 83 of the 185 storms (45 percent), within 2 km for 142 (77 percent) of the storms and within 3 km for 174 (94 percent) of the storms.

The work of Goyer (1975) suggests that seeding may affect the radar echo height. A possibility of dynamic seeding effects in hailstorms has also been suggested by others. However, the data in table 2 suggest that the forecast verification for maximum radar echo height seems to be just a little worse for the not-seeded storms sample than for the all-storms sample.

THE PREDICTORS

Model Predictors

A number of parameters have been extracted from the LMA model results to be used as predictors. They are listed in table 3. PMXSZ, the predicted maximum hailstone size, is actually obtained by using the LMA model in combination with the Maxwell nomogram (Renick and Maxwell, 1977). This nomogram gives hailstone size in terms of six size categories, from MAXU and TMAXU, two parameters obtained from the LMA model. The size categories are shot, pea, grape, walnut, golfball, and larger

TABLE 2
Forecast Verification of Maximum Radar Echo Height

Sample number	Sample	Number of storms in sample	% of storms for which predicted and observed max radar echo height are within 1 km	% of storms for which predicted and observed max radar echo height are within 2 km	% of storms for which predicted and observed max radar echo height are within 3 km	Number of outliers
1	All hailstorms from 1975 and 1976	185	45	77	94	12
2	All hailstorms from 1976	98	45	77	93	7
3	All hailstorms from 1975	87	45	75	94	5
4	All hailstorms from 1975 and 1976 with representative soundings	46	46	80	98	1
5	All hailstorms from 1976 with representative soundings	23	39	74	100	
6	All hailstorms from 1975 with representative soundings	23	52	87	96	1
7	All not-seeded hailstorms from 1975 and 1976	87	41	77	91	8
8	All not-seeded hailstorms from 1976	55	44	73	89	6
9	All not-seeded hailstorms from 1975	32	38	84	94	2
10	All not-seeded hailstorms from 1975 and 1976 with representative soundings	21	38	67	95	1
11	All not-seeded hailstorms from 1976 with representative soundings	13	46	62	100	
12	All not-seeded hailstorms from 1975 with representative soundings	8	25	75	88	1
13	All seeded hailstorms from 1975 and 1976	98	45	77	96	4
14	All seeded hailstorms from 1976	43	47	86	98	1
15	All seeded hailstorms from 1975	55	44	69	95	3
16	All seeded hailstorms from 1975 and 1976 with representative soundings	25	52	92	100	
17	All seeded hailstorms from 1976 with representative soundings	10	30	90	100	
18	All seeded hailstorms from 1975 with representative soundings	15	67	93	100	

TABLE 3
Predictors from the LMA Model

Symbol	Description	Units
PCB	Pressure at cloud base	mb
HCB	Height at cloud base	km MSL
TCB	Temperature at cloud base	C
HCTM	Height of cloud top; the height where the calculated updraft speed has decreased to 0	km MSL
HETM	Height of the radar echo top; the height where the calculated updraft speed has decreased to 10 ms^{-1}	km MSL
MAXU	Maximum updraft speed	ms^{-1}
TMAXU	Temperature at the level where the updraft speed is a maximum	C
MAXLWC	Maximum liquid water content	gm^{-3}
MAXPE	Maximum potential energy	Jg^{-1}
MAXLWCPE	Maximum liquid water content multiplied by the maximum potential energy	$J(g\ of\ water)(g\ of\ air)^{-1}m^{-3}$
THETAE	Equivalent potential temperature	K
CLDPT	Cloud depth	km
HFZL	Height of freezing level in cloud	km MSL
PMXSZ	Predicted maximum hailstone size	cm

than golfball. These size categories have been converted to hailstone diameters by assigning a mean diameter to each category. The mean diameters used in this study are based on Wojtiw (1975) and are as follows: shot = 0.2 cm, pea = 0.8 cm, grape = 1.6 cm, walnut = 2.4 cm. golfball = 4.0 cm, larger than golfball = 6.0 cm.

The various parameters from the LMA model listed in table 3 are obviously all related to each other to some extent. The relationships between these model "predictors" are discussed in a later section.

Synoptic Predictors

A number of studies have found that storms, occurring on days with appreciable wind shear in the vertical, exhibit greater organization and persistence than those forming in weakly sheared regions (Newton, 1966; Marwitz, 1972; Chisholm and Renick, 1972). Thus a number of wind parameters have been calculated to be used as supplementary predictors. These "wind predictors" are listed in table 4.

Seeding Predictors

Assuming that there is a detectable seeding effect, the magnitude of the effect should be dependent upon the amount of AgI expended on the storm, or the rate of AgI dispersion and possibly also upon the method by which the AgI was dispensed (that is cloud-top versus cloud-base seeding). Thus a large number of seeding predictors have been calculated so that any, or all, such effects can be detected. The seeding predictors are listed in table 5.

TABLE 4
Wind Predictors

Symbol	Description	Units
WSCL	Horizontal wind speed in sub-cloud layer	ms^{-1}
DSCL	Directional wind shear in sub-cloud layer	deg m^{-1}
WSSCL	Horizontal wind speed shear in cloud layer	s^{-1}
WMCL	Horizontal wind in mid-cloud layer	ms^{-1}

Relationships Among the Various Predictors

In order to determine the degree to which these various predictors are related to one another, correlation coefficients have been calculated for all possible pairs of predictors. As a precaution, distributions were drawn for all the predictors. These distributions showed that few of the predictors were normally distributed, at least not according to the samples on hand. To test for the statistical significance of the usual product-moment correlation coefficient, the distribution of the parameters must be known; a normal distribution is generally assumed in the readily available statistical programming packages. But since the predictors (nor the response variables for that matter) were not normally distributed both the Spear-

TABLE 5
Seeding Predictors

Symbol	Description	Units
CTF	Number of cloud-top flares	
TCTF	Time of cloud-top seeding	s
RCTF	Rate of cloud-top seeding	flares s^{-1}
GCTF	Total grams of AgI dispensed by cloud-top seeding	g
RGCTF	Rate of AgI dispensed by cloud-top seeding	gs^{-1}
CBF	Number of cloud-base flares	
TCBF	Time of cloud-base seeding	s
RCBF	Rate of cloud-base seeding	flares s^{-1}
GCBF	Total grams of AgI dispensed by cloud-base seeding	g
RGCBF	Rate of AgI dispensed by cloud-base seeding	gs^{-1}
TGFL	Total amount of AgI dispensed by both cloud-top and cloud-base seeding	g
RGTFL	Rate of AgI dispensed for both cloud-top and cloud-base seeding; RGCTF + RGCBF	gs^{-1}
TIME	Total time of seeding run	s
R2FL	Rate of AgI dispensed for total seeding run; TGFL/TIME	gs^{-1}

man's rank and the usual product-moment correlation coefficients were calculated for all pairs. To test for statistical significance of the Spearman's rank correlation coefficient, no distribution is assumed. Thus the Spearman's rank correlation coefficient has been used to determine whether or not a relationship exists between two parameters. In table 6, pairs of parameters are ranked according to their Spearman's rank correlation coefficient. Data is entered in table 6 only for those pairs of predictors for which the Spearman's rank correlation coefficient is statistically significant at the 10 percent level or better. As a matter of fact, correlation coefficients significant only at the 5 to 10 percent level are indicated by an asterisk. All Spearman's rank correlation coefficients without asterisks are significant at the 5 percent level or better. The second number for each pair of parameters in table 6 gives the corresponding product-moment correlation coefficient. The third number shows the number of storms used to calculate the correlation coefficient. (Any storm for which the value of either parameter is missing, or equal to zero, is deleted from the sample.)

Consider first the model predictors. It is gratifying to note that, in most cases, the Spearman's rank and the product-moment correlation coefficients are quite similar. Looking at specific parameters, it is obvious that PCB and HCB are very highly related to each other. TCB is very highly related to MAXLWC and THETAE. HCTM is highly related to HETM, MAXU, MAXPE, MAXLWCPE, THETAE, CLDPT, HFZL and PMXSZ and so forth. Note that TCB and MAXLWC are essentially water parameters whereas the remaining model predictors are essentially buoyancy or instability parameters.

Looking at the correlation coefficients for the wind predictors, it is apparent that they are all quite low. The highest correlation coefficients seem to be obtained for MWCL (the wind speed in the mid-cloud layer) with some of the model predictors such as MAXPE.

The correlations between the seeding predictors and the model predictors are generally quite low. The highest Spearman's rank correlations seem to be obtained for R2FL with a number of the model predictors such as HFZL, THETAE and HCTM. These correlation coefficients are all of the order of 0.3. However, the corresponding product-moment correlation coefficients are very much lower. This suggests that there are some extreme values in either or both of the data samples and the correlation coefficients may not be reliable. In any case, these correlations suggest that the total amount of AgI expended on a storm and the rate at which it is expended are both weakly dependent upon the maximum height of the storm. This may not be surprising. A storm that reaches a very high height may last a long time and be very intense. Obviously, seeding continues as long as the storm continues to be a threat.

Of the wind predictors, MWCL, the horizontal wind speed in the mid-cloud layer, exhibits the highest correlation with the seeding predictors. In particular, MWCL is related to the rate of cloud-base seeding. But even in this case the correlation coefficient is only about 0.3.

Aside from such obvious high correlations as those between, for example, CTF, TCTF and GCTF, parameters that are derived from one another, it is interesting to note that CTF, the number of cloud-top flares, (and parameters derived from it) correlate highly with TGFL, the total amount of AgI delivered to a storm. Actually the correlation between CTF and TGFL is considerably higher than the correlation between CBF, the number of cloud-base flares, (and parameters derived from it) and TGFL suggesting that more AgI is delivered to a storm by cloud-top seeding than by cloud-base seeding. On the other hand, the duration of the seeding (TIME) seems to be determined primarily by the cloud-base seeding. It is not surprising that the total amount of AgI delivered to a storm correlates highly with the duration of the seeding.

The data in table 6 have been separated into various subsets. From these subsets, it is apparent that correlations of PCB and HCB (the cloud-base pressure and height) with the remaining model predictors are considerably higher for the storms of 1976 than for the storms of 1975. On the other hand correlations between the remaining model predictors are generally higher for storms of 1975 than for those of 1976. No explanation for this effect has been found. Obviously the degree of relationship between the various model predictors depends upon the details of the soundings used for the storms in the samples.

Differences are also found, from year to year, in the degree of correlation between the various model predictors and the wind predictors. These correlations are all quite low, the highest coefficients are less than 0.3. But in 1975, model predictors seem to correlate slightly more with MWCL (the horizontal wind speed in the mid-cloud layer) and in 1976 model predictors seem to correlate slightly more with WSCL (the mean horizontal wind speed in the sub-cloud layer). The sample sizes for the two years are virtually identical.

Correlations between seeding predictors and model predictors are generally quite low in both years. No consistent pattern is evident in the differences in the correlations between seeding predictors and model predictors for the storms from 1975 and 1976.

TABLE 6
Correlations Between Predictors for all Hailstorms
from 1975 and 1976

Spearman rank C.C.	Product-moment C.C.	Number of storms	Predictor pair	Spearman rank C.C.	Product-moment C.C.	Number of storms	Predictor pair	Spearman rank C.C.	Product-moment of	Number of storms	Predictor pair
1.00	0.97	157	MAXPE-MAXU	0.77	0.76	193	PMXSZ-CLDPT	0.51	0.60	197	HFZL-MAXU
0.99	0.99	197	HETM-HCTM	0.77	0.74	193	CLDPT-MAXLWC	0.50	0.57	64	TIME-GCTF
0.99	0.99	197	MAXLWC-TCB	-0.76	-0.73	197	TMAXU-MAXU	0.50	0.01	102	R2FL-TGFL
0.99	0.96	85	GCBF-CBF	0.76	0.73	197	HFZL-MAXLWC				
0.98	0.99	64	RGTFL-RGCTF	-0.76	-0.66	197	MAXPE-TMAXU	0.46	0.58	64	TIME-CTF
-0.98	-0.98	197	HCB-PCB	0.76	0.66	102	R2FL-RGTFL	0.44	0.65	64	R2FL-RCTF
0.98	0.98	64	GCTF-CTF	0.75	0.85	64	TGFL-TCTF	0.42	0.49	197	PMXSZ-TCB
0.97	0.95	197	PMXSZ-MAXU	0.75	0.78	193	CLDPT-MAXU	0.41	0.15	188	MWCL-WSSCL
0.97	0.94	197	HFZL-THETAE	0.75	0.72	193	CLDPT-MAXPE	0.40	0.47	196	PMXSZ-MAXLWC
0.96	0.98	197	MAXLWCPE-MAXLWC	-0.74	-0.76	197	TMAXU-HETM				
0.96	0.94	197	MAXLWCPE-MAXU	0.74	0.72	85	TIME-TCBF	-0.39	-0.35	64	TIME-RGCTF
0.96	0.92	197	PMXSZ-MAXPE	-0.74	-0.67	197	PMXSZ-TMAXU	0.39	0.26	83	RCBF-MWCL
0.95	0.89	197	PMXSZ-MAXLWCPE	-0.73	-0.60	197	MAXLWCPE-TMAXU	0.38	0.50	197	MAXPE-TCB
0.94	0.94	193	CLDPT-HETM	-0.72	-0.74	197	TMAXU-HCTM	0.38	0.48	197	MAXU-TCB
0.93	0.99	64	RGCTF-RCTF	0.71	0.71	197	MAXLWC-PCB	-0.38	-0.36	197	HFZL-TMAXU
0.93	0.99	64	RGTFL-RCTF	0.71	0.66	102	TIME-TGFL	0.38	0.22	85	R2FL-RGCBF
0.93	0.94	193	CLDPT-HCTM	0.70	0.80	85	TGFL-GCBF	0.38	0.07	85	RGTFL-RGCBF
0.93	0.94	85	RGCBF-RCBF	-0.69	-0.72	193	CLDPT-TMAXU	-0.37	-0.35	197	THETAE-TMAXU
0.90	0.89	85	TCBF-CBF	-0.69	-0.68	197	MAXLWC-HCB	0.36	0.46	197	MAXPE-MAXLWC
				0.69	0.67	85	TIME-CBF	0.36	0.45	197	MAXLWC-MAXU
0.89	0.91	85	GCBF-TCBF	0.69	0.65	85	TIME-GCBF	0.36	0.21	101	TGFL-HETM
0.89	0.75	197	MAXLWCPE-HETM	0.68	0.72	85	TGFL-CBF	0.36	0.17	101	RGTFL-HFZL
0.87	0.75	197	MAXLWCPE-HCTM	0.68	0.65	197	TCB-PCB	-0.35	-0.34	64	TIME-RCTF
0.87	0.74	193	CLDPT-MAXLWCPE	-0.66	-0.62	197	TCB-HCB	0.35	0.27	85	R2FL-GCBF
0.85	0.92	64	TGFL-GCTF	0.65	0.61	197	THETAE-MAXLWCPE	0.35	0.20	101	TGFL-HCTM
0.83	0.80	197	PMXSZ-HETM	0.64	0.64	197	HFZL-MAXLWCPE	0.35	-0.05	101	R2FL-HFZL
0.83	0.79	197	HFZL-HCTM	0.64	0.62	197	HCTM-TCB	0.34	0.30	193	CLDPT-PCB
0.82	0.85	64	GCTF-TCTF	0.64	0.61	197	HETM-TCB	-0.34	-0.30	193	CLDPT-HCB
0.82	0.84	197	MAXU-HETM	0.61	0.74	85	TGFL-TCBF	0.34	0.25	83	RGCBF-MWCL
0.82	0.77	197	MAXPE-HETM	0.61	0.58	197	MAXLWC-HCTM	0.34	0.21	101	RGTFL-HCTM
0.82	0.77	197	THETAE-HCTM	0.61	0.57	197	MAXLWC-HETM	0.34	0.21	101	RGTFL-HETM
0.82	0.77	197	HFZL-HETM	-0.61	-0.39	64	RCTF-TCTF	0.34	0.19	101	TGFL-HFZL
0.81	0.91	64	TGFL-CTF	0.60	0.70	64	TIME-TCTF	0.34	0.15	85	R2FL-RCBF
0.81	0.80	197	PMXSZ-HCTM					0.34	0.03	85	RGTFL-RCBF
0.81	0.76	197	THETAE-TCB	0.58	0.60	197	MAXLWCPE-TCB	0.33	0.59	47	GCBF-TCTF
0.81	0.75	197	THETAE-HETM	-0.58	-0.39	64	RGCTF-TCTF	0.33	0.22	85	R2FL-CBF
0.80	0.83	197	MAXU-HCTM	0.57	0.61	197	PMXSZ-THETAE	0.33	0.06	101	R2FL-HCTM
0.80	0.77	197	MAXPE-HCTM	0.56	0.62	197	PMXSZ-HFZL	-0.32	-0.27	192	DSCL-WSCL
				0.56	0.57	197	MAXLWCPE-MAXLWC	0.32	0.21	101	TGFL-CLDPT
0.79	0.86	64	TCTF-CTF	-0.55	-0.38	64	RGTFL-TCTF	0.32	0.04	101	R2FL-HETM
0.79	0.77	197	HFZL-TCB	0.54	0.08	102	RGTFL-TGFL	0.31	0.63	47	TCBF-TCTF
0.79	0.73	193	CLDPT-THETAE	0.52	0.58	197	THETAE-MAXU	0.31	0.49	47	CBF-TCTF
0.78	0.75	193	CLDPT-TCB	0.52	0.57	197	THETAE-MAXPE	0.31	0.15	101	RGTFL-THETAE
0.78	0.74	197	THETAE-MAXLWC	0.51	0.66	64	R2FL-RGCTF	0 31	0.14	100	RGTFL-CLDPT
0.78	0.73	193	HFZL-CLDPT	0.51	0.61	197	HFZL-MAXPE	-0.31	-0.14	85	RCBF-TCBF

TABLE 6 continued

Spearman rank C.C.	Product-moment C.C.	Number of storms	Predictor pair	Spearman rank C.C.	Product-moment C.C.	Number of storms	Predictor pair	Spearman rank C.C.	Product-moment of	Number of storms	Predictor pair
0.31	-0.05	101	R2FL-THETAE	0.20	-0.08	101	R2FL-TCB	-0.16	-0.14	188	WSSCL-WSCL
0.29	0.20	100	TGFL-PMXSZ	-0.19	-0.20	101	TIME-TMAXU	0.16	0.12	100	RGTFL-PMXSZ
0.29	0.15	101	TGFL-THETAE	0.19	0.19	193	MWCL-HCTM	0.16*	0.09	84	TCBF-MAXU
0.29	0.01	100	R2FL-CLDPT	-0.19	-0.16	197	MAXLWCPE-HCB	0.16*	0.04	84	TCBF-MAXPE
0.28	0.21	102	TIME-PMXSZ	0.19	0.12	84	CBF-MAXU	0.15*	0.21	85	RGCBF-CBF
0.28	0.16	192	MWCL-PMXSZ	0.19*	0.12	64	RGCTF-MWCL	0.15*	0.20	84	GCBF-HETM
-0.27	-0.27	197	TMAXU-TCB	0.19	0.10	101	TGFL-TCB	0.15	0.17	193	MWCL-CLDPT
0.27	0.23	193	MWCL-MAXU	-0.19	0.11	47	CBF-RGCTF	0.15	0.16	193	MWCL-HFZL
0.27	0.20	193	MWCL-MAXPE	0.19*	0.08	64	CTF-MAXPE	-0.15*	-0.15	84	TCBF-TMAXU
-0.26	-0.16	101	TGFL-TMAXU	0.19	0.08	84	CBF-MAXPE	-0.15	-0.13	193	WSCL-HFZL
-0.25	-0.25	197	MAXLWC-TMAXU	0.19	0.07	101	R2FL-MAXLWC	-0.15	-0.11	193	WSCL-HCTM
0.25	0.17	193	MWCL-MAXLWCPE	0.19*	0.07	47	GCBF-RGCTF	0.15*	0.11	84	RGCBF-THETAE
0.25	0.14	188	WSSCL-TMAXU	0.19*	0.04	64	GCTF-MAXLWCPE	0.15*	0.10	84	GCBF-HCTM
0.25	0.14	64	CTF-HFZL	0.18*	0.18	84	RCBF-THETAE	0.15*	0.10	84	HETM-GCBF
0.25	0.07	101	RGTFL-TCB	0.18	0.16	197	MAXLWCPE-PCB	-0.15	-0.07	197	THETAE-HCB
0.24	0.22	101	TGFL-MAXLWCPE	-0.18	-0.12	193	WSCL-CLDPT	0.14*	0.14	101	TIME-HETM
0.24	0.13	64	GCTF-HFZL	0.18	0.11	197	THETAE-PCB	0.14*	0.13	101	RGTFL-MAXLWCPE
0.24	0.12	64	CTF-HETM	-0.18	-0.11	193	WSCL-PCB	-0.14	-0.10	193	WSCL-HETM
0.24	0.11	85	RGTFL-GCBF	-0.18*	-0.11	84	CBF-TMAXU	-0.14	-0.10	193	WSCL-THETAE
0.24	0.07	101	RGTFL-MAXLWC	-0.18	-0.10	101	R2FL-TMAXU	0.14*	0.03	84	CBF-MAXLWCPE
0.23	0.19	101	TIME-MAXU	0.18	0.09	84	GCBF-MAXU	0.14*	0.02	84	GCBF-MAXLWCPE
0.23	0.16	101	TGFL-MAXU	0.18*	0.07	63	CTF-PMXSZ	0.13*	0.14	101	TIME-HCTM
0.23	0.15	101	TIME-MAXPE	-0.18*	-0.07	62	CTF-WSSCL	0.13*	0.10	102	R2FL-PMXSZ
0.23	0.13	101	TGFL-MAXPE	0.18*	0.05	84	GCBF-MAXPE	0.13*	0.07	100	RGTFL-MWCL
0.23	0.13	83	RCBF-DSCL	0.18*	-0.00	82	RGCBF-WSSCL	0.13	0.06	197	HFZL-PCB
0.23	0.11	64	CTF-HCTM	0.17*	0.25	85	R2FL-TCBF	-0.12	-0.11	193	MWCL-PCB
0.23	0.10	83	RGCBF-DSCL	0.17	0.25	102	R2FL-TIME	0.11*	0.09	193	MWCL-HCB
0.23	0.07	85	RGTFL-CBF	-0.17*	-0.20	64	TGFL-RCTF	-0.11*	-0.09	193	WSCL-MAXLWCPE
-0.22	-0.15	193	WSCL-TCB	-0.17*	-0.19	64	GCTF-RCTF	0.10*	0.11	187	WSSCL-DSCL
-0.22	-0.14	101	RGTFL-TMAXU	0.17	0.19	193	MWCL-THETAE	-0.10*	-0.09	188	WSSCL-MAXPE
0.22	0.14	63	CTF-PMXSZ	-0.17*	-0.15	64	GCTF-TMAXU	-0.10*	-0.07	188	WSSCL-MAXU
0.22	0.13	64	GCTF-HETM	-0.17*	-0.12	64	CTF-TMAXU	-0.10*	-0.04	188	WSSCL-HCTM
0.22	0.12	84	GCBF-PMXSZ	0.17*	0.11	64	GCTF-MAXU	-0.10*	-0.03	188	WSSCL-HETM
0.22	0.06	64	CTF-MAXLWCPE	0.17	0.10	193	WSCL-HCB	-0.10*	-0.01	197	HFZL-HCB
0.22	-0.02	84	CBF-PMXSZ	0.17	0.10	101	TGFL-MAXLWC				
0.21	0.12	64	RCTF-MWCL	-0.17*	-0.09	62	GCTF-WSSCL				
0.21	0.11	64	GCTF-HCTM	0.17*	0.07	64	GCTF-MAXPE				
0.21	0.10	64	CTF-THETAE	-0.17*	-0.06	84	GCBF-TMAXU				
-0.21	-0.05	85	RGCBF-TCBF	0.17*	0.06	84	TCBF-PMXSZ				
0.21	-0.00	82	RCBF-WSSCL	0.16*	0.21	84	RCBF-HCTM				
0.20	0.20	193	MWCL-HETM	0.16*	0.21	84	RCBF-HETM				
0.20	0.13	101	TIME-MAXLWCPE	0.16*	0.21	84	GCBF-HCTM				
0.20*	0.13	63	GCTF-PMXSZ	0.16*	0.21	85	RGCBF-GCBF				
0.20*	0.12	64	CTF-MAXU	-0.16*	-0.18	64	TGFL -RGCTF				
				0.16*	0.16	85	TGFL-RGCBF				

Correlations between the seeding parameters and the wind predictors are all quite low.

A significant difference, between the two years, in the correlations between the various seeding predictors seems to be that CBF (and parameters related to it) correlate more highly with TGFL, RGTFL and TIME for storms from 1976 than for storms from 1975. This suggests that cloud base seeding was more frequent, in relation to cloud top seeding, in 1976 than in 1975.

Dropping all storms for which no representative soundings were available, from the all-storms sample, makes little difference in the apparent relationships between the various model predictors. Correlations between wind predictors, especially MWCL, and model predictors seem to be significantly higher for the storms with representative-soundings sample than for the all-storms sample. Typical correlations coefficients between MWCL and model predictors are now about 0.4.

It is conceivable that seeded and not-seeded storms are not quite alike; that is, it is possible that on average the storms in the seeded storm sample are slightly larger or smaller than the ones in the not-seeded storms sample. If this is the case, the relationships between the various predictors may well be somewhat different for seeded and not-seeded storms. For this reason, correlations between the various model and wind predictors have been calculated for the not-seeded storms sample and the seeded storms sample. These calculations show that the correlations between the model predictors are generally very slightly higher for the not-seeded storms sample than for the seeded storms sample. For the seeded storms sample, fairly high correlations exist between MWCL and various model predictors. No such high correlations exist for not-seeded storms. However, when only the not-seeded storms with representative soundings are considered, much higher correlations are obtained between wind predictors and model predictors. Also, for the seeded storms correlations between MWCL and the various model predictors are much higher when only storms with representative soundings are considered.

The not-seeded storms of 1976 seem to produce somewhat higher correlations between model predictors and wind predictors than the not-seeded storms of 1975 sample. A comparison of the seeded storms of 1975 with the seeded storms of 1976 shows that correlations between the various model predictors are generally higher for the 1975 sample than for that of 1976.

THE RESPONSE VARIABLES

Response Variables Derived From Hail Reports

Numerous response variables have been calculated from the hail reports sent in by voluntary observers. This data base has provided most of the response variables used in this study chiefly because it is readily available. The response variables calculated from data given by the voluntary observers are listed in table 7.

TABLE 7
Response Variables Calculated from Hail Reports sent in by Voluntary Observers

Symbol	Description	Units
RMHS	absolute maximum of the reported maximum hailstone sizes, known only in terms of 6 size categories, the mean diameter of each size category being used	cm
AMHS	average maximum of the reported maximum hailstone size	cm
AHM	average hail mass	Kgm^{-2}
AHF	average hailflux	$Kgm^{-2}\ s^{-1}$
AIE	average impact energy	Jm^{-2}
AREA	total hailswath area	km^2
AGP	total area covered by pea-sized and larger hail	km^2
AGG	total area covered by grape-sized and larger hail	km^2
AGW	total area covered by walnut-sized and larger hail	km^2
AGGP	total area covered by golfball-sized and larger hail	km^2
AGL	total area covered by larger than golfball-sized hail	km^2
SV1	ratio of AGP to AREA	
SV2	ratio of AGG to AREA	
SV3	ratio of AGW to AREA	
SV4	ratio of AGGP to AREA	
SV5	ratio of AGL to AREA	

A word of explanation is required for most of these parameters. AMHS was calculated by counting the number of reports in each of the two highest size categories reported for the maximum hailstone size and then setting AMHS equal to a weighted average of the two highest size categories. This parameter was calculated to account for instances where one observer grossly overestimated the maximum size of the hail. AHM was derived from the reported modal hailstone size and the average depth of hail or the average spacing between hailstones. The duration of the hailfall was also considered to calculate AHF. To calculate AIE, a hailfall velocity had to be assumed. In

order to calculate all the hailswath area parameters, plots of maximum hailstone size were produced, contours were drawn and then planimetered.

Response Variables From Radar Data

The only response variable derived from the radar data is the maximum radar echo height (MRT). Originally, numerous other response variables from radar data were planned. However, the extraction of the necessary radar data and the development of the necessary programs proved to be beyond the scope of the Cloud Modelling Group.

Relationships Between the Response Variables

It seemed reasonable that some of the response variables would be related to each other to some extent. To investigate possible relationships between the various response variables, Spearman's rank correlation coefficients as well as product-moment correlation coefficients have been calculated. These are presented in table 8. Data is entered in table 8 only for pairs of response variables for which the Spearman's rank correlation coefficient is statistically significant at the 10 percent level. Correlation coefficients that are statistically significant at the 5 to 10 percent level are indicated with an asterisk; all other Spearman's rank correlation coefficients are statistically significant at the 5 percent level or better.

Looking at table 8, it is apparent that the correlation between RMHS and AMHS is very high; they are virtually identical. Correlation coefficients greater than 0.5, are evident for AIE, AREA, MRT, AGP, AGG, AGW, AGL, SV1 and SV2 with RMHS and AMHS. Thus, all these parameters are related, to some extent, to maximum hailstone size. This is encouraging, because it suggests that a model that can predict maximum hailstone size reasonably well, can also predict these other parameters. AHM, AHF and AIE correlate well with each other because they are all calculated, to some extent, from the reported modal hailstone size and the average depth of, or spacing between, hailstones. The low correlation between AREA and MRT is somewhat surprising since they both correlate about equally well with the maximum size parameters. The high correlations between the various area parameters is interesting, as is the high correlation between MRT and the areas covered by the larger hailstones.

Is there a significant difference in these correlations between the storms from 1976 and those of 1975? Subsets of the data in table 8 show that the correlations of MRT with RMHS and AMHS are significantly lower for storms from 1976 than for storms from 1975. The correlation between MRT and AREA is also lower for the storms of 1976 than for those of 1975, as are the correlations between MRT and most of the other response variables.

Obviously, the accuracy of the data given on the hail reports will vary considerably from observer to observer. To reduce the influence of any one observer on the results, all storms for which less than five hail reports were received were dropped from the data sample and new correlation coefficients were calculated. Very little difference is evident between these new correlations and those in table 8.

Presumably, seeding will have some effect on all these response variables. Therefore, the relationships between the various response variables may be different for seeded storms and for not-seeded storms. Correlation coefficients, between the various response variables, have been calculated for the not-seeded storms sample and the seeded storms sample. The correlations between the maximum size parameters (RMHS and AMHS) and AREA and MRT are a little lower for the seeded storms, but there is really no significant difference in the correlations between the various response variables for seeded and not-seeded storms.

CORRELATIONS BETWEEN PREDICTOR AND RESPONSE VARIABLES FOR ALL STORMS

Spearman's rank and product-moment correlation coefficients have been calculated for all the predictor and response variables discussed in previous sections. In table 9, for each predictor-response pair, the first value given is the Spearman's rank correlation coefficient. As before, correlation coefficients have been entered in table 9 only for those predictor-response pairs for which the Spearman's rank correlation coefficient is statistically significant at the 10 percent level or better. In fact, Spearman's rank correlation coefficients that are significant at the 5 to 10 percent level are indicated with an asterisk. All other Spearman's rank correlation coefficients in table 9 are statistically significant at the 5 percent level or better. The second value given for each predictor-response pair is the product-moment correlation coefficient. A large difference between the product-moment and the Spearman's rank correlation coefficient for a given pair of parameters indicates the presence of extreme values in one or both of the samples used to calculate the correlation coefficients. The last entry for each pair of parameters is the number of storms in the two samples.

TABLE 8
Correlations Between Response Variables of all Hailstorms from 1975 and 1976

Spearman rank C.C.	Product-moment C.C.	Number of storms	Predictor pair	Spearman rank C.C.	Product-moment C.C.	Number of storms	Predictor pair	Spearman rank C.C.	Product-moment of	Number of storms	Predictor pair
0.98	0.99	116	AGP-AREA	0.58	0.41	60	SV3-AGW	0.39	0.22	60	SV1-AGW
0.97	0.97	208	AMHS-RMHS	0.58	0.36	15	SV2-AGL	0.38*	0.35	14	SV5-AIE
0.97	0.85	160	AIE-AHM	0.57	0.65	116	AREA-AMHS	-0.38*	0.02	14	SV5-AGG
0.93	0.99	15	AGL-AGGB	0.57	0.16	15	AGL-RMHS	0.37	0.45	56	AGW-MRT
				0.56	0.75	15	AGL-AGG	0.35*	0.35	15	AGL-AIE
0.86	0.85	14	SV5-SV4	0.55	0.61	193	MRT-AMHS	0.34	0.27	115	SV1-AIE
0.86	0.46	28	AGGB-AMHS	0.54	0.59	193	MRT-RMHS	0.33	0.39	109	SV1-MRT
0.85	0.96	103	AGG-AGP	0.54	0.38	60	AGW-AIE	-0.34	0.01	27	SV4-AREA
0.85	0.75	14	SV5-SV3	0.54	0.45	116	SV1-RMHS	0.33	0.29	101	SV2-AHM
0.83	0.33	15	AGL-AMHS	0.54	0.47	116	SV1-AMHS	0.33	0.30	60	SV3-AHM
0.81	0.94	103	AGG-AREA	0.54	0.19	28	SV1-AGGB	0.33	0.32	103	SV2-AGP
0.81	0.54	13	AGL-MRT	0.53	0.39	115	AGP-AIE	0.32	0.35	28	AGGB-AIE
0.80	0.62	60	AGW-AMHS	0.53	0.81	28	AGGB-AGG	0.32	0.24	116	SV1-AREA
0.80	0.54	25	AGGB-MRT	0.53	0.37	115	AREA-AIE	0.31	0.07	96	AGG-AHF
0.80	0.94	60	AGW-AGG	0.51	0.41	103	AGG-AIE	0.31	0.25	58	SV3-AHF
0.80	0.92	15	AGL-AGW	-0.51	-0.20	14	SV5-AREA	0.31	0.16	60	SV3-SV1
				0.51	0.69	28	AGGB-AGP	0.30	0.38	109	AGP-MRT
0.78	0.85	60	AGW-AGP	-0.51	-0.17	14	SV5-AGP	0.30	0.40	98	AGG-MRT
0.77	0.54	60	AGW-RMHS	0.50	0.58	15	AGL-AREA	-0.30*	0.03	27	SV4-AGP
0.77	0.83	60	AGW-AREA	0.50	0.50	15	SV3-AGL				
0.76	0.69	103	SV2-AMHS	0.50	0.51	27	SV4-AGGB	0.28	0.14	103	AGP-AHF
0.76	0.95	28	AGGB-AGW	0.50	0.43	27	SV4-SV2	0.26	0.15	103	AREA-AHF
0.73	0.55	134	AHF-AHM	0.50	0.61	15	AGL-AGP	0.26	0.36	109	MRT-AREA
0.73	0.77	27	SV4-SV3					0.25	0.26	160	MRT-AIE
0.71	0.32	28	AGGB-RMHS	0.49	0.19	15	SV1-AGL	0.25	0.28	103	SV2-AREA
				0.49	0.42	28	SV3-AGGB	0.23	0.14	113	SV1-AHM
0.69	0.57	24	SV4-MRT	0.48	0.16	58	AGW-AHF	0.22	-0.02	96	SV2-AHF
0.69	0.69	60	SV3-SV2	0.48	0.66	28	AGGB-AREA				
0.68	0.67	103	AGG-AMHS	0.48	0.48	98	SV2-MRT	-0.19	-0.08	123	MRT-AHF
0.67	0.6	103	AGG-RMHS	-0.48	-0.59	14	SV5-RMHS	0.14	0.12	134	AHF-AMHS
0.66	0.47	134	AIE-AHF	0.47	0.39	160	AHM-AMHS	0.12*	0.13	134	AHF-RMHS
0.66	0.67	116	AGP-RMHS	0.47	0.58	14	SV4-AGL	0.12*	0.11	149	MRT-AHM
0.66	0.59	103	SV2-SV1	0.46	0.26	103	SV1-AGG				
0.64	0.58	172	AIE-AMHS	0.44	0.38	160	AHM-RMHS				
0.64	0.59	103	SV2-RMHS	0.44	0.24	60	AGW-AHM				
0.64	0.41	103	SV2-AGG	0.44	0.28	116	SV1-AGP				
0.63	0.57	172	AIE-RMHS	0.43	0.37	60	SV3-RMHS				
0.63	0.66	116	AREA-RMHS	0.43*	0.25	14	SV5-SV2				
0.62	0.50	60	SV3-AMHS	0.42	0.28	113	AREA-AHM				
0.60	0.67	116	AGP-AMHS	0.42	0.29	113	AGP-AHM				
0.60	0.36	60	SV2-AGW	0.42	0.48	103	SV2-AIE				
0.60	0.31	28	SV2-AGGB	0.42	0.45	60	SV3-AIE				
				0.41	0.46	56	SV3-MRT				
				0.41	0.08	27	SV4-SV1				
				0.40	0.27	101	AGG-AHM				
				0.40*	0.26	12	SV5-MRT				
				0.40	0.26	27	SV4-AMHS				

Looking at table 9, correlation coefficients greater than 0.5 are apparent for:

HCTM, HETM, MAXU, MAXPE, MAXLWCPE, PMXSZ	with RMHS
HCTM, HETM, MAXU, MAXPE, MAXLWCPE, THETAE, PMXSZ	with AMHS
CBF, GCBF	with AREA
HCTF, HETM, MAXU, TMAXU, MAXPE, MAXLWCPE, THETAE, CLDPT, HFZL, PMXSZ	with MRT
CBF, GCBF	with AGP
HCTM, HETM, MAXU, TMAXU, MAXPE	with AGGB
HCTM, HETM, MAXU, TMAXU, MAXPE MAXLWCPE, CLDPT, PMXSZ, DSCL, RCBF	with AGL
HCTM, HETM	with SV3
CFB, TCBF, GCBF, TIME	with SV4
RCTF, CBF, TCBF, RCBF, GCBF, TIME	with SV5

It is interesting to note that the seeding predictors correlate highly with some of the hailswath area response variables (including some of the severity ratio response variables). Furthermore, it is mostly predictors concerned with cloud-base seeding that correlate highly with the area response variables.

Subsets of the data in table 9 show that for the model predictors, correlations between predictors and response variables are generally much higher for the storms of 1975 than for the storms of 1976. This may be due to the many more "outliers" found in the storms of 1976 than in the storms of 1975. For the seeding predictors, the correlations between predictor and response variables seem to be slightly higher for the storms of 1976 than for the storms of 1975.

The severity ratios SV1, SV2, SV3, SV4 and SV5 were calculated because of the results of Mather (1977). However, Summers (1978) has shown that the interpretation of a change in severity ratio is difficult.

The correlations between model predictors and response variables are considerably higher for the storms from 1975 than for the storms from 1976. This is true of the all-storms sample, the sample containing only the storms with representative soundings and five or more hail reports, the not-seeded storms sample and the seeded storms sample.

For seeded storms the model predictors seem to correlate more highly with maximum hailstone size and some of the area parameters than they do for not-seeded storms. On the other hand, for not-seeded storms the model predictors seem to correlate more highly with MRT and the severity ratios than they do for seeded storms.

It does not seem possible to draw any conclusions about the effect of sounding representativeness and the number of hail reports because of the extremely small sample size when all other storms are excluded.

SOME PREDICTOR-RESPONSE RELATIONSHIPS

Predictor-Response Pairs

In the previous section, for some of the response variables, a number of predictor variables were identified as promising parameters for inclusions in a predictor-response relationship. Simple linear regressions between some predictor variables and response variables, are given in table 10. It should be recalled here that all predictor variables are calculated while all response variables are measured. Given in table 10 are the number of storms in the not-seeded (N) category, the number of storms in the seeded (S) category, the calculated correlation coefficient between the predictor and response variables in question for the not-seeded storms sample and the seeded storms sample, and the direction of the difference in the simple linear regression lines for the seeded and not-seeded samples. These data are given for a number of predictor-response variable pairs both for a number of subsets of the all-storms sample and for the whole sample. S > N signifies that for a given value of the predictor (HCTM in the case of the first row) the response variables (RMHS in the case of the first row) has a larger value for seeded storms than for not-seeded storms. Note that the observed differences between seeded and not-seeded storms have *not* been tested for statistical significance.

HCTM with RMHS

The correlation coefficient between HCTM and RMHS for both the seeded storms sample and the not-seeded storms sample is over 0.5. The linear regression lines suggest that for the larger storms, for a given predicted maximum storm height, seeded storms tend to produce slightly larger hail than not-seeded storms. This suggestion is even stronger for the storms from 1976 only (row two of table 10). Note, however, that the correlation coefficient between HCTM and RMHS for the not-seeded storms from 1976 is significantly lower than that for the seeded storms from 1976. This may be due to the fact that, as discussed earlier, most of the "outliers" are in the not-seeded storms from 1976 sample. The opposite trend, if anything, is suggested in row three of table 10, which gives the relations between HCTM and RMHS for all storms from 1975. Furthermore, the correlation coefficient between HCTM and RMHS is very much higher for both seeded and not-seeded storms from 1975 than it is for storms from 1976. The regression lines derived for the

TABLE 9
Correlations Between Predictors and Response Variables for all Hailstorms from 1975 and 1976

Spearman rank C.C.	Product-moment C.C.	Number of storms	Predictor pair	Spearman rank C.C.	Product-moment C.C.	Number of storms	Predictor pair	Spearman rank C.C.	Product-moment of	Number of storms	Predictor pair
-0.95	-0.59	7	TCBF-SV5	0.53	0.57	185	MAXU-MRT	0.44	0.45	59	CLDPT-SV3
				-0.53	-0.53	185	TMAXU-MRT	0.44	0.50	60	PMXSZ-SV3
-0.86	-0.35	15	TMAXU-AGL	0.53	0.55	185	MAXPE-MRT	-0.44*	-0.32	14	TCTF-SV4
				0.53	0.55	184	PMXSZ-MRT	0.43	0.33	116	MAXLWCPE-SV1
-0.78	-0.62	13	TCBF-SV4	0.53	0.32	28	HETM-AGGB	0.43	0.39	103	THETAE-SV2
-0.78	-0.51	7	GCBF-SV5	0.53	0.53	60	HCTM-SV3	0.43	0.13	28	HFZL-AGGB
0.74	0.73	185	HCTM-MRT	0.52	0.51	197	THETAE-AMHS	0.43*	0.01	14	RCTF-AGGB
0.73	0.72	185	HETM-MRT	0.52	0.51	60	HETM-SV3	0.43	0.59	60	MAXLWCPE-SV3
-0.73	-0.56	13	GCBF-SV4	-0.52	-0.61	9	TIME-SV5	-0.42	-0.42	197	TMAXU-RMHS
0.70	0.68	181	CLDPT-MRT	0.51	0.41	28	MAXU-AGGB	-0.42	-0.42	197	TMAXU-AMHS
0.70	0.41	15	MAXU-AGL	0.51	0.46	28	MAXPE-AGGB	0.42	0.49	58	TCBF-AREA
0.70	0.46	15	MAXPE-AGL	0.50	0.48	185	TCB-MRT	0.42	0.46	60	MAXLWCPE-AGW
0.70	0.46	8	RCTF-SV5	0.50	0.49	193	CLDPT-RMHS	0.42	0.51	114	CLDPT-SV1
				0.50	0.49	193	CLDPT-AMHS	0.42	0.27	28	PMXSZ-AGGB
0.68	0.51	15	MAXLWCPE-AGL	0.50	0.05	14	RCTF-SV4	0.42	0.01	16	RGTFL-AGGB
0.68	0.22	15	PMXSZ-AGL	-0.50	-0.42	16	TIME-SV4	0.42	0.55	60	MAXU-SV3
0.67	0.65	186	HFZL-MRT					0.42	0.59	60	MAXPE-SV3
0.66	0.61	185	THETAE-MRT	0.49	0.54	198	HFZL-AMHS	0.42*	0.29	14	MAXLWCPE-SV5
-0.65	-0.51	13	CBF-SV4	0.49	0.37	60	PMXSZ-AGW	0.42	0.44	26	CLDPT-SV4
0.64	0.32	15	HCTM-AGL	0.48	0.49	116	HFZL-SV1	-0.42	-0.34	16	TGFL-SV4
-0.64	-0.37	28	TMAXU-AGGB	0.48	0.38	27	HCTM-SV4	0.41	0.32	102	TGFL-RMHS
0.62	0.31	15	HETM-AGL	0.47	0.45	185	MAXLWC-MRT	0.41	0.39	116	TCB-SV1
0.61	0.60	196	PMXSZ-RMHS	0.47	0.43	60	MAXU-AGW	-0.41	-0.25	27	TMAXU-SV4
0.60	0.58	197	MAXPE-RMHS	0.47	0.48	60	MAXPE-AGW	0.41	0.33	60	THETAE-SV3
0.60	0.60	197	MAXU-RMHS	0.47	0.42	27	CLDPT-AGGB	0.40	0.39	103	TCB-SV2
0.60*	0.89	7	RCBF-AGL	0.47	0.39	52	GCBF-AGG	0.40	0.41	116	MAXU-SV1
				0.47	0.20	30	GCBF-AGW	0.40	0.36	116	MAXLWC-SV1
0.59	0.58	197	HETM-AMHS	0.47	0.38	27	HETM-SV4	0.40	0.36	116	MAXPE-SV1
0.59	0.53	197	MAXLWCPE-RMHS	0.47	0.52	60	HFZL-SV3	0.40	0.38	101	CLDPT-SV2
0.59	0.54	185	MAXLWCPE-MRT	0.46	0.36	60	HCTM-AGW	0.40	0.37	116	PMXSZ-SV1
0.59	0.58	196	PMXSZ-AMHS	0.46	0.45	28	MAXLWCPE-AGGB	0.40	0.46	58	TCBF-AGP
-0.59	-0.38	15	DCSL-AGL	0.46	0.47	103	HFZL-SV2	0.40	0.19	30	RGCBF-AGW
0.59*	0.44	7	RCBF-SV5	0.46	0.23	30	CBF-AGW				
0.58	0.59	197	HCTM-AMHS	0.45	0.51	198	HFZL-RMHS	0.39	0.37	103	MAXLWC-SV2
0.58	0.58	197	HETM-RMHS	0.45	0.53	116	HCTM-SV1	0.39	0.32	65	TGFL-AGP
0.58	0.59	197	MAXU-AMHS	0.45	0.35	60	HETM-AGW	0.38	0.33	65	TGFL-AREA
0.58	0.58	197	MAXPE-AMHS	0.45	0.53	116	HETM-SV1	0.38	0.25	100	TGFL-MRT
0.57	0.58	197	HCTM-RMHS	0.45	0.46	116	THETAE-SV1	0.38	0.32	43	CTF-SV1
0.57	0.53	197	MAXLWCPE-AMHS	0.45	0.39	52	CBF-AGG	-0.38	-0.38	30	TCBF-SV3
0.57	0.46	58	CBF-AREA	0.45	0.15	14	MAXU-SV5	0.37	0.36	85	CBF-RMHS
0.57	0.45	58	GCBF-AREA	0.45	0.23	14	MAXPE-SV5	0.37	0.32	85	GCBF-RMHS
-0.55*	-0.51	7	CBF-SV5	0.44	0.43	103	HCTM-SV2	-0.37	-0.31	60	TMAXU-AGW
0.54	0.33	28	HCTM-AGGB	0.44	0.42	103	HETM-SV2	0.37	0.28	27	HFZL-SV4
0.54	0.47	15	CLDPT-AGL	0.44	0.46	27	MAXU-SV4	0.36	0.29	102	TIME-RMHS
0.54	0.44	58	CBF-AGP	0.44	0.52	27	MAXPE-SV4	0.36	0.32	43	GCTF-SV1
0.54	0.44	58	GCBF-AGP	0.44	0.51	27	MAXLWCPE-SV4	0.36	0.41	103	MAXLWCPE-SV2

TABLE 9 continued

Spearman rank C.C.	Product-moment C.C.	Number of storms	Predictor pair	Spearman rank C.C.	Product-moment C.C.	Number of storms	Predictor pair	Spearman rank C.C.	Product-moment of	Number of storms	Predictor pair
0.35	0.42	166	MAXU-AIE	0.29	0.32	197	TCB-RMHS	0.24	0.12	87	TIME-AIE
0.35	0.45	166	MAXPE-AIE	0.29	0.35	116	PMXSZ-AREA	0.24*	0.20	43	CTF-AGP
0.35	0.26	102	TGFL-AMHS	0.29	0.24	193	MWCL-RMHS	0.24	0.23	52	RCBF-SV2
0.35	0.36	116	PMXSZ-AGP	0.29	0.22	63	CTF-MRT	0.23	0.22	156	MAXPE-AHM
0.35	0.15	30	TCBF-AGW	0.29	0.26	114	MWCL-SV1	0.23	0.27	166	THETAE-AIE
0.34	0.21	55	TCTF-AIE	0.28	0.35	116	MAXU-AREA	0.23	0.03	114	MWCL-AREA
0.34	0.39	103	MAXU-SV2	0.28	0.36	116	MAXPE-AREA	0.23	0.20	64	CTF-RMHS
0.34	0.41	103	MAXPE-SV2	0.28	0.28	85	CBF-AMHS	0.23	0.15	64	TCTF-AMHS
0.34	0.18	59	TGFL-AGG	0.28	0.25	85	GCBF-AMHS	0.23	0.06	65	R2FL-AREA
0.33	0.38	165	PMXSZ-AIE	0.28	-0.02	100	R2FL-MRT	0.23	0.28	114	CLDPT-AGP
0.33	0.28	55	CTF-AIE	0.28	0.38	103	MAXU-AGG	0.23	0.23	116	HFZL-AGP
0.33	0.07	100	RGTFL-MRT	0.28	0.41	103	MAXPE-AGG	0.23	0.15	52	RCBF-AGG
0.33	0.37	116	MAXU-AGP	0.28	0.17	58	RGCBF-AGP	-0.23	-0.27	36	TIME-SV3
0.33	0.38	116	MAXPE-AGP	-0.28*	-0.26	28	TCTF-SV3	0.22	0.22	156	MAXU-AHM
0.33	0.11	28	THETAE-AGGB	-0.27	-0.26	166	TMAXU-AIE	0.22	0.31	167	HFZL-AIE
0.33	0.24	60	HFZL-AGW	0.27	0.28	197	MAXLWC-RMHS	0.22	0.18	64	CTF-AMHS
0.33	0.35	103	PMXSZ-SV2	0.27	0.23	52	CTF-AHM	0.22	0.11	87	TIME-AHF
-0.33	-0.31	60	TMAXU-SV3	0.27	0.20	43	TCTF-AREA	0.22	0.17	100	TIME-MRT
0.32	0.33	197	TCB-AMHS	0.27	0.13	52	GCTF-AHM	-0.22	-0.27	116	TMAXU-AGP
0.32	0.42	166	MAXLWCPE-AIE	0.27	0.21	63	GCTF-MRT	0.22	0.22	101	MWCL-SV2
0.32	0.25	55	GCTF-AIE	0.27	0.32	103	HETM-AGG	0.22*	0.30	43	TCTF-SV1
0.32	0.18	43	TCTF-AGP	-0.27	-0.33	116	TMAXU-SV1	0.22	0.23	65	TGFL-S V1
0.32	0.20	52	RGCBF-AGG	0.27	0.35	103	PMXSZ-AGG	0.22	0.05	65	R2FL-AGP
-0.32	-0.27	30	GCBF-SV3	0.27*	-0.07	36	TIME-AGW	0.21	0.20	155	PMXSZ-AHM
0.31	0.34	166	HETM-AIE	0.27	0.34	60	TCB-SV3	-0.21	-0.18	149	WSSCL-AHM
0.31	0.24	193	MWCL-AMHS	0.27*	0.19	30	RGCBF-SV3	0.21*	0.20	45	TCTF-AHF
0.31	0.21	52	TCTF-AHM	-0.26	-0.23	45	RGCTF-AHF	0.21	0.19	64	GCTF-RMHS
0.31	0.23	87	TGFL-AIE	0.26	0.18	84	TGFL-AHM	0.21	0.16	73	CBF-AIE
0.31	0.21	65	TIME-AREA	0.26	0.18	102	TIME-AMHS	0.21	0.12	58	RCBF-AREA
0.31	0.20	28	TCB-AGGB	0.26	0.33	103	HCTM-AGG	0.21	0.06	102	RGTFL-RMHS
0.31	0.23	28	MAXLWC-AGGB	0.26	0.03	114	MWCL-AGP	0.21	0.19	116	THETAE-AGP
0.31	0.35	116	MAXLWCPE-AGP	0.26	0.05	42	TCTF-AGG	0.21	0.23	103	HFZL-AGG
0.31	0.35	59	CLDPT-AGW	0.26	0.27	52	RGCBF-SV2	-0.21*	-0.20	43	RGCTF-AGP
0.31	0.33	52	TCBF-AGG	0.26	0.07	59	TIME-AGG	0.20	0.17	181	MWCL-MRT
0.31	0.01	36	TGFL-AGW	0.25	0.33	116	MAXLWCPE-AREA	0.20*	0.15	64	GCTF-AMHS
0.31	0.19	65	TIME-AGP	0.25	0.18	83	GCBF-MRT	0.20*	0.22	43	GCTF-AREA
-0.31	-0.25	30	CBF-SV3	-0.25	-0.25	103	TMAXU-SV2	-0.20	-0.20	43	RGCTF-AREA
0.31	0.17	30	RCBF-SV3	0.25	0.39	103	MAXLWCPE-AGG	0.20	0.11	73	GCBF-AIE
0.30	0.35	166	HCTM-AIE	0.25	0.13	60	THETAE-AGW				
0.30	0.29	197	MAXLWC-AMHS	0.25	0.21	43	GCTF-AGP	0.19	0.17	156	HCTM-AHM
0.30	0.32	85	TCBF-RMHS	0.25	0.28	60	MAXLWC-SV3	0.19	0.17	156	HETM-AHM
0.30	0.16	58	RGCBF-AREA	0.24	0.29	116	HCTM-AREA	0.19	0.19	156	MAXLWCPE-AHM
0.30	0.32	116	HCTM-AGP	0.24	0.29	116	HETM-AREA	-0.19*	-0.18	52	RGCTF-AHM
0.30	0.31	116	HETM-AGP	0.24	0.26	163	CLDPT-AIE	0.19	0.22	85	TCBF-AMHS
0.30*	0.20	27	PMXSZ-SV4	0.24	0.16	83	CBF-MRT	0.19	0.06	102	RGTFL-AMHS

TABLE 9 continued

Spearman rank C.C.	Product-moment C.C.	Number of storms	Predictor pair	Spearman rank C.C.	Product-moment C.C.	Number of storms	Predictor pair	Spearman rank C.C.	Product-moment of	Number of storms	Predictor pair
0.19	0.15	87	TIME-AHM	0.17*	-0.07	59	WSCL-AGW	0.14	0.10	156	THETAE-AHM
0.19	0.00	102	R2FL-AMHS	0.16	0.26	114	CLDPT-AREA	0.14	0.13	156	HCB-AHM
-0.19	-0.27	103	TMAXU-AGG	-0.16	-0.14	162	DSCL-AIE	0.13	0.10	153	CLDPT-AHM
0.19	0.18	103	THETAE-AGG	-0.16	-0.07	125	WSSCL-AHF	-0.13	-0.16	152	DSCL-AHM
0.19	0.30	101	CLDPT-AGG	0.16	0.06	163	MWCL-AIE	-0.12*	-0.12	156	PCB-AHM
0.19*	0.12	58	RCBF-AGP	0.16*	0.04	73	TCBF-AIE	0.12*	0.13	166	HCB-AIE
0.19*	0.05	59	R2FL-AGG	0.16	0.17	116	TCB-AGP	-0.11*	-0.12	166	PCB-AIE
0.18	0.20	116	HFZL-AREA	-0.16	-0.18	101	WSCL-SV2	0.11*	0.15	166	TCB-AIE
-0.18*	-0.18	55	RGCTF-AIE	0.15	0.17	116	THETAE-AREA	-0.11*	-0.10	193	WSCL-RMHS
0.18	0.16	83	TCBF-MRT	0.15*	0.26	85	RGCBF-AMHS	-0.10*	-0.12	197	PCB-RMHS
0.18	-0.02	102	R2FL-RMHS	0.15	0.17	116	MAXLWC-AGP	-0.10	-0.14	197	PCB-AMHS
-0.18*	-0.07	60	PCB-AGW	0.15	0.19	103	MAXLWC-AGG	0.10*	0.12	197	HCB-RMHS
-0.17	-0.16	156	TMAXU-AHM	0.15*	-0.01	101	MWCL-AGG	0.10*	0.13	197	HCB-AMHS
-0.17	-0.26	116	TMAXU-AREA	0.14*	0.05	99	WSSCL-SV2				
0.17*	0.25	85	RCBF-AHMS	-0.14	-0.14	159	WSSCL-AIE				
0.17*	0.21	83	RGCBF-MRT	-0.14	-0.12	181	WSCL-MRT				
0.17	0.20	103	TCB-AGG	0.14	0.11	157	HFZL-AHM				

storms from 1976 suggest that there is little difference in the relationship between HCTM and RMHS for seeded and not-seeded storms, but for a given predicted maximum height, not-seeded storms produce slightly larger hail than seeded storms.

Row four of table 10 summarizes the relations between HCTM and RMHS for all storms from 1975 and 1976 with representative soundings and five or more hail reports. However, sample sizes are too small to draw any conclusions.

HCTM with MRT

A scatter diagram for HCTM (Cld Top Ht) versus MRT (Max Radar Top) for the storms of 1975 and 1976 is shown in figure 3. Note that the correlation coefficient between HCTM and MRT is reasonably high for both seeded and not-seeded storms and that the correlation coefficients for the two samples are virtually identical. The linear regression lines suggest little difference in the relationship between HCTM and MRT for seeded and not-seeded storms. The same conclusion can be drawn from the scatter diagram for the storms of 1976, summarized in row six of table 10. In fact, the correlation coefficients between HCTM and MRT are virtually the same as in row five for both seeded and not-seeded storms. Row seven of table 10 summarizes the relations between HCTM and MRT for storms from 1975 only. Again, the same conclusions apply to the storms of 1975 and the correlation coefficients between HCTM and MRT are still very much the same as in the other two samples.

The storms with representative soundings and five or more hail reports have been separated out and the results are summarized in row eight of table 10. Note that for these storms, the correlation coefficients between HCTM and MRT are slightly higher than those obtained for the all-storms samples. Furthermore, the regression lines derived suggest that for a given predicted maximum cloud height, seeded storms grow slightly taller than not-seeded storms. In any case, the not-seeded storms sample is exceedingly small.

The regression lines for the seeded and not-seeded samples of HCTM versus MRT have been tested for statistical significance of the difference. A variety of statistical tests were used. All subsets of the whole data set were also tested. All the results obtained indicated no statistically significant difference in maximum echo top between seeded and not-seeded storms. This suggests that no dynamic seeding effects are realized by seeding a hailstorm.

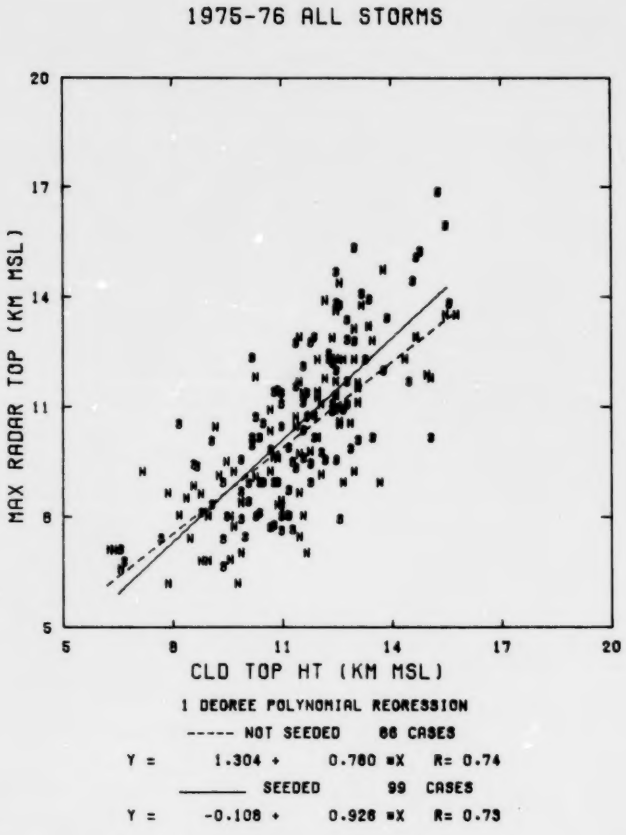

FIGURE 3. Scatter diagram of HCTM (Cld Top Ht) versus MRT (Max Radar Top) for all storms from 1975 and 1976. "S" represents a data point for a seeded storm, "N" for a not-seeded storm. The solid line is a linear regression line for the "S" data points, the dashed for the "N" data points. Equations for the regression lines, number of data points in each sample (seeded and not-seeded) and correlation coefficients for each sample are also given.

HCTM with AREA

For all samples, the correlation coefficients between HCTM and AREA are quite low, always less than 0.5. But in all samples, the correlation coefficient between HCTM and AREA is much higher for the seeded storms than for the not-seeded storms. The seeded storms samples seem to contain the storms with the largest hailswath areas.

HCTM with SV3

Recall that severity ratio SV3 is the ratio of the area covered by walnut-sized and larger hailstones to the total hailswath area. The correlation coefficient between HCTM and SV3 is somewhat higher for seeded storms than for not-seeded storms, but the two correlation coefficients

TABLE 10
Correlations Between Various Predictor — Response Pairs for Not-Seeded and Seeded Storms Samples

(Differences between seeded (S) and not-seeded (N) samples have not been tested for statistical significance)

Row	Predictor-Predictand Pair	Sample	Number of Storms in Sample N	Number of Storms in Sample S	Correlation Coefficient N	Correlation Coefficient S	Direction of Results
1	HCTM-RMHS	All hailstorms from 1975 and 1976	96	101	0.55	0.62	S > N
2		All hailstorms from 1976	56	44	0.34	0.50	S > N
3		All hailstorms from 1975	40	57	0.76	0.71	S < N
4		All hailstorms from 1975 and 1976 with representative soundings and 5 or more hail reports	8	17	0.51	0.64	-
5	HCTM-MRT	All hailstorms from 1975 and 1976	86	99	0.74	0.73	S > N
6		All hailstorms from 1976	54	44	0.71	0.74	S = N
7		All hailstorms from 1975	32	55	0.77	0.72	S > N
8		All hailstorms from 1975 and 1976 with representative soundings and 5 or more hail reports	8	17	0.76	0.86	S > N
9	HCTM-AREA	All hailstorms from 1975 and 1976	51	65	0.14	0.39	S > N*
10		All hailstorms from 1976	30	26	0.04	0.48	S > N
11		All hailstorms from 1975	21	39	0.22	0.37	S > N
12		All hailstorms from 1975 and 1976 with representative soundings and 5 or more hail reports	8	17	0.07	0.32	S > N
13	HCTM-SV3	All hailstorms from 1975 and 1976	24	36	0.48	0.58	-
14		All hailstorms from 1976	14	14	0.21	0.10	S < N
15		All hailstorms from 1975	10	22	0.80	0.61	S = N
16		All hailstorms from 1975 and 1976 with representative soundings and 5 or more hail reports	8	16	0.84	0.69	-
17	MAXPE-RMHS	All hailstorms from 1975 and 1976	96	101	0.42	0.72	S > N
18		All hailstorms from 1976	56	44	0.17	0.67	S > N
19		All hailstorms from 1975	40	57	0.70	0.80	S < N
20		All hailstorms from 1975 and 1976 with representative soundings and 5 or more hail reports	8	17	0.44	0.72	-
21	MAXPE-MRT	All hailstorms from 1975 and 1976	86	99	0.49	0.60	S > N
22		All hailstorms from 1976	54	44	0.36	0.50	S > N
23		All hailstorms from 1975	32	55	0.70	0.64	S = N
24		All hailstorms from 1975 and 1976 with representative soundings and 5 or more hail reports	8	17	0.41	0.66	S = N
25	MAXPE-AREA	All hailstorms from 1975 and 1976	51	65	-0.02	0.49	S > N
26		All hailstorms from 1976	30	26	-0.05	0.63	S > N
27		All hailstorms from 1975	21	39	-0.02	0.48	S > N
28		All hailstorms from 1975 and 1976 with representative soundings and 5 or more hail reports	8	17	0.05	0.47	S > N
29	MAXPE-SV3	All hailstorms from 1975 and 1976	24	36	0.60	0.60	S < N
30		All hailstorms from 1976	14	14	0.42	-0.02	S < N
31		All hailstorms from 1975	10	22	0.71	0.63	S < N
32		All hailstorms from 1975 and 1976 with representative soundings and 5 or more hail reports	8	16	0.88	0.70	S < N

TABLE 10 continued

Row	Predictor-Predictand Pair	Sample	Number of Storms in Sample N	Number of Storms in Sample S	Correlation Coefficient N	Correlation Coefficient S	Direction of Results
33	PMXSZ-RMHS	All hailstorms from 1975 and 1976	96	100	0.50	0.70	S > N
34		All hailstorms from 1976	56	44	0.27	0.66	S > N
35		All hailstorms from 1975	40	56	0.75	0.75	S < N
36		All hailstorms from 1975 and 1976 with representative soundings and 5 or more hail reports	8	17	0.68	0.78	S = N
37	PMXSZ-MRT	All hailstorms from 1975 and 1976	86	98	0.53	0.56	S > N
38		All hailstorms from 1976	54	44	0.39	0.50	S > N
39		All hailstorms from 1975	32	54	0.73	0.58	S = N
40		All hailstorms from 1975 and 1976 with representative soundings and 5 or more hail reports	8	17	0.34	0.72	S = N
41	PMXSZ-AREA	All hailstorms from 1975 and 1976	51	65	0.00	0.50	S > N
42		All hailstorms from 1976	30	26	0.01	0.56	S > N
43		All hailstorms from 1975	21	39	-0.01	0.48	S > N
44		All hailstorms from 1975 and 1976 with representative soundings and 5 or more hail reports	8	17	0.30	0.60	S > N
45	PMXSZ-SV3	All hailstorms from 1975 and 1976	24	36	0.55	0.48	S < N
46		All hailstorms from 1976	14	14	0.40	-0.13	S < N
47		All hailstorms from 1975	10	22	0.62	0.54	S = N
48		All hailstorms from 1975 and 1976 with representative soundings and 5 or more hail reports	8	16	0.95	0.60	S = N

*Underlining of the entry in column (Direction of results) signifies that the difference is fairly large.

are still reasonably similar. The regression lines indicate little difference in the relationship between HCTM and SV3 for seeded and not-seeded storms.

However, for all the storms from 1976 sample (Table 10) there is very little relation between HCTM and SV3 for both seeded and not-seeded storms. On the other hand, for all the storms from 1975 a very high correlation between HCTM and SV3 is found for both seeded and not-seeded storms (Table 10). The regression lines derived suggest little difference in the relation between HCTM and SV3 for seeded and not-seeded storms.

MAXPE with RMHS

Note the very large difference in correlation coefficient for MAXPE with RMHS between the seeded and the not-seeded storms samples. This large difference is probably due to all the "outliers" in the not-seeded storms from 1976 sample. Because of these outliers, little confidence can be placed in the conclusion to be drawn from this sample, namely that for a given predicted parcel energy, seeded storms produced larger hail. However, for the storms of 1975, the correlation coefficient between MAXPE and RMHS is fairly similar for seeded and not-seeded storms and the derived regression results suggest that for a given predicted parcel energy, seeded storms produced slightly smaller hail than did not-seeded storms.

MAXPE and MRT

Note that the correlation coefficient between MAXPE and MRT is significantly lower for not-seeded storms than for seeded storms.

MAXPE with AREA

MAXPE (Parcel Energy) is shown plotted against AREA (Hailswath Area) in figure 4 for all hailstorms from 1975 and 1976. The results, summarized in table 10, are all quite similar for the subsets and the whole data set for these two parameters. Namely, a reasonably high correlation

coefficient between MAXPE and AREA is found for seeded storms and absolutely no correlation for not-seeded storms. All four samples also indicate considerably larger hailswath areas (for a given value of the predictor) for seeded storms than for not-seeded storms.

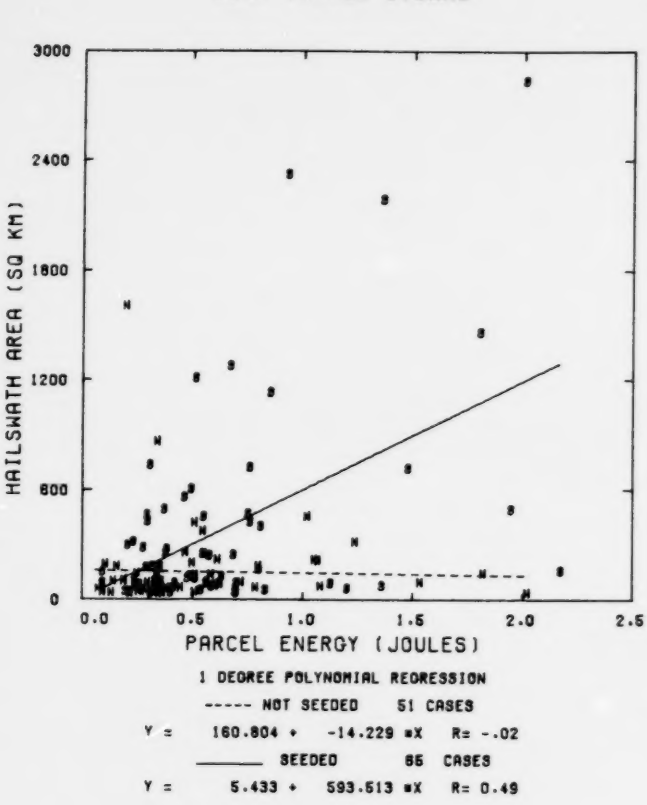

FIGURE 4. Scatter diagram of MAXPE (parcel energy) versus AREA (hailswath area.)

MAXPE with SV3

The four samples in table 10 all show similar results, that is, correlation coefficients between MAXPE and SV3 that are reasonably high and reasonably similar, for both the seeded and not-seeded storms samples, and regression lines that suggest a slightly higher severity ratio for not-seeded storms for a given value of predicted maximum parcel energy.

PMXSZ with RMHS

Figure 5 shows a scatter diagram of PMXSZ (Predicted Max Dia) versus RMHS (Reported Max Dia) for all storms from 1975 and 1976. (Both predicted maximum hailstone diameter and reported maximum hailstone diameter are known only in terms of six size categories. Data points have been plotted at the mean diameter for each size category. Since there exists only a limited number of possible positions on the graph of PMXSZ versus RMHS, many data points fall on top of each other.) Note that the correlation coefficient between PMXSZ and RMHS is significantly lower for the not-seeded storms sample than for the seeded storms sample. This effect is even more evident in the results for the storms of 1976 only.

PMXSZ with MRT

The results suggest that, for a given predicted maximum hailstone diameter, seeded storms grow a little taller than do not-seeded storms.

PMXSZ with AREA

All samples show the same results, that is, fairly high correlation, of the order of 0.5, between PMXSZ and AREA for seeded storms and absolutely no relation between the parameters for not-seeded storms.

PMXSZ with SV3

The regression lines for all samples lead to the same conclusion: there is little difference in severity ratio between seeded and not-seeded storms.

MULTIPLE LINEAR REGRESSIONS

For a number of the response variables, a stepwise least-squares multiple linear regression was performed to determine those predictor variables which could serve as useful covariates for evaluating a hail suppression project. Only predictor variables with partial correlations significant at the 5 percent level, or better, were chosen for the regression. Although a total of 208 storms were analyzed, the actual sample sizes for the various regressions are generally smaller because all missing values were simply deleted. The seeding predictors were not included in this analysis.

Some of the results are shown in table 11. In interpreting these results, one must note that all predictor variables derived from the model are related to one another. These predictor variables can be separated into three groups; one group consisting of variables that correlate highly with energy parameters, another group with water parameters, and a third group with both energy and water parameters. Thus, the fact that in one sample the best predictor for RMHS is PMXSZ and, in another sample it is MAXU, is of little consequence since PMXSZ and MAXU are highly correlated (correlation coefficient of 0.97).

However, the fact that for one sample HFZL is the best predictor of RMHS is significant. Another problem with the results in table 11 is that, for some response variables, in particular for AIE and AREA, the significance tests must be interpreted with caution as the regression residuals are not normally distributed.

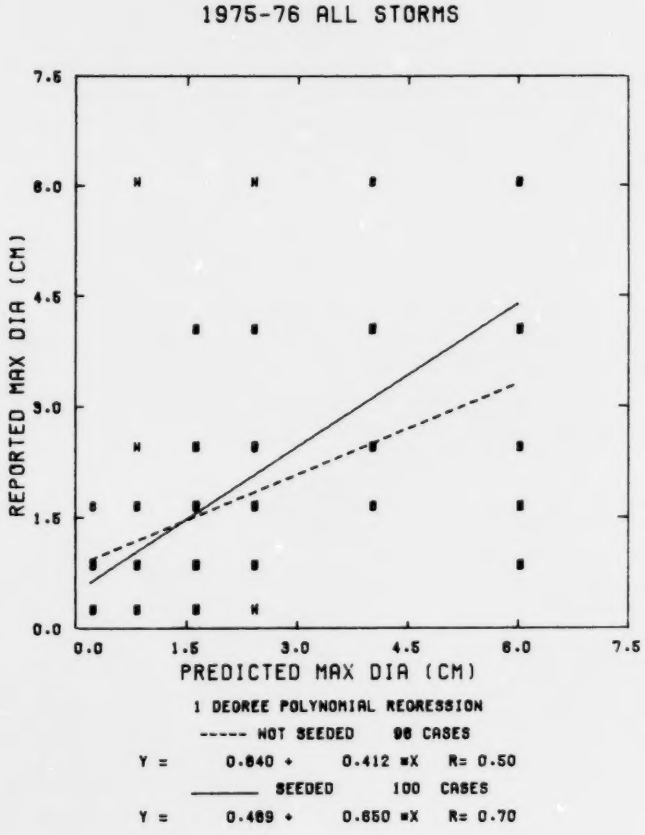

FIGURE 5. Scatter diagram of PMXSZ (predicted max. diam.) versus RMHS (reported max. diam.).

CONCLUSIONS

In spite of the poor accuracy of the data, easily obtainable predictor variables, that should be of major help in the evaluation of a hail suppression project, have been identified for some response variables. More accurate input data for the model should result in even higher correlation coefficients (English and Wong, 1976). Although differences in the regression results have been found between the seeded and not-seeded samples, and also between the storms of 1975 and those of 1976, these differences may be due largely to the inhomogeneity of the samples. This topic is addressed further in the next section.

HAILSTORM CLIMATOLOGY

COMPARISON BETWEEN THE STORMS OF 1975 AND THOSE OF 1976

In the second section, it was noted that the storms of 1976 often behaved differently from the storms of 1975. For a number of predictor-response pairs, correlations obtained for samples containing the storms of 1975 were significantly higher than the correlations obtained for samples containing the storms of 1976. It was suggested that one of the reasons for the differences were the large number of "outliers", especially "maximum hailstone size outliers" in the not-seeded storms of 1976 sample. But could there be other reasons as well? For instance, the method used to obtain cloud base could be expected to yield more accurate results for the very large storms and considerably less accurate results for the small storms. Could it be that the 1976 sample contains more small storms than the 1975 sample?

On average, the storms of 1975 had a higher, but colder cloud base and consequently a somewhat lower liquid-water content. However, the storms of 1975 sample contained a few, more, very low energy storms and a few, more, high energy storms than did the sample of 1976. The 1975 sample seems to have more storms at the extremes of the spectrum, whereas the 1976 sample has more storms in the middle of the spectrum. It is also apparent that, on average, the storms of 1975 produced larger hail than did the storms of 1976. The 1975 sample also contains some storms that were taller than the storms from 1976, but the 1975 sample also seems to contain a few shorter storms. The areas of the hailswaths of 1975 were about the same as those of 1976, but the frequency distribution of hailswath areas seems more continuous for the storms of 1975 than for the storms of 1976.

COMPARISON BETWEEN SEEDED AND NOT-SEEDED STORMS

Another common occurrence in the scatter diagrams shown in the previous section was radically different correlation coefficients for some of the predictor-response pairs between the seeded and not-seeded storms samples. It has already been shown that most of the "maximum hailstone size outliers" are in the not-seeded storms samples. These outliers were shown to be due mainly to storms that occurred at night or in the mountains; conditions under which little information is available for calculating cloud-base temperatures and heights. Furthermore, it seems possible that the not-seeded storms samples may contain a number of storms that

were really marginal, so marginal in fact that they were not seeded even though they did produce small hail. It seems entirely possible then that the "not-seeded" storm samples contain more small storms for which the predictors calculated would be quite inaccurate. To investigate this possibility, frequency distributions of some of the predictor and response variables were drawn for seeded and not-seeded storms.

TABLE 11
Multiple Regression Results

Sample	Response variable	Predictor variables chosen	Multiple correlation coefficient	Significance of multiple regression
All hailstorms from 1975 and 1976	RMHS (192 of 208)*	PMXSZ HFZL PCB	0.65	.0000
	AIE (162 of 208)*	MAXPE DSCL	0.46	.0000
	AREA (112 of 208)*	MAXPE	0.36	.0001
	MRT (180 of 208)*	HCTH HFZL	0.74	.0000
	SV3 (58 of 208)*	MAXPE	0.68	.0000
All not-seeded hailstorms from 1975 and 1976	RMHS (92 of 106)*	HFZL MAXLWC HCB	0.67	.0000
	AIE (76 of 106)*	MAXPE	0.42	.0002
	AREA	NO PREDICTORS CHOSEN		
	MRT (82 of 106)*	HCTH	0.74	.0000
	SV3 (23 of 106)*	MAXPE DSCL	0.85	.0000
All seeded hailstorms from 1975 and 1976	RMHS (100 of 102)*	MAXU	0.73	.0000
	AIE (86 of 102)*	MAXPE PCB	0.52	.0000
	AREA (65 of 102)*	PMXSZ	0.50	.0000
	MRT (98 of 102)*	HCTH	0.73	.0000
	SV3 (35 of 102)*	MAXPE	0.67	.0000

* Number of storms included in sample

On average, the seeded storms have slightly higher and colder cloud bases than do the not-seeded storms and consequently slightly lower liquid-water contents. Very little difference is shown in (predicted) maximum parcel energy between seeded and not-seeded storms. However, seeded storms tend to be just a little taller than not-seeded storms.

Turning to the response variables, it appears that the seeded storms produced slightly larger hail. A comparison of the seeded storms and the not-seeded storms distributions of maximum radar echo height suggests that the seeded storms sample contains just a few taller storms than does the not-seeded storms sample. Both in 1975 and in 1976, the storms with the largest hailswaths were invariably seeded. One possible reason for this may be that the storms with the largest hailswaths generally cross the boundary between the north and south project area. To check for this possibility, the frequency distributions of measured hailswath areas were recalculated, with all storms that crossed the boundary between the north and south project area omitted. But the areas of the seeded hailswaths are still somewhat larger than the areas of the not-seeded hailswaths.

DISTRIBUTIONS OF REPORTED MAXIMUM HAILSTONE DIAMETER

Carte and Held (1978) studied data derived from hail reports sent in, for many years, by a network of voluntary observers located in the vicinity of Pretoria and Johannesburg, South Africa. Among other results, they concluded that remarkably little variation from year to year is shown by certain variables, among them relative frequencies of the size categories for the largest and most common hailstones. As a matter of fact, they suggest that an operational hail suppression program could be evaluated by comparing frequency distributions of the sizes of the largest and most common hailstones occurring in a year for seeded years and for preceding years.

Results presented in the previous section have shown that, although minor differences were evident, no gross differences were found between seeded and not-seeded storms of 1975 and 1976, aside from the tremendous difference in hailswath area. Thus, frequency distributions of reported maximum hailstone size for seeded storms and for not-seeded storms could be compared, as well as a frequency distribution, for pre-seeding years with one for seeded years. By comparing frequency distributions of reported maximum hailstone size for the seeded storms of 1975 and 1976 and for the not-seeded storms of the same period, it is evident that the seeded storms produced somewhat more large hail than did the not-seeded storms. Furthermore, many more hail reports are received for seeded storms than for not-seeded storms. This almost suggests that seeded storms are surveyed more carefully. On the other hand, it could simply be a reflection of the fact that seeded storms generally have larger hailswaths.

It seemed worthwhile to investigate the natural variation in the frequency distribution of reported maximum hailstone size from year to year. Wojtiw (1975) gives data from which frequency distributions of reported maximum hailstone size can be calculated for the years 1956 to 1973. From these 17 frequency distributions, a 17-year average frequency distribution of reported maximum hailstone

size and the maximum deviation from the average in the 17 years for each size category were derived. All seeded and not-seeded storms frequency distributions for 1975 and 1976 storms lie well within the 17-year maximum deviation from the average.

It seemed interesting to compare the frequency distributions of reported maximum hailstone size for 1975 and 1976, when there was randomized seeding in the northern project area, with those of 1977 and 1978 when full operational seeding took place in both the north and south areas. The data suggests, that, in 1977, hail in the project area was smaller than it was in the years from 1956 to 1973 and, in 1978 it was as small as it was during 1956 to 1973. On the other hand, in 1975 hail was more or less as large as it was in the 17-year period. Since 1975 and 1976 can be considered to be three quarter seeded years and 1977 and 1978 full seed years, the trend is probably climatic to a large extent.

STORMS WITH NEGATIVE BUOYANCY AT CLOUD BASE

Marwitz (1973) suggested that negatively buoyant updrafts (at cloud base) are a common phenomenon of severe hailstorms in northeastern Colorado. Fankhauser and Mohr (1977) suggest that negative buoyancy at cloud base seems to act as a modulator of storm intensity by inhibiting premature release of potential instability. A search through the LMA model results for all the storms of 1975 and 1976 revealed that 116 of the 208 hailstorms had negative buoyancy at cloud base. According to the reasoning of Fankhuaser and Mohr, one would expect that the storms with negative buoyancy at cloud base would, on average, be more severe than the ones without negative buoyancy at cloud base. Thus, frequency distributions of some of the hailstorms parameters presented were recalculated for the storms with negative buoyancy at cloud base only and for the storms without negative buoyancy at cloud base only. Surprisingly, there is little difference, on average, between the two classes of storms.

SEEDING STATISTICS

It was mentioned previously that seeding methods changed between the summer of 1975 and 1976. For a detailed description of the reasoning behind the change and the new seeding method, see Barge *et al.* (1976). Prior to 1976, cloud-base seeding was conducted in the region of the strongest updraft at cloud-base and cloud-top flares were dropped into growing cloud towers; in 1976, both cloud-base seeding and cloud-top seeding were moved further out, away from the main storm, into the "new growth zone" of hailstorms. It is difficult to assess the effect of the change in location of the seeding, but changes in the intensity of the seeding can readily be documented. Much higher amounts of AgI were expended on some storms in 1976 than in 1975. Strangely enough, the rates of cloud-top and of cloud-base seeding were actually higher in 1975 than in 1976, but the cloud-base and cloud-top seeding times were considerably longer in 1976 than in 1975.

Considering the differences in seeding methods between 1975 and 1976, it appears possible that different relationships between the various predictor-response pairs might exist for the seeded storms from 1975 and for the seeded storms from 1976. The only consistent difference however, is that SV3, for a given value of any of the predictors, is always lower for the seeded storms from 1976 than for the seeded storms from 1975. Since all other results are not consistent, no conclusions can be drawn about the effect of changing the seeding techniques.

SUMMARY AND CONCLUSIONS

THE SIMULATION OF THE GROWTH OF HAIL EMBRYOS

Much of the groundwork for the development of a realistic model for simulating the growth of hail embryos has been accomplished. Preliminary results from the model should be available early in 1980. The model is expected to provide a firm theoretical basis for cloud seeding as a means of suppressing hail. It is also expected to allow considerable refinement of seeding methods and to test the efficacy of hail suppression with other seeding agents.

SIMPLE NUMERICAL CLOUD MODELS AS POTENTIAL TOOLS IN EVALUATING HAIL SUPPRESSION TECHNIQUES

The outstanding problem in evaluating a hail suppression project is determining what would have happened if no treatment had been applied to the storms. In this study, predictors calculated with a very simple numerical model are used to answer this question. In order to calculate these predictors, only a "representative" temperature and humidity sounding and a reasonably accurate cloud-base height and temperature are required. These measurements can be made before the storm is seeded.

Actually, how "representative" a sounding needs to be has not been established. When only storms with representative soundings are used, results sometimes improve significantly, but at other times, become worse. Using only storms with representative soundings reduces the sample size to one quarter of the original sample. Thus, it is impossible to separate the effects of the drastic reduction in sample size and of the representativeness of the sounding.

The model used is very sensitive to the specified cloud-base height and temperature. A number of ways of determining the cloud base for a given storm were investigated. Aircraft measurements were obviously best. The method used in this study requires surface temperatures and dew-point temperatures just ahead of the maximum development (as seen from radar data) of the storm. Mixing the lowest 75 mb of the sounding seemed to be the worst method of determining cloud base. If model predictors are to be used in any future evaluation of a hail suppression project, every effort should be made to obtain cloud base temperatures accurate to within ½ degree or better.

A total of fourteen predictors were calculated from the model. However, these predictors were all related to one another to some degree. A study of the correlations between the various predictors suggested that just two would be sufficient, a water predictor and a buoyancy (energy) predictor. Supplementary predictors were calculated from wind data and a number of seeding predictors were also calculated. The wind and seeding predictors were generally not related to the model predictors.

A number of response variables were calculated from hail reports made by voluntary observers; one response variable, the maximum radar echo height, was determined from radar data. As was the case with the predictors, most of the response variables were found to be related to one another to some degree.

The correlations between all possible predictor-response pairs were calculated and a number of predictor-response pairs were identified for which the correlation coefficients were in the range 0.5 to 0.8. Predictors which correlated highly with some of the response variables were almost always of the model type; the wind and seeding predictors were found to correlate highy with a response variable only very occasionally, and in such cases, it was generally a response variable based on hailswath area. A number of regression models were developed which give a (multiple) correlation in the range 0.5 to 0.8. The most important predictor seemed to be MAXPE and its derivations (such as MAXU and PMXSZ). This agrees with the findings of Foote and Mohr (1979). The height of the freezing level (HFZL), cloud depth (CLDPT) and cloud base parameters such as PCB, HCB and TCB also seemed to be significant predictors.

Only very simple response variables have been used in this study. Presumably, more powerful response variables could be obtained from radar data or hailpad data. Possibly a combination of several simple response variables could be used to devise a better measure of the hail produced by a storm.

Some differences were found in the results for the two years. These differences have been ascribed largely to the large number of "outliers" in the 1976 data sample and also to the fact that the storms from 1975 represent a more even spread over the whole spectrum of hailstorm intensity than do the storms of 1976.

Some differences have also been found between seeded and not-seeded storms. It must be pointed out here that most of these differences have not been tested for statistical significance. An investigation of the frequency distributions of various hailstorm parameters for seeded and not-seeded storms showed that such differences cannot be attributed to sample differences, that is, the storms in the seeded samples are not materially larger or smaller than the storms in the not-seeded samples. Subjectively evaluating the differences found, there is no difference in maximum storm height between seeded and not-seeded storms. Most likely there is also no difference in maximum hailstone size between seeded and not-seeded storms. There seems to be a definite trend, however, for seeded storms to have larger hailswaths than not-seeded storms.

The correlation coefficients between the various predictors and AREA are mostly rather small. It is clear that no adequate predictors have been found for the area of a hailswath. It is possible, therefore, that the observed difference in hailswath area between seeded and not-seeded storms is due to some climatic factor.

Summers (1978), upon reanalyzing the data from the Nelspruit project (Mather, 1977), concluded that the severity ratio decreased on days when seeding occurred because the total "area hit by hail" apparently increased by 19 to 33 percent. (Mather defined his severity ratio as the ratio of the "area damaged to 100 percent" to the total "area hit by hail".) Summers further concluded that the "area damaged to 100 percent" was more or less the same on seeded and not-seeded days. In the present study, it was found that, for a given value of any of the predictors used, the severity ratio was smaller for seeded storms than for not-seeded storms, but the hailswath area was larger for seeded storms than for not-seeded storms. (Here, severity ratio is defined as the ratio of the area covered by walnut or larger hailstones to the total hailswath area.)

Chapell *et al.* (1971) found that, under certain conditions, the duration of precipitation from cold orographic clouds could be increased by seeding with ground generators. If seeding with AgI can increase the duration of precipitation from orographic clouds, it is conceivable that it could also increase the duration of precipitation in a hailstorm.

An increase in the duration of the hailfall from a hailstorm would generally result in an increase in the hailswath area.

In calculating all the predictors and response variables, a wealth of climatological information was accumulated on the storms of 1975 and 1976. These data could be very useful in planning future weather modification experiments.

ACKNOWLEDGMENTS

The members of the Cloud Modelling Group are very grateful to the Alberta Weather Modification Board for funding these projects. We are also deeply indebted to Dr. G.G. Goyer for much helpful guidance. R.K.W. Wong, of the Evaluation Group, provided considerable assistance with some of the statistical aspects of this study. The Storm Environment Group provided considerable sounding data.

REFERENCES

Barge, B.L. and F. Bergwall, 1976: Fine scale structure of convective storms associated with hail production. Report 76-2, Atmospheric Sciences Division, Alberta Research Council, Edmonton, Alberta. In two volumes.

_____, _____, G.G. Goyer, and J.H. Renick, 1976: Fine scale structure of convective storms — implications for cloud seeding in Alberta. Report 76-3, Atmospheric Sciences Division, Alberta Research Council, Edmonton, Alberta, 19 pp.

Barlow, F.D., B. Kochtubajda and M. English, 1980: Predictor and response variables for the hailstorms of 1975 and 1976. Natural Resources Notes 80-1, Atmospheric Sciences Department, Alberta Research Council, Edmonton, Alberta, 60 pp.

Browning, K.A. and G.B. Koote, 1976: Airflow and hail growth in supercell storms and some implications for hail suppression. Quarterly Journal of the Royal Meteorological Society, 102, pp. 499-533.

Carte, A.E. and G. Held, 1978: Variability of hailstorms on the South African Plateau. Journal of Applied Meteorology, 17, pp. 365-373.

Chappell, C.F., L.O. Grant and P.W. Mielke, Jr., 1971: Cloud seeding effects on precipitation intensity and duration of wintertime orographic clouds. Journal of Applied Meteorology, 10, pp. 1006-1010.

Cherry, N. and R.R. Rogers, 1972: The interaction of Alberta hailstorms with environmental air. Report 72-2, Atmospheric Sciences Division, Alberta Research Council, Edmonton, Alberta, p. 17.

Chisholm, A.J., 1970: Estimate of precipitation growth environment in the updraft core of Alberta hailstorms. Preprints, Conference on Cloud Physics, Ft. Collins, AMS, Boston.

_____, and M. English, 1973: Alberta hailstorms. Meteorological Monographs, 14, 98 pp.

_____, and J.H. Renick, 1972: The kinematics of multicell and supercell Alberta hailstorms. Report 72-2, Atmospheric Sciences Division, Alberta Research Council, Edmonton, Alberta, pp. 124-131.

English, M., 1973: Alberta hailstorms, Part II: Growth of large hail in the storm. Meteorological Monographs, 14, pp. 37-98.

_____, 1976: Current research in hailstorms and their modification: Numerical modelling program. Report 76-1. Atmospheric Sciences Division, Alberta Research Council, Edmonton, Alberta, pp. 21-33.

_____, 1977: Current research on hailstorms and their modification. Cloud Modelling: A possible role for simple numerical cloud models in the evaluation of a hail suppression project. Report 77-3. Atmospheric Sciences Division, Alberta Research Council, Edmonton, Alberta, pp. 21-27.

English, M., B.L. Barge and R.G. Humphries, 1980: Cloud physics research aircraft program: Summary of operations and preliminary aircraft and radar observations. Atmospheric Sciences Department, Alberta Research Council, Edmonton, Alberta. In preparation.

_____, and R.K.W. Wong, 1976: Simple numerical cloud models as potential tools in evaluating hail suppression techniques; WMO International Conference on Weather Modification, WMO , Geneva, Switzerland, pp. 357-361.

Fankhauser, J.C., 1976: Structure of an evolving hailstorm, Part II: Thermodynamic structure and airflow in the near environment. Monthly Weather Review, 104, pp. 576-587.

_____, and C.G. Mohr, 1977: Some correlations between various sounding parameters and hailstorm characteristics in northeast Colorado. Preprints, 10th Conference on Severe Local Storms, Omaha, pp. 218-225.

Flueck, J.A. and P.W. Mielke, Jr., 1977: Design and evaluation of hail suppression experiments. Meteorological Monographs, 16, pp. 225-235.

Foote, G.B. and C.G. Mohr, 1979: Results of a Randomized Hail Suppression Experiment in Northeastern Colorado, Part VI, Post-Hoc Stratification by Storm Intensity and Type. Journal of Applied Meteorology, 18, 1589-1600.

Goyer, G.G., 1975: Time-integrated radar echo tops as a measure of cloud seeding effects. Journal of Applied Meteorology, 14, pp. 1362-1365.

Hirsch, .H., 1971: Computer modelling of cumulus clouds during project Cloud Catcher. Report 71-7. Institute of Atmospheric Sciences, South Dakota School of Mines and Technology, Rapid City, South Dakota, 61 pp.

Hudson, H.R., 1970: On the relationship between horizontal moisture convergence and convective cloud formations. ESSA Technical Memorandum, ERLTM-NSSL45, NSSL, Norman, Oklahoma.

Kochtubajda, B., and M. English, 1980. The areal distribution of hailfall for 1975 and 1976. Atmospheric Sciences Department, Alberta Research Council, Edmonton, Alberta. In preparation.

Mahrt, L., 1977: Influence of low-level environment on severity of High Plains moist convection. Monthly Weather Review, 105, p. 1315.

Marwitz, J.D., 1972: The structure and motion of severe hailstorms. Parts I, II and III. Journal of Applied Meteorology, 11, pp. 166-201.

———, 1973: Non-hydrostatic pressures in severe thunderstorms. Preprints, 8th Conference on Severe Local Storms, Denver, pp. 14-17.

Mather, G.K., 1977: An analysis of a possible crop response to hail suppression seeding: The Nelspruit Hail Suppression Project. Journal of Applied Meteorology, 16, pp. 959-970.

Maxwell, B., 1974: Alberta hail project field program 1974: Meteorological Section. Report No. 1. Interim Weather Modification Board, Alberta Agriculture, Three Hills, Alberta, pp. 20-21.

Newton, C.W., 1966: Circulations in large sheared cumulonimbus. Tellus, 18, pp. 699-713.

Renick, J.H., and J.B. Maxwell, 1977: Forecasting hailfall in Alberta. Meteorological Monographs, 16, pp. 145-151.

Robitaille, F., C. Sackiw, J. Mason and F. Barlow, 1979: The Storm Environment Program, Atmospheric Sciences Report 79-1, Volume 2.

Summers, P.W., 1978: Comments on "an analysis of a possible crop response to hail suppression seeding: The Nelspruit Hail Suppression Project". Journal of Applied Meteorology, 17, pp. 1084-1090.

Warner, C., 1976: Case studies of seeded Alberta hailstorms. Scientific Report MW-86. Stormy Weather Group, McGill University, Montreal, Canada, 72 pp.

Wojtiw, L., 1975: Climatic summaries of hailfall in Central Alberta (1957 - 1973). Report 75-1. Atmospheric Sciences Division, Alberta Research Council, Edmonton, Alberta, 101 pp.

Wong, R.K.W., 1977: Further analysis of the Alberta hailcrop insurance data. Report 77-3. Atmospheric Sciences Division, Alberta Research Council, Edmonton, Alberta, pp. 73-97.

APPENDIX

DETERMINING THE CLOUD BASE

The correlation between predicted and reported maximum hailstone size, with the predicted size being obtained from the LMA model and the Maxwell nomogram, for some hail days from the summer of 1975 was investigated by English and Wong (1976). They found that when aircraft-measured, cloud-base parameters were used as input into the models, along with a "representative" temperature and humidity sounding, a statistically significant correlation coefficient of about 0.85 was obtained for predicted and reported maximum size. However, aircraft-measured cloud-base temperature and height are available only for seeded storms, since these measurements were made by the pilots of the seeding planes. Thus, alternate methods for obtaining reasonably accurate cloud-base parameters were investigated.

Cherry and Rogers (1972) analyzed a number of serial temperature and humidity soundings taken at Penhold on three days when storms passed close to Penhold. They concluded that the LMA model gives cloud bases and storm tops that are consistent with those observed, when the initial parcel is obtained by mixing adiabatically the air from the lowest 300 to 500 m of the atmosphere. Fankhauser and Mohr (1977) assumed mixing to occur in the lowest 50 mb for storms in northeast Colorado. (This corresponds, approximately, to the 500 m of Cherry and Rogers.) However, Hudson (1970) suggests mixing the lowest 100 mb. Therefore, as a first attempt, cloud bases were determined by mixing the lowest 75 mb of the atmosphere.

One criterion used by Cherry and Rogers (1972) to determine the depth of the mixing layer was that the storm top predicted by the LMA model be equal to the measured radar echo top of the storm. It seems reasonable, then, to use the measured radar echo top to derive the cloud base to be used as input into the LMA model. Thus, for a given storm, the LMA model was run with a variety of cloud-base heights and temperatures and the cloud-base parameters that gave the best agreement between the predicted and observed storm top were then used to determine other model predictions such as maximum hailstone size.

Mahrt (1977) who studied the influence of the low-level environment on the severity of High Plains convection, concluded that the mixed layer tends to be thinner and more moist on hail days compared to cumulus congestus days. This suggests that using a standard mixing layer depth to determine cloud base would tend to underestimate convection on severe storm days and overestimate it on less severe days. Indeed, English and Wong (1976) found that, when cloud base was determined by mixing the lowest 75 mb, both the LMA model and the Hirsch model underestimate the hailstone size considerably on days when hailstorms occur, and overestimate the convection on days when no storms occurred. (This suggests further that if a standard mixing layer depth is used to determine cloud base, a model such as the LMA model cannot be used to predict the occurrence of hail on a yes-no basis.) Marwitz (1972), Browning and Foote (1976) and Fankhauser (1976) lead to the conclusion that after development of severe, well-organized, moist convection, updrafts seem to originate close to the surface. Furthermore, Chisholm and English (1973) and Renick and Maxwell (1977) used surface temperatures and surface dew-point temperatures just ahead of the maximum radar development of a storm to determine cloud base. Thus cloud bases were also determined from surface observations ahead of the storms.

English (1977) compared correlation coefficients obtained between predicted and reported maximum hailstone size when cloud bases were determined, by the various methods, for a sample of hailstorms for which aircraft-measured, cloud-base parameters were available. A correlation coefficient of 0.92 was obtained when aircraft-measured cloud bases were used, of 0.83 when cloud bases were determined from radar echo tops and of 0.40 when cloud bases determined by mixing the lowest 75 mb were used. A correlation coefficient of about 0.7 was obtained when cloud bases determined from surface temperature and dew-point temperatures were used. When aircraft-measured, cloud-base heights and temperatures for 14 hail days from 1975 were compared with relevant soundings, English and Wong (1976) found that on those days little mixing occurred and thus surface temperatures and dewpoint temperatures would give cloud bases in better agreement with the aircraft measurements.

Since there has been some suggestion that storm tops could be affected by seeding (Goyer, 1975) cloud bases have been determined from surface temperatures and dew-point temperatures for the results presented in this report.

THE CLOUD PHYSICS PROGRAM

M. English

T. Krauss

TABLE OF CONTENTS

	Page
Introduction	51
The basic concept	51
The cloud physics research aircraft program	51
Secondary projects	52
The data collected	52
Thunderstorm penetrations	52
Procedure	52
The Rocky Mountain House storm	53
A typical cloud turret from the Rocky Mountain House storm	54
Cumulus penetrations and dry ice experiments	56
Cumulus penetrations	56
Dry ice experiments	56
The procedure	58
The first dry ice experiment — 15 August	58
The second dry ice experiment — 18 August	58
Comparison of a seeded and a not-seeded cloud	58
The data available	58
The not-seeded cloud	58
The seeded cloud	60
Conclusion	63
The bright band study	64
Introduction	64
Results	64
Summary and Conclusions	67
Summary	67
Conclusions	67
Suggestions	68
Acknowledgments	68
References	69
Appendix A	71
Appendix B	73

ILLUSTRATIONS

Page

Figure 1. Synthesis of a hailstorm showing hypothesized regions of hailstone embryo birth and growth, and hail growth 51
Figure 2. Cloud photograph taken from the spotter aircraft at 1657 of southeastern side of Rocky Mountain House storm 53
Figure 3. Photograph of thin sections of a few hailstones collected from the Rocky Mountain House storm 54
Figure 4. Radar echo of Rocky Mountain House storm at 1550 MDT and at an elevation of 1.9 degrees 55
Figure 5. An example of a cloud droplet spectrum measured in a turret of the Rocky Mountain House storm 55
Figure 6a. Images from the 2D-C probe in a typical updraft region of cloud turrets associated with the Rocky Mountain House storm 57
Figure 6b. Images from the 2D-C probe in a typical downdraft region of cloud turrets associated with the Rocky Mountain House storm 57
Figure 7. Liquid water content and ice crystal concentration from the 2D-C probe 59
Figure 8. Images recorded by the PMS 2D-C probe during the first penetration of the not-seeded cloud 61
Figure 9. Images recorded by the PMS 2D-C probe during the sixth (last) penetration of the not-seeded cloud 62
Figure 10. Particle images recorded by the PMS 2D-C probe during the first two penetrations of the seeded cloud, before seeding with dry ice 63
Figure 11. Particle images recorded by the PMS 2D-C probe during the third penetration of the seeded cloud, i.e. the first penetration after this dry ice seeding 64
Figure 12. Particle images from the sixth penetration of the seeded cloud, the last penetration at the -9°C level 65
Figure 13. Vertical cross-section for the bright band study flight and the corresponding S-band radar reflectivity 66
Figure 14. Size distribution of particles measured by the 2D-C probe at different elevations on 16 August 1978 66

TABLES

Table 1. Properties of a typical cloud turret from the Rocky Mountain House storm 56
Table 2. Summary of observations made in penetrations of the not-seeded cloud 61
Table 3. Summary of observations made in penetrations of the seeded cloud ... 62

APPENDICES

Appendix A. Summary of hailstorms penetrated by the cloud physics research aircraft 70
Appendix B. Summary of cumulus clouds penetrated by cloud physics research aircraft 72

THE CLOUD PHYSICS PROGRAM

Marianne English

Terry Krauss

INTRODUCTION

THE BASIC CONCEPT

The study of "fine scale reflectivity patterns" by Barge and Bergwall (1976) lead to the hypothesis that hailstone embryos originate in the rather weak convective zone near the upwind edges of the storm, designated the "new growth zone". Apparently, hail starts to grow in this zone well before the first echoes are received from cloud turrets; the hail then develops within time-dependent updrafts and finishes growing in the mature storm (Fig. 1). Marwitz (1978) came to similar conclusions through the study of vertical streaks in radar echoes of thunderstorms.

During the first three years of the Alberta Weather Modification Board's five-year hail suppression project, seeding was conducted on the mature portion of the storm at cloud base, in the region of the most intense updraft, and at cloud top on the well developed cloud turrets. As a result of the findings of Barge *et al.* (1976) the seeding methodology was changed so that, ideally, only the new growth zone would be seeded. It was reasoned that if hail growth starts in the new growth zone, then conditions must be altered there in order to affect the growth of hail.

The current seeding methodology in Alberta is therefore dependent upon the hypothesis that hail embryos originate on the fringes of storms in the new growth zone. It is essential that this hypothesis be examined and verified in detail. Furthermore, it seems highly desirable to quantify the conceptual model by developing a numerical model that is consistent with it. Since statistical evaluations of hail suppression projects have generally been inconclusive so far, one hopes to deduce reasonably firm answers to the question of what effect cloud seeding may have on the production of rain and hail through a *realistic* numerical model.

THE CLOUD PHYSICS RESEARCH AIRCRAFT PROGRAM

Cloud photography observations suggest that particles sufficiently large to grow into hail embryos in about 10 min must be present in the new growth zone if hail embryos are to originate there. Innovative radar techniques have been used to glean information on the first echo stage (Renick, 1971) and the mature stage (Chisholm and English, 1973) of Alberta hailstorms, but the new growth zone cannot be examined in a like manner. Only a well-instrumented, cloud physics research aircraft can

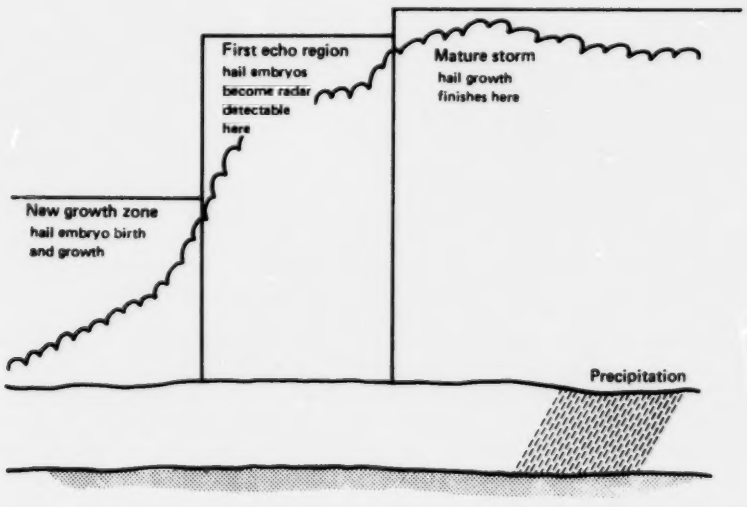

FIGURE 1. Synthesis of a hailstorm showing hypothesized regions of hailstone embryo birth and growth, and hail growth.

measure particle size in the new growth zone. The cloud physics research aircraft program was designed to obtain the required measurements.

As part of this program, the Alberta Research Council contracted with the University of Wyoming for the operation of their Queen Air in conjunction with the Alberta Hail Project during the first three weeks of August 1978. The Alberta Research Council also initiated the sponsorship of a graduate student in cloud physics at the University of Wyoming. This graduate student played the role of technician on board the Queen Air. Many members of the Atmospheric Sciences Division of the Alberta Research Council and staff of the Alberta Weather Modification Board, as well as staff of Intera Environmental Consultants, contributed greatly to the field project of the cloud physics research aircraft program.

The cloud physics research aircraft field project is described in detail by English *et al.* (1979).

SECONDARY PROJECTS

The primary objective of the cloud physics research aircraft program was to obtain aircraft measurements necessary to test the proposed conceptual model, to derive a numerical model and to test with these models the effects of cloud seeding on the growth of hail and rain. As storms do not occur on every day in August and to fully utilize the research aircraft, a number of secondary projects were designed to be carried out when the weather was not suitable for the primary objective. The secondary projects are listed below in order of priority.

(A) Cumulus Penetrations
Cumulus clouds of various sizes and in different locations were penetrated in support of a rain augmentation study. A few of these cumulus clouds were seeded with dry ice to stimulate the growth of precipitation.

(B) Rocky Mountain House Area Genesis Study
On one convective day, the aircraft flew at a low level along the mountains measuring temperature, humidity and wind. This experiment is expected to shed some light on preferred regions for hailstorm formation.

(C) Bright Band Study
A radar phenomenon called a "bright band" is often observed on days with widespread rain. Whereas considerable data have been collected worldwide, by observing bright bands with conventional weather radars, very few polarization radar data, in conjunction with cloud physics aircraft data, have been collected on bright bands. Thus, during a classic bright-band situation, the cloud physics research aircraft made several passes over a disdrometer site, flying above, at and below the 0°C level to measure particle types and sizes.

(D) Collecting Water Samples
About 5 bags of rain or cloud water, from approximately cloud-base level, were collected for isotope analysis.

THE DATA COLLECTED

Details concerning the data collected for both the primary and secondary objectives can be found in English *et al.* (1979). In summary, a total of 24.2 hours of research missions were flown by the Queen Air from 7 to 18 August (1978), inclusive. About 11.2 hrs were spent on thunderstorm penetrations (the primary objective), 7.8 hrs on cumulus penetrations, 3.4 hrs on a Rocky Mountain House Area Genesis Study flight and 1.8 hrs on a bright-band, study flight. Clearly, analyses of the data collected are still in their infancy. However, a few, preliminary results are already available. The results gathered so far from the cloud-physics data will be discussed in this report. Thus, this report covers the primary objective (thunderstorm penetrations) as well as the cumulus penetrations and a portion of the bright-band study. Since the Rocky Mountain House Area Genesis Study involved no cloud-physics data, results from this flight will be discussed by the Storm Environment Group. No results are available from the water samples.

THUNDERSTORM PENETRATIONS

PROCEDURE

On a day when thunderstorms were expected, the Research Operations Director would watch the radar screen for signs of a storm suitable for penetration by the research aircraft. Once a suitable storm was detected, the research aircraft was directed to launch and proceed to the storm. Provided it was not required for seeding, another project aircraft with an observer/photographer onboard would be launched soon after the research aircraft was directed to take off. Observations from this "spotter aircraft" together with ground-radar information would be used to determine clouds suitable for penetration by the research aircraft. Once a target was chosen, "the spotter aircraft" would fly in a location suitable for photographing the cloud. Typically this would mean an altitude of about 6 km at about 16 km in front of the storm. If the storm to be penetrated appeared to be reasonably steady-state and long-lasting, the cloud physics research aircraft would first make a number of penetrations at about the – 10°C level at various horizontal distances from the edge of the radar echo of the storm. Then, it would slowly descend to cloud base making a number of penetrations en route. If time permitted, the aircraft would again climb to about the – 10°C level, making more penetrations. With short-lived, non-steady storms, the research aircraft would simply penetrate repeatedly at about the – 10°C level until the storm decayed.

In all, seven hailstorms were penetrated in the manner described above. These seven storms are described, and the data collected on them are summarized, in Appendix A. Of the seven storms, the Rocky Mountain House Storm is perhaps the best case study obtained during the cloud physics research-aircraft field project. The data analyses, to date, have concentrated on this storm. Although analyses on the Rocky Mountain House Storm are still in early stages, a few, very preliminary results are already apparent. These are given in the next sections.

THE ROCKY MOUNTAIN HOUSE STORM

A complete radar echo history of the storm, as well as some cloud photographs, temperature and humidity soundings and hailswath map are shown in English *et al.* (1979). The storm reached its maximum reflectivity of 67 dBZ at about 1650 MDT. The location of maximum reflectivity and maximum cloud tower growth seemed to fluctuate continuously from the very southern tip of the main storm to the southeast. At about 1640 MDT, a new echo formed just to the west of the southernmost tip of the storm. A photograph of the new growth zone, on the southeastern side of the storm, taken from the spotter aircraft at about the time of maximum reflectivity is shown in figure 2.

One sample of hailstones from the Rocky Mountain House storm was obtained. This sample has been analyzed by N.C. Knight (of the National Center for Atmospheric Research) with a view to determining the type of embryos which produced the stones. She reports (private communications) that all 28 stones in the sample had graupel embryos. A photograph of some thin sections of a few of the 28 stones is shown in figure 3. Note that conical graupel embryos are clearly visible.

Approximately 14 cloud penetrations were made on the Rocky Mountain House storm during the time period 1543 to 1748. A list of the events when the liquid-water content, as measured by the Axially Scattering Spectrometer Probe (ASSP), was 0.2 gm ^{3} or greater was made. (Each event is a 10 sec average.) The list contains 84 events, thus the data set corresponding to the 84 events constitutes 840 sec or 14 min of in-cloud data. From these 14 min of in-cloud data, a set of distribution curves has been compiled of some of the parameters measured during the cloud penetrations. These distribution curves, therefore, give a good indication of the characteristics, and in a sense constitute a climatology, of the "typical", or average, cloud turret in the new growth zone for this particular storm. This "typical" cloud turret is discussed more fully in the next section.

FIGURE 2. Cloud photograph taken from the spotter aircraft at 1657 of southeastern side of Rocky Mountain House storm.

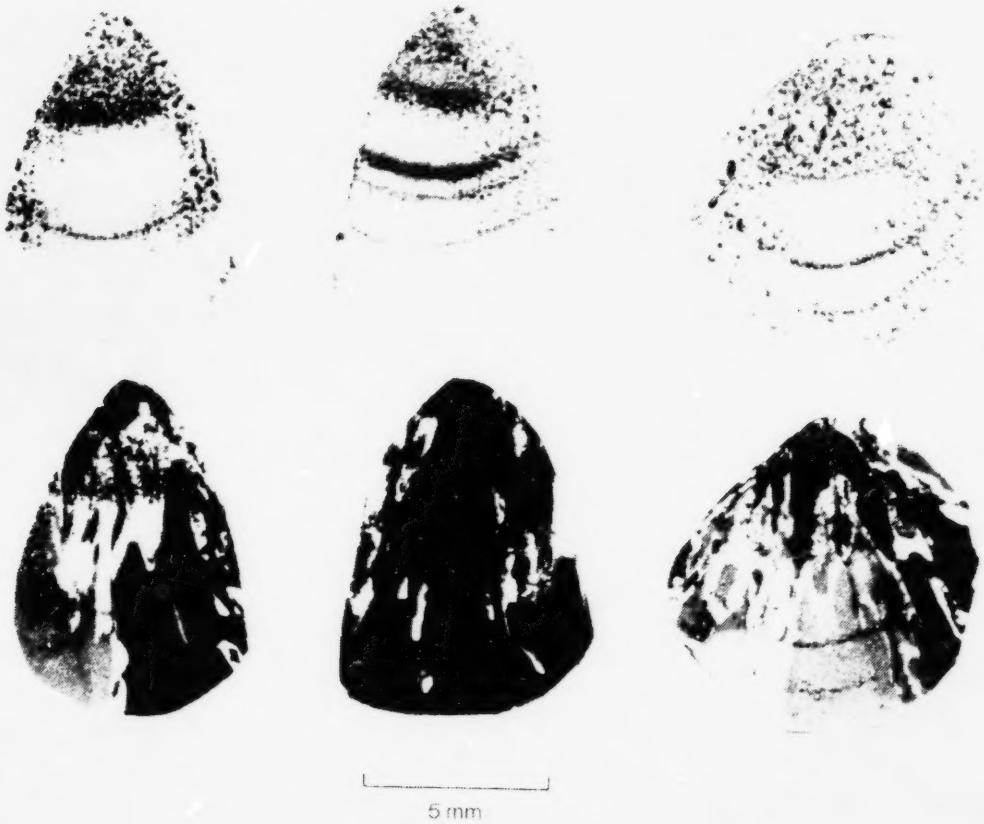

FIGURE 3. Photograph of thin sections of a few hailstones collected from the Rocky Mountain House storm (courtesy of N.C. Knight).

A TYPICAL CLOUD TURRET FROM THE ROCKY MOUNTAIN HOUSE STORM

The radar echo of the Rocky Mountain House storm at 1550:52 MDT is shown in figure 4. The PPI is at the 1.9 elevation angle (approximately 10,900 ft or 3.3 km above ground level) and the contours indicate equivalent radar reflectivity in 10 dBZ intervals, starting at 20 dBZ. A portion of the research aircraft flight track is also shown.

As mentioned earlier, 14 min of in-cloud data were collected during penetrations in the new growth zone. A typical cloud penetration lasted for approximately 1 min. The true air speed of the aircraft was typically 75 ms $^{-1}$. Thus the average horizontal dimension of the typical cloud turret was approximately 4.5 km.

Most of the penetrations occurred at altitudes between 4.4 and 4.8 km, predominantly in the temperature range of -6 to -10°C.

The typical θ_e value (potential temperature) within cloud was near 322° K. By comparison, the environmental value for θ_e at the 4.6 km level was near 316 K. This suggests tremendous buoyancy inside the cloud turrets.

Typical, cloud-droplet, number concentrations were 300 to 500 cm^{-3}. Maximum liquid-water contents observed were near 1.8 gm^{-3}. The liquid-water content as measured by the Johnson - Williams device showed good agreement with that measured by the ASSP. The mean cloud-droplet diameter for the cloud-droplet spectra as measured by the ASSP was near 14 μm. A typical cloud-droplet spectrum is shown in figure 5. The concentration of particles > 25 μm, computed from images recorded by the PMS 2D-C probe, was typically less than 1 per liter (1 l^{-1}), although particle concentrations in excess of 50 l^{-1} were found to occur approximately 2.5 percent of the time. These particles are generally ice crystals or graupel particles; no images indicative of raindrops were found.

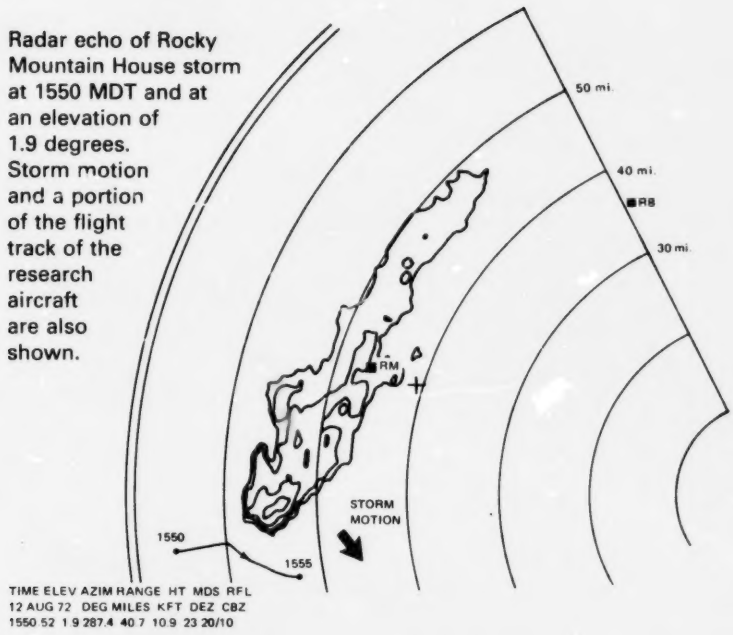

FIGURE 4. Radar echo of Rocky Mountain House storm at 1550 MDT and at an elevation of 1.9 degrees. Storm motion and a portion of the flight track of the research aircraft are also shown.

The PMS 2D-C probe scans a volume along the flight path of the aircraft and records the two dimensional images of all particles lying in that volume. The sample volume is approximately 4 ls^{-1}. The probe is generally operated with the aperture aligned vertically, so that the two-dimensional images are those that would correspond to a view of the particles from above. The resolution of the probe is 25 μm in both dimensions, and this is also the minimum-detectable particle size. Images are recorded as bit patterns on magnetic tape. There are 32 independent elements (bits) and so the maximum dimension measurable is 32 × 25 μm = 800 μm. The images recorded by the 2D probe can generally be classified as raindrops, graupel or ice crystals, and artifacts. Raindrop images are smooth and round (Cooper, 1978), graupel particles are rough and produce an irregular shape. Artifacts are usually streakers, (images produced by water shedding across the upstream edge of the probe and across the aperture). Streakers are usually long compared to their widths, for example, six times as long as they are wide.

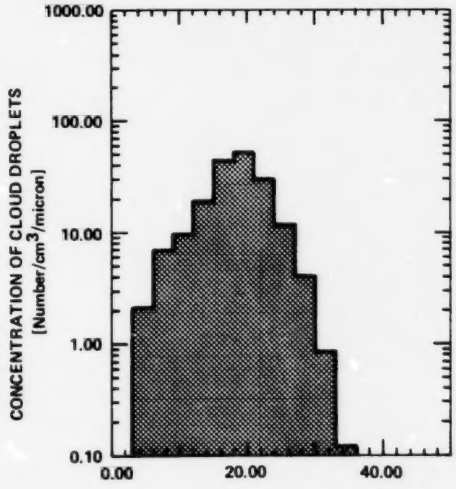

FIGURE 5. An example of a cloud droplet spectrum measured in a turret of the Rocky Mountain House storm. The mean diameter ($\bar{D}$) is 16.7 μm and the coefficient of dispersion ($\sigma/\bar{D}$) is 0.29. The droplet spectrum represents a 5 second average during the time period 1551:00 to 1551:05. The number concentration (N) is 543 cm^{-3} and the liquid water content is 1.63 gm^{-3}.

Images from the 2D-C probe in a typical updraft region from 1551:05 to 1551:08 are shown in Figure 6(a). The "streaker" images are indicative of liquid water streaming off the probe. No large particles were detected. In figure 6(b), images are shown from the 2D-C probe for a downdraft region from 1551:12 to 1551:21 MDT. The images in the downdraft region are indicative of rimed, plate-like ice crystals, approximately 300 μm in diameter and about 10 l^{-1} in concentration.

Both updrafts and downdrafts were experienced with equal incidence. Apparently, the predominant wind direction was between 200 and 270 degrees, or, approximately southwesterly. The typical wind speed for this day was near 10 ms^{-1}. The eddy dissipation rate computed from the MRI turbulence meter measurement was commonly near 120 cm^2s^3. The measurements described above are summarized in table 1. These preliminary observations show that the cloud turrets in the new growth zone are vigorous and contain much supercooled water. The horizontal motions show that these turrets are moving towards the main storm approximately at right angles to the storm motion. They would travel the distance to the storm in about 15 min. The cloud-droplet spectra indicate that the Alberta hailstorm is more maritime in nature than the severe storms which have been extensively studied in Colorado and Montana (see Cannon *et al.*, 1974 for Colorado and Cooper, 1978 for Montana).

CUMULUS PENETRATIONS AND DRY ICE EXPERIMENTS

CUMULUS PENETRATIONS

Cumulus penetrations were carried out on five days. These five days are described, and the data collected is summarized, in Appendix B. By 12 August, a reasonable amount of data had already been collected on towering cumulus clouds in Alberta. It seemed timely to try to determine the possible effect of introducing artificial ice crystals into the clouds.

DRY ICE EXPERIMENTS

Would the microphysics of clouds with artificial ice crystals be different from that of natural clouds? If changes in the microphysics were produced by artificial ice crystals, would (or could) those changes hasten the growth of rain? To answer such questions, a few, dry-ice, seeding experiments were conducted; the logistics of seeding with dry ice were tested on 12 August.

Although AgI has been used for all cloud seeding in Alberta in the past five years, these cumulus, cloud-seeding experiments were conducted with dry ice as the seeding agent. Dry ice was used primarily because it produces an immediate effect. Thus dry-ice plumes are much easier to find and effects can be anticipated more easily. Other advantages of dry ice are that it is effective at warmer temperatures than AgI and it leaves no residual. A prob-

TABLE 1
Properties of a Typical Cloud Turret from the Rocky Mountain House Storm

Horizontal dimension	4.5 km
Altitude of aircraft penetrations	4.4 to 4.8 km
Temperature at penetration level	−6 to −10°C
θ_e in cloud	322°K
θ_e out of cloud	316°K
Cloud droplet concentrations	300 to 500 cm^{-3}
Maximum liquid water content	1.8 gm^{-3}
Mean cloud droplet diameter	14 μm
Concentration of particles >25 μm	<1 l^{-1}
Large particles in updraft regions	none
Large particles in downdraft regions	rimed, plate-like, 300 μm, 10 l^{-1}
Maximum updraft speed	12 ms^{-1}
Maximum downdraft speed	−8 ms^{-1}
Predominant wind direction	200 to 270 degrees
Horizontal wind speed	10 ms^{-1}
Eddy dissipation rate	120 cm^2s^3

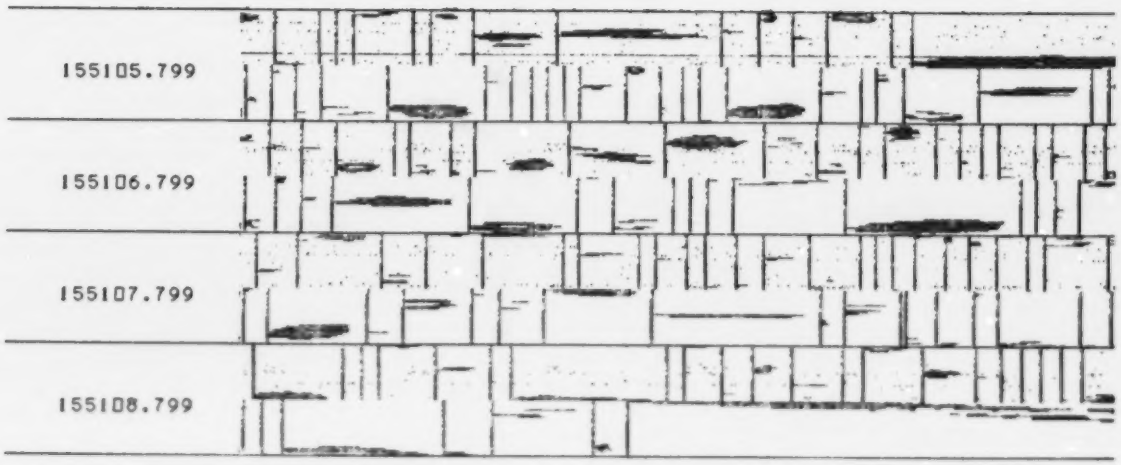

Updraft Region

FIGURE 6a. Images from the 2D-C probe in a typical updraft region of cloud turrets associated with the Rocky Mountain House storm. The distance between the horizontal lines is 800 μm. The vertical lines between images are time bars. The numbers at the beginning of the rows give the time when the first image in the row was recorded. Time advances from left to right.

*Distance between horizontal lines is 800 microns. Time advances from left to right.

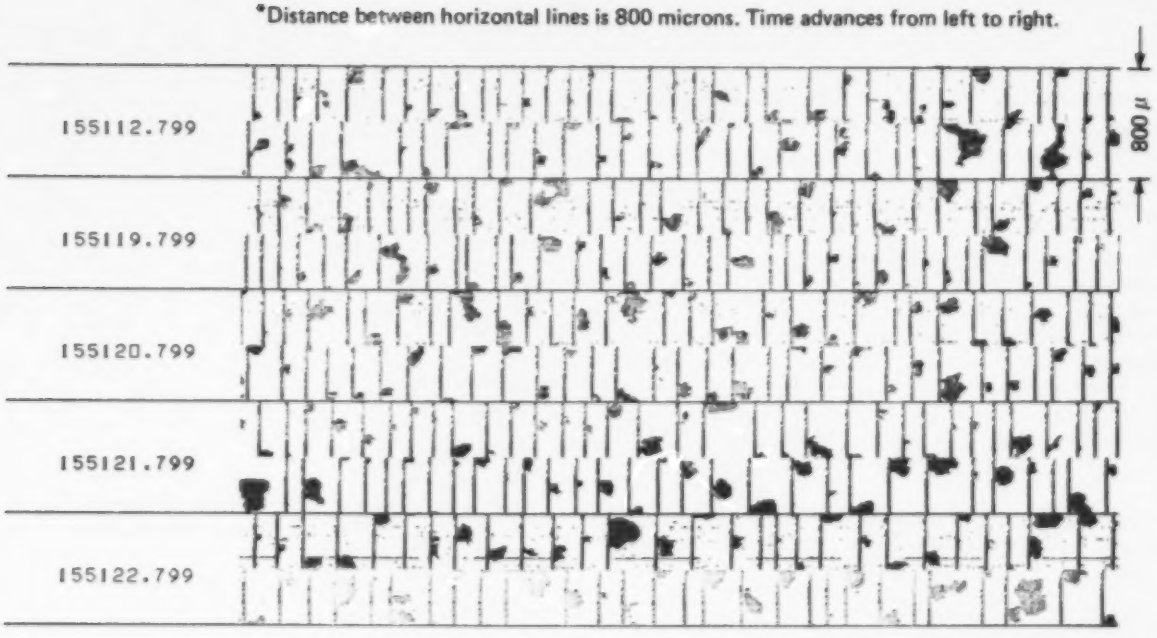

Downdraft Region

FIGURE 6b. Images from the 2D-C probe in a typical downdraft region of cloud turrets associated with the Rocky Mountain House storm.

lem with dry ice is that it requires direct injection into the location where it is to act. This presents no problem, however, when experimenting with cumulus clouds and with the new growth zone of hailstorms. For a more detailed discussion of the advantages and of the nucleation efficiency of dry ice see Holroyd *et al.* (1978).

The Procedure

Experimental design for the dry-ice, seeding missions had the research aircraft and the spotter aircraft working in tandem. The research-aircraft crew and the spotter-aircraft crew would, together, choose a suitable cloud. The research aircraft would then penetrate the cloud at about the −10°C level and the spotter aircraft would follow a few kilometers behind and about 500 m above. If sufficient liquid water and no ice crystals were detected by the research aircraft, the spotter aircraft would be given the go ahead to seed with dry ice on their penetration. The dry ice was in pellet form in a small container and the observer/photographer on the spotter aircraft would simply eject a few pellets at a time from the aircraft. The research aircraft would then make a penetration through the cloud, perpendicular to the seeding track, to look for seeding effects. The spotter aircraft would stand off to photograph the cloud. The research aircraft would then make successive passes through the cloud at lower and lower altitudes to follow the growth of the ice crystals produced by the seeding.

The First Dry Ice Experiment — 15 August

The first of the seeded clouds was seeded with 2 scoops of dry ice, equivalent to about 450 gm. Ice-crystal concentrations in the cloud increased considerably after seeding. During the last two penetrations, the liquid-water content was quite low, possibly due to the growth of the ice crystals. However, there was no sign of precipitation from the seeded clouds, nor from any of the clouds in the area.

The second of the seeded clouds was seeded with 1½ scoops of dry ice, equivalent to about 350 gm. Ice-crystal concentrations increased quite dramatically after the seeding. During the last penetration, the liquid-water content and the ice-crystal concentration were both significantly lower than in previous penetrations. This may have been due to the growth and aggregation of the ice crystals. Some signs of precipitation from this cloud were noted by the observer on the spotter aircraft.

The last cloud that was seeded was very small. No increase in the ice-crystal concentrations was found after seeding.

It should be noted that cloud-base temperatures were rather cold on this day (±1°C). Therefore, liquid-water contents in the clouds were quite low. More dramatic effects are anticipated in clouds with warmer cloud bases and more liquid water.

The Second Dry Ice Experiment — 18 August

The research aircraft penetrated a number of clouds prior to seeding. One cloud was penetrated six times; in addition, two clouds were seeded and penetrated a number of times. Unfortunately, both clouds seem to have been overseeded since ice-crystal concentrations greater than 100 l^{-1} were recorded after seeding. The desired seeding rate should have produced tens of ice crystals per litre.

As was the case on 15 August, the cloud bases on 18 August were again rather high (2.8 km) and cold (0°C). The clouds on 18 August were more vigorous, however.

The penetrations through the not-seeded cloud suggest that only very small ice-crystal concentrations occur naturally in some cumulus clouds, even in a period of 17 min. In the two seeded clouds, a dramatic increase in the ice-crystal concentrations occurred almost immediately after seeding. Data from the last penetration through one of the seeded clouds suggest that ice crystals fell from the cloud. Possibly, they evaporated very quickly. In any case, the observer on the spotter aircraft found no evidence of precipitation from either of the seeded clouds.

COMPARISON OF A SEEDED AND A NOT-SEEDED CLOUD

The Data Available

The initial results of the dry-ice, seeding experiments appear relatively exciting. Consequently, some cloud-physics data is presented here even though no in-depth analysis of these data has yet been made. It was thought that the dramatic effects of seeding with dry ice could be highlighted best by comparing two, rather similar clouds, one seeded and one not-seeded.

Since no not-seeded clouds were investigated for any length of time, on 15 August, the examples of a seeded and a not-seeded cloud have been taken from the research mission of 18 August.

Both seeded clouds were obviously overseeded on 18 August. However, the second seeded cloud exhibited lower, maximum, ice-crystal concentrations after seeding and so is presented as the example of a seeded cloud. Because the initial water content in the seeded cloud was a little less than that of the not-seeded cloud, one would expect the development of precipitation to be slightly favored in the not-seeded cloud.

The Not-Seeded Cloud

The simplest way to determine the exact times of the cloud penetrations is to determine when the recorded

liquid-water content exceeded about 0.2 gm^{-3}. The liquid-water content measured by the Johnson-Williams device during penetrations of the not-seeded cloud is shown as a function of time in figure 7. (The ASSP onboard the research aircraft was not in operation on 18 August.) The Johnson-Williams instrument uses the cooling rate of a heated wire to measure liquid-water content. The probe responds to only the liquid-water content in the cloud; it underestimates the liquid-water content if there is a significant amount in droplet sizes larger than 30 to 50 μm. Because of the difficulty in maintaining proper adjustment of the zero level, the instrument is generally given a positive bias. Note that in figure 7, the base line for the liquid-water trace (for the not-seeded cloud) is something like 0.4 gm^{-3}. Thus 0.4 gm^{-3} must be subtracted from the value of the liquid-water trace to obtain the true liquid-water content.

Also shown in figure 7 is the concentration of ice crystals measured by the PMS 2D-C probe. This instrument was discussed briefly in the second section. Whereas the concentrations shown in figure 7 are obtained from the raw data, computer processing of the recorded images can eliminate all obvious artifacts. Furthermore, computer processing can also include a correction factor for the sample volume when viewing very small crystals. (It has been found that very small crystals are "in focus" and are "accepted" within a smaller volume than large crystals.) Corrected concentrations for the six penetrations of the not-seeded cloud are shown in parenthesis in table 2

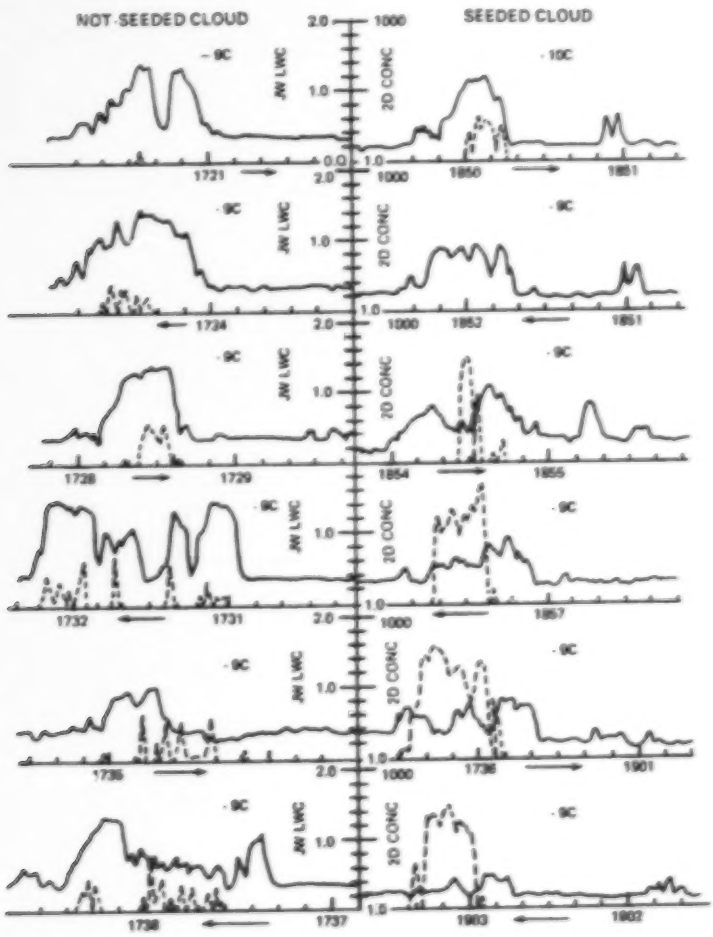

FIGURE 7. Liquid water content(-) and ice crystal concentration(...), from the 2D-C probe, as a function of time for the 6 penetrations of the not-seeded cloud and the 11 penetrations of the seeded cloud. Note the logarithmic scale of the concentration trace.

FIGURE 7 continued

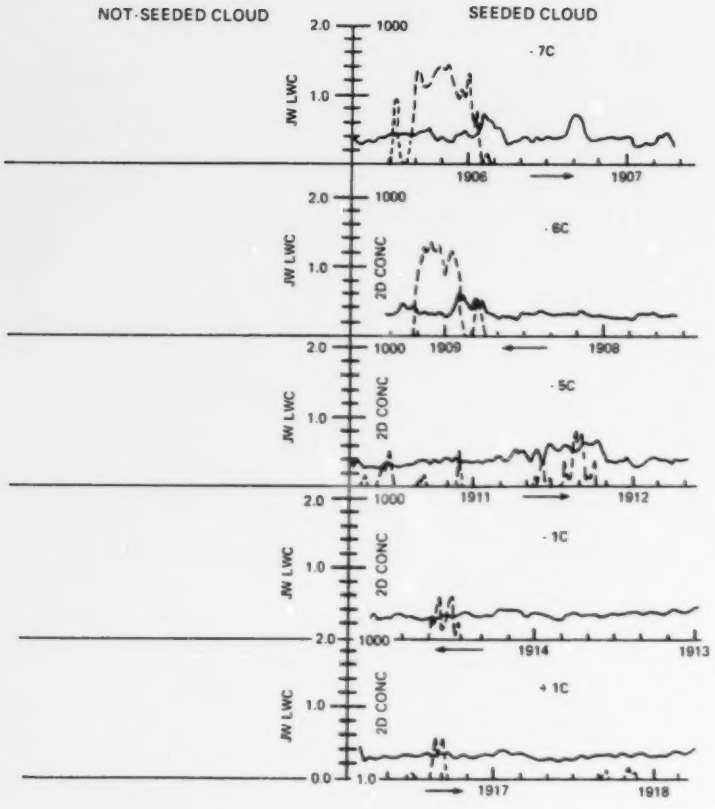

along with the maximum concentration read from figure 7. Although recorded images should be carefully scrutinized before accepting concentrations derived by the computer processing, in most cases, the processed concentrations are reliable to a factor of two accuracy (Cooper, 1978).

Table 2 also shows some other pertinent information on the penetrations. Note that the maximum water content remains fairly constant at about 1 gm^{-3}, except for one penetration. The ice-crystal concentration seems to increase with time at first, but then remains more or less steady at about 10 l^{-1}. Even though only updraft speeds are shown in table 2 downdraft regions were also encountered in the cloud. The penetrations were all made at about the $-10°C$ level and successive penetrations are generally in opposite directions. (For this reason, time advances first from left to right and then from right to left in figure 7).

Crystal-size distributions have been determined from the PMS 2D-C probe data and a mean, ice-crystal diameter for each penetration has been calculated. This mean diameter is also shown in table 2. Note that there is no consistent increase in mean crystal size nor in crystal concentration with time, that is with successive penetrations. However, because of the low, ice-crystal concentration, the mean crystal diameter is probably not representative.

Actual particle images for the first and last penetrations of the not-seeded cloud are shown in figures 8 and 9. Note that the records of 2D images contain mostly streakers which are indications of liquid water only.

The Seeded Cloud

Liquid-water content and 2D ice-crystal concentration are also shown as a function of time, for the time period 1845 to 1920 when the seeded cloud was penetrated, in figure 7. As was done for the not-seeded cloud, the actual penetration times can be determined from the liquid-water content. Where the water content is very small, the approximate time of the penetration can be determined from the ice-crystal concentration.

TABLE 2
Summary of Observations Made in Penetrations of the Not-seeded Cloud

Penetration time	Heading deg	Maximum ice crystal concentration l^{-1}	Maximum liquid water content gm^{-3}	Maximum updraft speed ms^{-1}	Mean crystal diameter μm
1720:20 - 1721:00	180	~ 1 (0.7)*	1.0	5	83*
1724:00 - 1724:40	350	~ 7 (0.6)	1.0	2	133
1728:10 - 1728:40	170	~10 (2.4)	1.0	3	92
1731:00 - 1732:20	320	~10 (1.9)	1.1	4	91
1735:00 - 1735:20	155	~10 (1.8)	0.6	3	56
1737:20 - 1738:30	320	~10 (1.4)	0.9	5	176

* Corrected values derived from raw data by further computer processing to eliminate streakers and aperture effects.

Table 3 shows some pertinent information from these penetrations. Note that the ice-crystal concentration increases dramatically after seeding and attains much higher values than were attained in the not-seeded cloud. Furthermore, the mean crystal diameter increases steadily up to the eighth penetration, by which time the water content had decreased substantially. This suggests, very strongly, that the artificial ice crystals grow very rapidly until the water content is nearly depleted. As the penetrations are made at lower levels in the cloud (evidenced by the warmer temperatures), the ice-crystal concentration decreases. The mean crystal diameter increases in going from the $-9°C$ level to the $-6°C$ level. Thereafter, the ice-crystal concentration becomes so low that the mean crystal size is probably not representative. This suggests that the decrease in ice-crystal concentration with decreasing altitude may be due to aggregation to some extent.

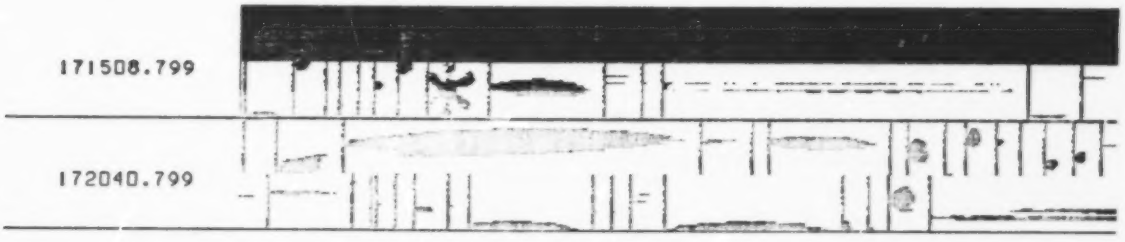

FIGURE 8. Images recorded by the PMS 2D-C probe during the first penetration of the not-seeded cloud.

TABLE 3
Summary of Observations Made in Penetrations of the Seeded Cloud

Penetration time	Heading deg	Temperature deg C	Maximum ice crystal concentration l^{-1}	Maximum liquid water content gm^{-3}	Maximum updraft speed ms^{-1}	Mean crystal diameter μm
1849:40 - 1850:20	130	−10	~ 10	1.0	4	
1851:40 - 1852:30	30	− 9	0	0.8	5	
CLOUD SEEDED						
1854:00 - 1855:00	210	− 9	~200 (292)	0.9	2	48
1857:00 - 1857:40	10	− 9	~300 (36)	0.8	2	104
1859:30 - 1902:00	210	− 9	~200 (28)	0.6	1	123
1902:40 - 1903:10	15	− 9	~200 (23)	0.4	−1	120
1905:50 - 1906:20	225	− 7	~100 (50)	0.4	10	138
1908:40 - 1909:10	30	− 6	~100 (25)	0.3	3	141
1911:10 - 1912:00	220	− 5	~ 30 (1.4)	0.2	6	118
1914:10 - 1914:30	20	− 1	~ 10	0.1	3	
1916:30 - 1917:00	210	+ 1	~ 7	0.0	6	

FIGURE 9. Images recorded by the PMS 2D-C probe during the sixth (last) penetration of the not-seeded cloud.

Actual particle images from the PMS probe are shown in figures 10 to 12. Figure 10 shows particle images recorded during the first two penetrations made before seeding commenced. The size of the images is proportional to the size of the actual ice crystals. (The PMS 2D-C probe will record large water drops, also. However, images of large water drops are generally very smooth and round. The images in figures 10 to 12 appear to be mostly ice crystals and graupel rather than large water drops.) The concentration of particles is given by the number of images recorded in a given time period. The time period noted at the beginning of each record applies to the first image of the record.

Figure 11 shows particle images recorded during the first penetration after seeding. Note how very many more images there are here and how very small they are. During the following three penetrations, particle concentrations remained high, but the particles became successively bigger (Fig. 12). Even though the largest particles the 2D-C probe can measure are 800 μm, images suggestive of a few, millimeter-sized particles were evident by 1903, about 10 min after seeding.

Conclusion

A quick glance through all the data collected during the two, dry-ice experiments shows that ice crystals were produced (by the hundreds) where there were few before. These crystals then grew at the expense of the available cloud water. The data do not show that precipitation-size particles were produced necessarily, but one must recall that the clouds treated were far from ideal with cold, cloud-base temperatures (~0°C) and consequently with little liquid water to begin with.

Isaac *et al.* (1978) show that similar results can sometimes be produced by seeding cumulus clouds with AgI.

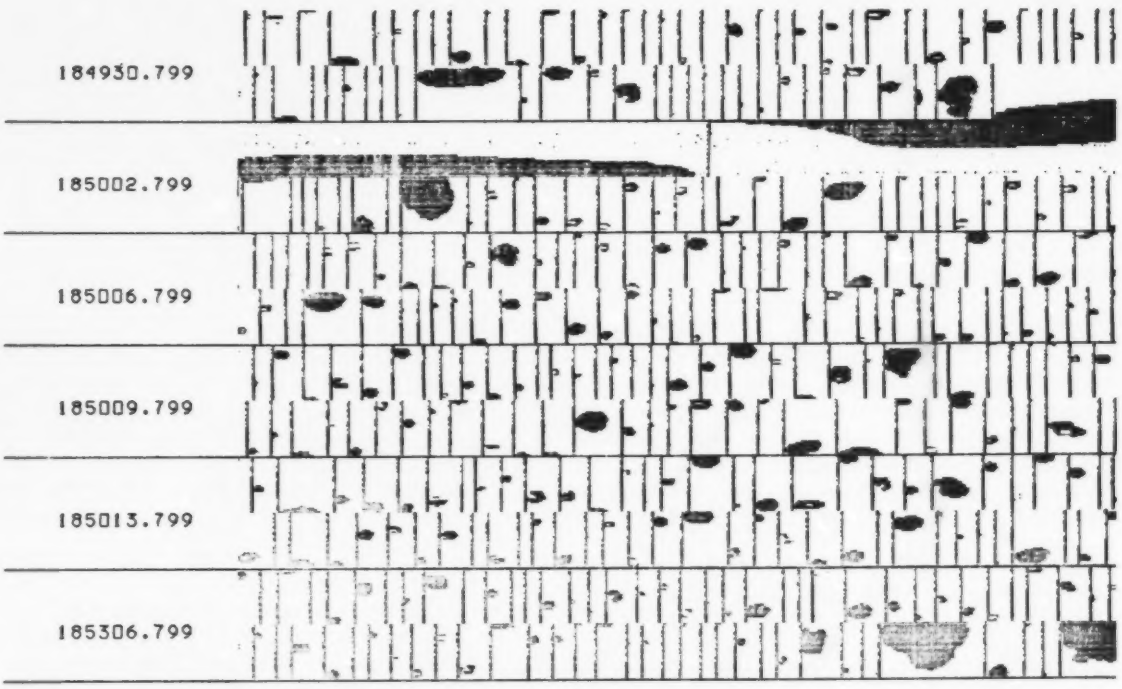

FIGURE 10. Particle images recorded by the PMS 2D-C probe during the first two penetrations of the seeded cloud, before seeding with dry ice.

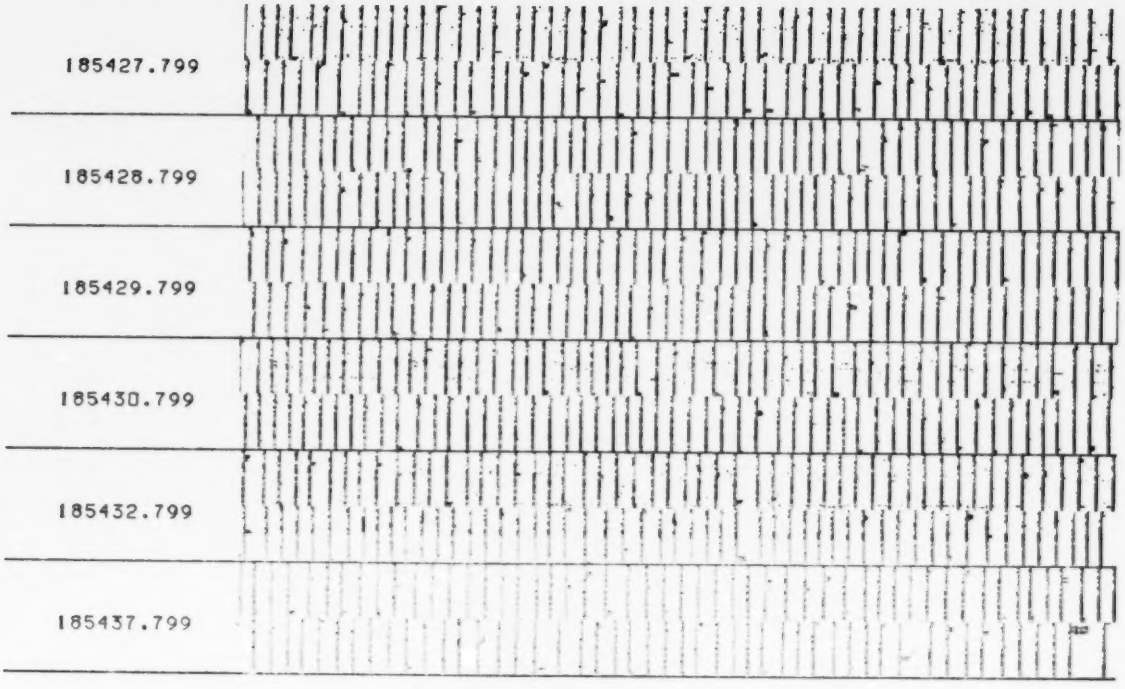

FIGURE 11. Particle images recorded by the PMS 2D-C probe during the third penetration of the seeded cloud, i.e. the first penetration after the dry ice seeding.

THE BRIGHT BAND STUDY

INTRODUCTION

On 16 August, widespread rain occurred throughout the project area and the radar showed a very good bright band. (The bright band is a horizontal layer of enhanced radar reflectivity located just beneath the melting layer of clouds; see the vertical profile of radar reflectivity, approximately over Innisfail, shown in figure 13.) Rainfall rates (near Innisfail) were about 2 mm hr^{-1}, total rainfall amounted to 7.6 mm during the period 1350 to 1659.

The research aircraft was launched at 1425 to make a series of passes over the disdrometer sites above, at, and below the 0°C level, the approximate level of the bright band. The desired measurements were particle type, size and concentration. Figure 13 shows the flight path. Marwitz *et al.* (1979) have analyzed the aircraft data collected during the flight. The radar data, for this day, have been analyzed in detail by Humphries and Barge (1979). A summary of their results follows; a more complete description of their analyses appear in Marwitz *et al.* (1979) and Humphries and Barge (1979).

RESULTS

Figure 13 shows that the aircraft flew back and forth approximately at the −7°C, −4°C, −1°C, +2.5°C and +8.0°C levels and then made a rapid ascent back through the cloud. Note the peak (at 49 dBZ) in the reflectivity curve at about 2 km elevation. This peak reflectivity is 15 dBZ greater than the reflectivity at the −7°C level and 10 dBZ greater than the reflectivity at the 8°C level. Another noteworthy feature is the fact that the temperature measurements show an isothermal layer 200 m thick at a temperature near 0°C. This layer is due to cooling of the air by melting particles.

The particle-size distributions and average microphysical characteristics for the −7°C, −4°C, −1°C and +2.5°C constant elevation legs of the flight are shown in figure 14. This diagram shows that the average concentration of ice crystals was highest at the −4°C level. Apparently, the average size of the particles remained nearly constant.

From 2D-C images recorded by the PMS probe along the flight legs above the 0°C layer, Marwitz *et al.* (1979) con-

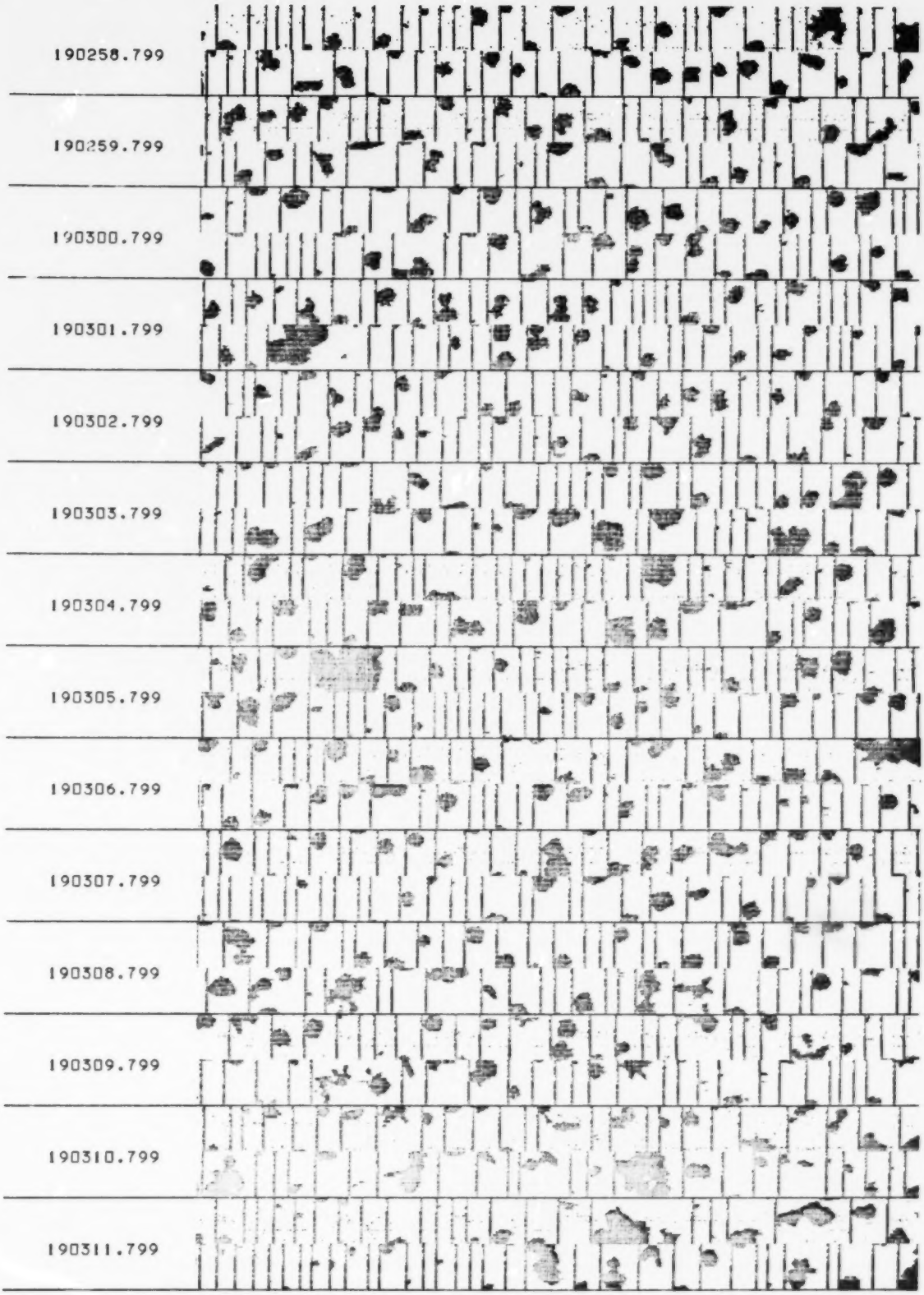

FIGURE 12. Particle images from the sixth penetration of the seeded cloud, the last penetration at the −9°C level.

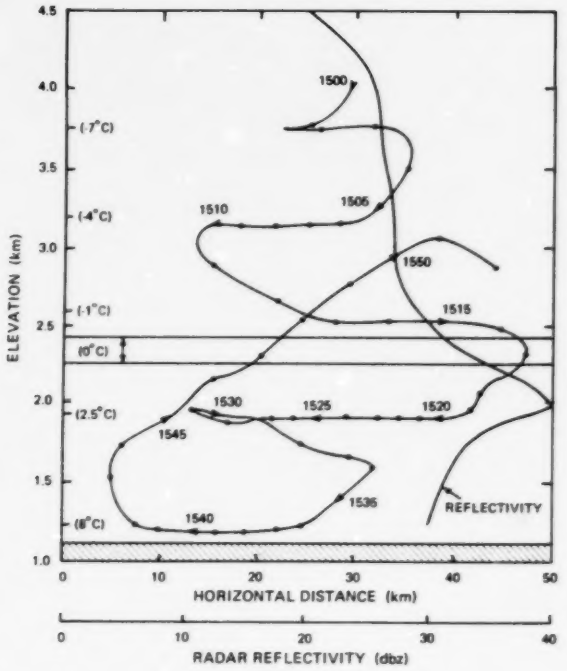

FIGURE 13. Vertical cross-section for the bright band study flight and the corresponding S-band radar reflectivity. Temperatures at which the constant elevation legs were flown are shown as well as the 0°C location (taken from Marwitz *et al.*, 1979)

clude that "large stellar-like or aggregate-like particles dominated the number concentration except at −4°C. At −4°C, there were also a large number of needles which were typically less than 800 μm in size. The average size of the stellar-like particles appeared to increase slightly as the air temperature increased. As well, the largest particle was found at the warmest temperature (−1°C). It was 5.5 mm in length." From 2D-C images recorded when the plane was rapidly descending through the melting layer, Marwitz *et al.* (1979) conclude that melted particles first appear at about the 0.6°C level and that by about the 1.7°C level almost all particles have melted. However, a few unmelted particles still existed at temperatures of about 2.4°C. Another conclusion was that there was an increase in size of the largest particles detected, down to a level where the temperature was about 1.3°C. At the 1.3°C level, the largest ice-water particle (>1 cm) was seen. At warmer temperatures, there were few particles of comparable size, presumably due to drop breakup. Furthermore, "the location of the large particle at the 1.3°C level was close to the height of the maximum reflectivity, and its presence suggests that the bright band is attributable to a very few large particles as compared to a large number of smaller particles".

To summarize, Marwitz *et al.* (1979) conclude that:

(a) the large increase in ice-crystal concentrations of sizes <1 mm between −7°C and −4°C (Fig. 14) was caused by the growth of needles between these two levels;

(b) the large decrease in the concentration of small particles from the −4°C to the −1°C level was probably due to aggregation;

(c) the water-drop spectrum can at least partially be explained as the result of melting and drop breakup;

(d) aggregation above the melting level is probably the primary cause of the bright band;

(e) the heat extracted from the environment by the melting precipitation is sufficient to produce an isothermal melting layer a few hundred meters thick;

(f) concentration changes by more than a factor of 10 were produced within a temperature change of 6.5°C and;

(g) when a bright band is present, the vertical gradients of all microphysical parameters are far greater than the corresponding horizontal gradients.

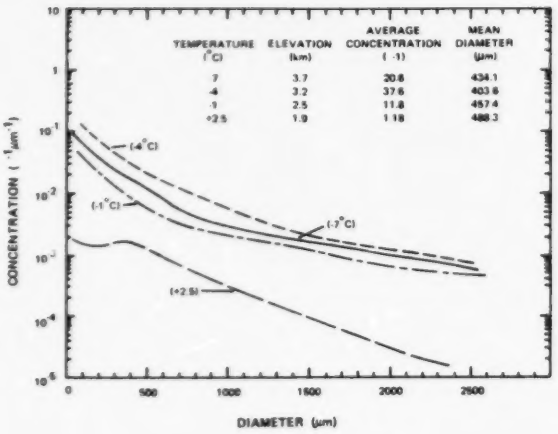

FIGURE 14. Size distribution of particles measured by the 2D-C probe at different elevations on 16 August 1978. The corresponding concentrations and mean diameters are also shown (taken from Marwitz *et al.*, 1979)

Humphries and Barge (1979) conclude (from the reflectivity, CDR and correlation data) that the particles below the melting level are large, wet and non-spherical, falling without any preferred orientation.

SUMMARY AND CONCLUSIONS

SUMMARY

During the period 1 August to 21 August, 1978, the Atmospheric Sciences Division (ASD) of the Alberta Research Council (ARC) operated a cloud physics research aircraft program in conjunction with the Alberta Hail Project. The primary objective of the program was to obtain the aircraft measurements necessary to test the proposed conceptual model and to develop a realistic, numerical model to test the effects of seeding storms with AgI on the growth of hail and rain. To obtain the aircraft measurements, ARC contracted with the University of Wyoming for the use of their specially instrumented Queen Air and for the services of a pilot and a scientist. The Queen Air operated under Intera's letter of agreement with Air Traffic Control and Intera controllers directed the plane.

To take advantage of the variety of weather situations experienced while the Queen Air was in Alberta, a number of secondary aircraft projects were devised and executed. Of a total of 24.2 hours of research missions flown during the period of the experiment, about 11.2 hrs were spent on thunderstorm penetrations, 7.8 hrs on cumulus penetrations, 3.4 hrs on a Rocky Mountain House Area Genesis Study (RAGS) and 1.8 hrs on a bright-band study.

The thunderstorm penetration missions entailed flying through the new growth zone on the edges of thunderstorms at various levels, measuring particle types, sizes and concentrations as well as state parameters. Such measurements were obtained from seven thunderstorms, including one particularly successful mission on 12 August (the Rocky Mountain House Storm).

The cumulus penetration missions required flying through cumulus clouds making the same kind of measurements as in the thunderstorm-penetration flights. A number of these cumulus clouds were seeded with dry ice in an attempt to stimulate the development of rain.

The Rocky Area Genesis Study was designed to confirm the hypothesis that surface winds, channelled up the river valleys, produce convergence over the higher ground between the river valleys and so initiate the formation of hailstorms. For the one successful RAGS flight, the Queen Air flew just above and along the foothills, measuring the subcloud winds several kilometers upwind of the convective clouds.

For the bright-band study flight, the Queen Air made a series of passes over two disdrometer sites, flying above, at and below the 0°C level (the approximate level of the Bright Band) measuring particle types, sizes and concentrations as well as state parameters.

In conclusion, many excellent data were collected, not only for the primary objective, but also for some secondary projects. Significant scientific progress surely will result from this program. Although firm conclusions can come only from detailed analysis of the recorded data, some preliminary results are presented in this report. In particular, a profile of a typical cloud turret in the new growth zone of the Rocky Mountain House storm is presented. Also, some cloud-physics data for a seeded (with dry ice) and a not-seeded cumulus cloud are shown. Finally, preliminary results of the analysis of the aircraft data for the bright-band, study flight are given.

CONCLUSIONS

It was expected that a first-class, thunderstorm-penetration program could be operated successfully with existing facilities and with a full-scale, operational, cloud-seeding program in progress since the Alberta Hail Project's radar system and the University of Wyoming's cloud physics research aircraft are among the best in the world. On the other hand, it was remarkable since there was little time for planning (because of the uncertain funding) and no time for mistakes (because of the short field project and unpredictable weather). Nevertheless, many excellent data were collected, not only for the primary objective of determining the precipitation processes active in the new growth zone of Alberta thunderstorms, but also for a number of secondary projects. Significant scientific results have already resulted from this project and many more are forthcoming.

In the second section, a profile of a typical cloud turret in the new growth zone of the Rocky Mountain House storm is presented. This preliminary analysis shows that the cloud turrets in the new growth zone are vigorous and contain much supercooled water. The horizontal motions on that day show that the cloud turrets in the new growth zone migrate toward the main storm, approximately at right angles to the storm motion. They travel the distance to the storm in about 15 min. The cloud-droplet spectra indicate that the Alberta hailstorm is more maritime in nature than the severe storms which have been studied extensively in Colorado and Montana.

Some cloud physics data are presented, in the third section, of a cumulus cloud seeded with dry ice and of a similar not-seeded cumulus cloud. The data collected during two, dry-ice-seeding experiments show that ice crystals were produced by the hundreds where there were few before. These crystals then grew at the expense of the available cloud water. The data do not show that precipitation-sized particles were produced necessarily, but the clouds treated were far from ideal with cold, cloud-base temperatures and consequently with little cloud water to begin with. More dramatic effects are expected from clouds with a higher cloud-base temperature and more liquid water.

The preliminary analysis of the aircraft data from the bright-band study suggests that the bright band is due mainly to aggregation above the melting level. This analysis further suggests that the heat extracted from the environment by melting precipitation below the freezing level causes an isothermal melting layer a few hundred meters thick.

The use of a spotter aircraft, to photograph the small clouds penetrated, seems to be a first for Alberta. The cloud photos will provide a macrophysical framework for the microphysical measurements by the aircraft and will facilitate linking the aircraft data to the radar measurements.

A lasting benefit to the Alberta Hail Project will undoubtedly be the spirit of cooperation and understanding among all involved which was fostered by the cloud physics research aircraft program. Another lasting benefit will be the fresh ideas brought to us by the University of Wyoming crew. The use of dry ice in the cumulus-seeding experiments and the logistics of these seeding experiments were largely based on their recommendations.

SUGGESTIONS

A suggestion for the future is to instigate a scientific, performance-monitoring system of the seeding operations to complement Intera's own monitoring and training program. For example, a reevaluation of the cloud-top, seeding logistics may be warranted since it is now evident that for some storms the cloud tops in the new growth zone are rather low; that is, they do not seem to reach anywhere near the −7°C level, the level where cloud-top flares ignite. Consequently, portions of cloud-top flares may burn above intended seeding targets. It may be advisable to adjust the seeding altitude or the burn time of the flares to ensure that most of the nuclei released by the flares are released in cloud.

Also, a reconsideration of seeding reagent may be desirable. Given the apparently warm cloud tops of the clouds in the new growth zone and the dramatic effect of seeding with dry ice demonstrated by the dry-ice experiments, dry ice should be considered as a seeding reagent.

The pilots of the seeding planes have a fantastic opportunity to develop a climatology of hailstorms and of cumulus clouds in Alberta that would be invaluable in planning future seeding operations and research experiments. This would require better instrumentation (for instance, more accurate thermometers) on the planes.

The results of the dry-ice, seeding experiments are quite encouraging for a rain stimulation experiment. More such experiments should therefore be carried out, possibly with a more sophisticated seeding method. As some researchers have reported similar results from seeding cumulus clouds with silver iodide, some silver iodide seeding of cumulus clouds should be tried.

Even the few preliminary results given in this report for the dry-ice experiments and the bright-band study show the tremendous power of a cloud physics research aircraft in furthering weather modification. It is therefore suggested that Alberta should direct more effort in this direction and, possibly, should even consider acquiring a suitably equipped cloud physics research aircraft of its own. Such an aircraft could be designed by government agencies but operated and maintained by a private corporation.

ACKNOWLEDGMENTS

Drs. B.L. Barge and R.G. Humphries were instrumental in initiating the cloud physics, research aircraft program and indispensable in the operation of the field project. Without their constant perseverance and assistance this program would never have started. We are also very grateful to Dr. G.G. Goyer for his understanding, advice and encouragement. J. Renick, D. Deibert and K. Grandia were also extremely helpful. Many other staff members of the Atmospheric Sciences Divison, the Alberta Weather Modification Board and Intera assisted the program. Finally, we are deeply indebted to the Alberta Weather Modification Board for financing this project.

REFERENCES

Barge, B.L. and F. Bergwall, 1976: Fine scale structure of convective storms associated with hail production. Report 76-2, Atmospheric Sciences Division, Alberta Research Council, Edmonton, Alberta. In two volumes.

Barge, B.L., F. Bergwall, G.G. Goyer and J.H. Renick, 1976: Fine scale structure of convective storms — implications for cloud seeding in Alberta. Report 76-3, Atmospheric Sciences Division, Alberta Research Council, Edmonton, Alberta, 19 pp.

Cannon, T.W., J.E. Dye and V. Toutenhoofd, 1974: The mechanism of precipitation formation in northeastern Colorado cumulus. II. Sailplane measurements. Journal of Atmospheric Sciences, 31, pp. 2148-2151.

Chisholm, A.J. and M. English, 1973: Alberta hailstorms. Meteorological Monograph, 14, 98 p.

Cooper, W.A., 1978: Cloud physics investigations by the University of Wyoming in HIPLEX 1977. Report No. AS119. Department of Atmospheric Science, College of Engineering, University of Wyoming, Laramie, 320 p.

English, M., B.L. Barge and R.G. Humphries, 1979: Cloud physics research aircraft program: Summary of operations and preliminary aircraft and radar observations. Atmospheric Sciences Division, Alberta Research Council, Edmonton, Alberta. In preparation.

Holroyd, E.W., A.B. Super and B.A. Silverman, 1978: The practicability of dry ice for on-top seeding of convective clouds. Journal of Applied Meteorology, 17, pp. 49-63.

Humphries, R.G. and B.L. Barge, 1979: Polarization and dual wavelength observations of the bright band. Submitted to IEE Transactions on Geoscience Electronics.

Isaac, G.A., R.S. Schemenauer, R.A. Stuart, A.J. Chisholm and J.I. MacPherson, 1978: Cumulus cloud measurements in northern Canada. Preprints, Conference on Cloud Physics and Atmospheric Electricity, Issaquah, Washington, pp. 363-370.

Marwitz, J.D., 1978: Vertical streaks in radar echoes from convective clouds. Preprints, 18th Weather Radar Conference, Atlanta, Georgia, pp. 260-265.

Marwitz, J.D., R.E. Stewart, T.S. Karacostas and B.E. Martner, 1979: Interim Report on the Sierra Cooperative Pilot Project, 1977-78 Season. Department of Atmospheric Science, College of Engineering, University of Wyoming, Laramie.

Renick, J.H., 1971: Radar reflectivity profiles of individual cells in a persistent multicellular Alberta hailstorm. Preprints, Seventh Conference on Severe Local Storms. American Meteorological Society, Kansas City, pp. 66-70.

APPENDIX A

SUMMARY OF HAILSTORMS PENETRATED BY THE CLOUD PHYSICS RESEARCH AIRCRAFT

THE SYLVAN LAKE STORM OF 7 AUGUST

During the most intense part of its lifetime, the storm was close to the radar, so that radar coverage was not optimum. However, a quick scan through the radar data suggests that the storm had echo tops of about 9.0 km MSL and a maximum reflectivity of about 59 dBZ. The storm lasted about 1¼ hours and produced pea-sized hail (~0.8 cm in diameter).

The research aircraft made 13 penetrations of this storm from about the −10°C to the −3°C level. Some of the noteworthy features found were:

(a) the winds were very strong and cell motion was rapid;
(b) in regions of updraft, speeds reached a maximum of 9 ms^{-1}, θ_e a maximum of 327 K and the in-cloud temperature at 5.2 km was −4.5°C whereas the out-of-cloud temperature at the same level was −10°C;
(c) at their flight levels (−10°C to −3°C), the edge of the visible cloud appeared to be almost identical to the edge of the radar echo and no new growth zone was apparent;
(d) the storm was surrounded by a mid-level stratocumulus cloud deck;
(e) much ice and little liquid water were observed in the clouds, ice-crystal concentrations of 25 to 100 l^{-1} were common;
(f) ice crystals were found at very warm temperatures like −3°C and −4°C, but no ice crystals were found during a penetration at −5°C.

THE PENHOLD STORM OF 10 AUGUST

A quick scan through the radar data for this storm suggests that the maximum echo top may have been about 10.4 km MSL. The maximum reflectivity was probably between 50 and 60 dBZ. Storm duration was about two hours and pea-sized hail was produced by the storm.

The storm was well advanced and already decaying when the cloud physics research aircraft reached it. In spite of this, seven penetrations were made, all at about the −10°C level. Some particularly noteworthy observations made during the penetrations were:

(a) very high ice crystal concentrations were encountered during the first two penetrations;
(b) at the flight altitude (~−10°C) the storm appeared to have no cloud-top seeding targets; there was no shelf cloud;
(c) no drops larger than about 20 μm in diameter were encountered;
(d) the liquid-water content measured in one of the penetrations was close to adiabatic.

THE RIMBEY STORM OF 10 AUGUST

A quick scan through the radar data for this storm suggests that maximum echo tops were about 13.1 km MSL and maximum reflectivities were in the range 50 to 60 dBZ. One report of grape-sized hail from this storm was received, most of the reports specified pea as the maximum size. The storm lasted about two hours.

The research aircraft made one pass through this storm on their way to a storm further north. Two further passes through the storm were made upon returning from the storm in the northwest, but by this time the Rimbey storm was decaying rapidly.

The observer on the "spotter aircraft" commented on some particularly noteworthy features of this storm, namely:

(a) big, impressive, cloud towers were seen to be associated with the storm;
(b) small turrets were seen building on the west side of the storm;
(c) apparently, ice crystals were falling from the large anvil back into the storm.

The crew of the research aircraft, on the other hand noted that:

(a) their first penetration was through an active turret on the southwest side of the storm;
(b) prior to their second penetration, they flew between two cells and, once on the south side, observed some very active, visually-impressive turrets to the east even though the storm was decaying rapidly;
(c) the second and third penetrations were through these active turrets to the east where they encountered strong, smooth, sustained updrafts, lots of liquid water, very little ice and no radar echo;
(d) again, no drops larger than about 20 μm in diameter were encountered;
(e) again, there were no apparent cloud-top seeding targets at or near the flight level of the research aircraft; the clouds in the new growth zone were at a much lower altitude.

THE DRAYTON VALLEY STORM OF 10 AUGUST

An isolated echo northwest of the radar moved into the project area at about 1525. At that time it had a maximum reflectivity of 58 dBZ and was about 80 to 90 miles away. Apparently, maximum reflectivities greater than 60 dBZ occurred before the storm moved into the project area. The storm probably had a maximum radar echo top of about 12.2 km MSL. Only two hail reports from this storm were received, both giving the maximum size as pea. By 1700 the storm was decaying rapidly.

Six penetrations of this storm were made by the cloud physics, research aircraft. The crew emphasized that:

(a) during their earlier penetrations, they were flying through a lens-type cloud;
(b) later in the flight, some turrets started to build on the south-east edge of the storm so that on the east of their runs they were spending most of their time in turrets;
(c) no drops larger than 20 μm were encountered;
(d) there appeared to be no cloud-top seeding targets at or near their flight altitude.

THE ECKVILLE STORM OF 11 AUGUST

There exists some confusion about how many storms were actually investigated during this research mission. Apparently both the spotter aircraft and the research aircraft arrived to find an obviously dissipating storm. After a number of penetrations on some "old" turrets of the decaying storm, a "new cell" seemed to develop in the vicinity of the dissipating storm. The dissipating storm and the "new cell" were connected by clouds but were not obviously associated with one another. The "new cell" developed turrets and a new growth zone and eventually produced heavy rain. The old storm apparently produced pea- and grape-sized hail.

Noteworthy observations were that ice-crystal concentrations in the mature towers of the dissipating storm were high (100 to 200 l^{-1}) and liquid-water contents were quite low, whereas ice-crystal concentrations were very low and water contents high, initially, in the "new cell". With time, the ice-crystal concentrations increased and the water content decreased. Apparently water drops greater than 30 μm in diameter were encountered for a very short time.

THE ROCKY MOUNTAIN HOUSE STORM OF 12 AUGUST

During its most intense phase, the Rocky Mountain House Storm seemed to exhibit a maximum radar reflectivity of about 67 dBZ and a maximum radar echo top of about 10.4 km. The storm was long-lived, it started about 1415 and dissipated about 1730. Numerous reports of grape-sized hail were received. One sample of hailstones was collected for analysis. The storm had a relatively warm, cloud-base temperature of +7°C.

The research aircraft made numerous penetrations on the south side of the storm. About half the penetrations were made at about the −10°C level and half at lower levels. Of particular interest were the high updraft speeds occasionally encountered by the research aircraft, the relatively low, ice-crystal concentrations and the high, liquid-water contents.

THE RED DEER STORM OF 15 AUGUST

At about 1915 a small, intense storm popped out of the ground clutter about 16 km northeast of the radar. The storm reached a maximum reflectivity of about 68 dBZ and lasted about 30 min. A quick scan through the radar data suggests that the storm had echo tops to about 9.4 km once it was out of the ground clutter. A number of grape-sized hail reports can be attributed to this storm. The research aircraft made three low-level penetrations through this storm.

More detailed information on all these storms can be found in English *et al.* (1979).

APPENDIX B

SUMMARY OF CUMULUS CLOUDS PENETRATED BY CLOUD PHYSICS RESEARCH AIRCRAFT

CUMULUS PENETRATION OF 7 AUGUST

The research aircraft made four penetrations, at an altitude of 4.6 km, of some clouds near Sundre. The spotter aircraft remained about 16 km to the east, at an altitude of 5.2 km, to photograph the clouds. Apparently, the first penetration by the research aircraft was through a number of inconsequential clouds in the area. By the second penetration, a very vigorous cumulus cloud had developed. On the third penetration, the cloud was producing a radar echo of about 35 dBZ, and the research aircraft flew right through the echoing part of the cloud and encountered updrafts of 6 ms^{-1}. The last penetration was again through the echoing portion of the cloud but by this time the echo was much weaker.

CUMULUS PENETRATION OF 9 AUGUST

Some suitable, towering, cumulus clouds were found northeast of Calgary, near Drumheller. The research aircraft penetrated four different clouds during this mission. Apparently none of the clouds were vigorous enough to produce a radar echo. It is noteworthy that small graupel, 500 to 800 μm in diameter was encountered on one penetration. Also, rimed dendrites with diameters of about 800 μm, and rimed needles with lengths of about 600 μm were noted.

CUMULUS PENETRATION OF 12 AUGUST

Two or three cumulus clouds in the vicinity of the Rocky Mountain House storm were penetrated once. Actually, the main object of this part of the flight was to test logistics for a dry-ice, seeding experiment. Although one of the cumulus clouds was actually seeded, it had a strong radar echo and significant concentrations of ice crystals prior to seeding.

CUMULUS PENETRATION OF 15 AUGUST

On this day, suitable cumulus clouds for penetration by the research aircraft were found near Sullivan Lake. Three clouds were penetrated, once each. Three other clouds were penetrated once, then seeded with dry ice, and then penetrated again a number of times.

CUMULUS PENETRATIONS OF 18 AUGUST

Four cumulus clouds were penetrated once each by the research aircraft on this day. In addition, a fifth cloud was penetrated six times during a period of about 17 min. During these 17 min, liquid-water contents remained high and ice-crystal concentrations remained low. This fifth cloud was meant to serve as a comparison to two further clouds penetrated on this day. These two further clouds were both seeded with dry ice.

ATMOSPHERIC SCIENCES DIVISION
RESEARCH, OPERATIONS, AND EVALUATION
IN THE
ALBERTA HAIL PROJECT

1974 - 1978

VOLUME 1 The Summary

— Summary of ARC Report to AWMB: G.G. Goyer

VOLUME 2 The Research

VOLUME 2-A Meteorology and Modelling

— The Storm Environment Program: F.E. Robitaille

— The Cloud Modelling Program: M. English et al.

— The Cloud Physics Program: M. English

VOLUME 2-B Radar Meteorology

— Digital Weather Radar Data for Computer Novices: J. Ramsden et al.

— Calculations of Dual Wavelength Ratios for Non-Rayleigh Oblate Spheroids at Weather Radar Wavelengths: R.G. Humphries and B.L. Barge

— Polarization and Dual Wavelength Radar Measurements of Rain, Snow, and Hail: B.L. Barge and R.G. Humphries

VOLUME 2-C Precipitation Studies

— Sampling Statistics of Alberta Hailpad Data: L. Wojtiw and E.P. Lozowski

— Hailsize Distributions from Hailpad Data: L. Wojtiw

— Factors Affecting Hailcrop Damage: L. Wojtiw

— The Dispersion of Silver Iodide in Cloud Seeding Experiments: E. Zacharuk et al.

— Analysis of Rainfall Data from the Precipitation Network: L. Wojtiw

— The Analysis of Historical Rainfall Patterns in the Alberta Hail Project Area: R.K.W. Wong

VOLUME 3 The Operations

— Radar Engineering, Operations, and Applications: S. Leung

— Data Processing in the Alberta Hail Project: M. Johnson

— Documentation of Computer Software for Processing Digital Weather Radar Data at the Alberta Council: J. Ramsden et al.

— Extraction of CAPPIs' from Logged Radar Data: B. Folliott and J. Ramsden

— Hailpad Data Collection and Reduction: L. Wojtiw

VOLUME 4 — The Evaluation: R.K.W. Wong and N. Chidambaram.